MEASUREMENT OF RESIDUAL STRESS IN THIN DIAMOND FILMS BY RAMAN SPECTROSCOPY AND THE BEAM DEFLECTION EQUATION

By

Naoufel Turki

A THESIS

submitted to
Michigan State University
in partial fulfillment of the requirements
for the degree of

MASTER OF SCIENCE

Department of Materials Science and Mechanics

1996

ABSTRACT

MEASUREMENT OF RESIDUAL STRESS IN THIN DIAMOND FILMS BY RAMAN SPECTROSCOPY AND THE BEAM DEFLECTION EQUATION

By

Naoufel Turki

The properties of natural diamond and the effect of deposition parameters on the deposited synthetic diamond films were reviewed. A new model for calculating thermal expansion mismatch stress between the film and the substrate is proposed. Residual stress in a diamond film deposited by MPCVD on a silicon substrate was measured from the change in substrate curvature according to Stoney's equation and from the shift in the Raman peak position at 1332.5 cm^{-1}. Both methods were found to measure the average stress in the diamond film. Assumptions made to derive stress equations for both methods were not truly satisfied. Polycrystalline diamond film presents a problem for the Raman Shift method and the non uniformity in the diamond film thickness coupled with the anisotropy of the single crystal substrate and possible texture in the diamond film create obstacles to directly applying Stoney's stress equation. The magnitude of the stress measured from Stoney's equation and Raman shift are comparable to reported values in the literature.

TABLE OF CONTENT

LIST OF TABLES

LIST OF FIGURES

LIST OF SYMBOLS USED

ε_{th}: Thermally induced strain

σ_{th}: Thermally induced stress.

ε: Total residual strain in the thin film.

σ_R: Total residual stress in the thin film.

T: Temperature.

T_s: Substrate temperature.

E_s: Young's modulus of the substrate material.

E_f: Young's modulus of the film material.

α_s: Thermal expansion coeficient of the substrate.

α_f: Thermal expansion coeficient of the film.

t_s: Substrate thickness.

t_f: film thickness.

νs: Poisson ratio of the substrate material.

ν_f: Poisson ratio of the film material.

ρ: Radius of curvature of the films-subtrate composite.

1- INTRODUCTION

1.1 Overview

Due to its excellent properties, synthetic diamond films are being increasingly used and studied.

In this work, a detailed review of the properties of natural diamond is presented in section 2.1 to serve as a basis for comparison with the properties of deposited synthetic diamonds. Depositions techniques and the effects of deposition parameters on the properties of synthetic diamonds are discussed in the remainder of chapter 2.

Residual stress measurement in thin diamond films is the main topic in this thesis. A review of the effect of film properties (film thickness and grain size) as well as the effect of deposition parameters on the magnitude and sign of residual stress in thin films is discussed in chapter 3.

In chapter 4, x-ray and energy gap stress measurement techniques are briefly discussed while a detailed discussion of stress measurement from the curvature change in a coated substrate and the Raman peak position shift are presented in section 4.3 and 4.4. Stress calculation formulas are derived and the two methods are analyses in terms of the assumptions made and the applicability of those assumptions to the specific silicon-diamond system used in the experimental procedure.

In chapter 5, a new model is presented for calculating the thermal stress that develops in diamond films upon cooling to room temperature from the deposition temperature. The temperature dependence of the thermal expansion mismatch between the diamond film and the silicon substrate and the Young's modulus temperature dependence are considered in the proposed model.

The experimental procedure is presented in chapter 6, while the experimental results are given in chapter 7. Calculation of the stress by the two methods and discussed of the results is presented in chapter 8. Conclusion and recommendations are given in chapter 9.

1.2 Background

In 1909, Stoney [1] discovered large internal stresses in electroplated films. Since then, many researchers have studied the nature and effects of internal residual stress on thin films.

Residual stress in thin films can cause undesirable properties. Internal stresses induced by the deposition process induce buckling of the beam-substrate composite [2], and can promote interface cracking, by providing additional driving force for crack propagation. Argon and Gupta [3] found that SiC films deposited on single crystal silicon wafer by plasma assisted chemical vapor deposition (PACVD) process, delaminated spontaneously under residual stress, when the thickness of the film is above a critical value of about 1 μm [3]. Cracking was also

observed at the interface of semiconductor films (GaP, GaAs, InP) grown on silicon substrates, due to residual stress [4]. Strains up to $2x10^{-3}$ were measured in the semiconductor films.

In silicon coating on Pitch-55 carbon fibers, the coating trapped a large concentration of hydrogen. The trapped hydrogen in the film resulted in large compressive residual stresses in the silicon film. Upon embedding the coated fibers in the metal matrix, hydrogen diffused to the metal matrix leaving voids behind which resulted in severe debonding of the fibers from the metal matrix [3]. Blunberg [5] reported that super conducting critical temperature in thin films increased with decreasing film thickness. An increase in film thickness also resulted in an increase in the residual stress. Freedman [6] reported that thermal stress at 275°C due to thermal expansion mismatch was sufficient to induce a phase change to a tetragonal structure in nickel films on NaCl substrate. The stress was compressive and measured -1.0 GPa.

It is evident that the existence of residual stress in thin films affects their properties. Therefore, it is critical to understand the behavior and dependences of film stress so that the film-substrate composites behave as they are designed.

There is an exhaustive amount of literature on the mechanisms and measurement of residual stress in thin metal films. A lesser amount however does exist for dielectric thin films. At a given temperature, internal stress has two components: intrinsic and extrinsic. Extrinsic stresses result from thermal expansion coefficient mismatch between the

substrate and the film which in turn depends on the difference between film growth temperature, during deposition and stress measurement temperature.

Intrinsic stresses are growth stresses arising from such effects as incomplete structural ordering processes, which could result in lattice misfit strains. Intrinsic stresses can also arise from contamination of the film. Internal stresses are therefore a strong function of the deposition process and parameters such as deposition temperature, pressure, rate, film thickness, sputtering ion beam energy as well as other parameters [7,8]. Choice of film and substrate materials can reduce residual stresses arising from thermal expansion mismatch and lattice mismatch. However, residual stress elimination or reduction can best be pursued by changing the deposition parameters. Controlling all these material and deposition parameters can affect both the magnitude and the sign of internal stresses.

Measured stresses in carbon films are usually compressive [7,9]. The magnitude of the stress for CVD diamond is about 1 GPa [9]. The magnitude of the compressive stresses in DLC films deposited by ion beam sputtering methods are higher than in CVD films. Tensile stresses in CVD films have also been observed [10]. While compressive stresses are understood, tensile stresses in CVD diamond films are not so easily explained. The grain boundary relaxation model (GBRM) has been proposed to explain the origin of the tensile intrinsic stresses in CVD diamond [10]. Compressive stresses are thought to be due to ion

bombardment in sputtered films and to impurities in CVD films [9,11,12]. When diamond is deposited on silicon the lattice mismatch strain is tensile in the diamond films. However, thermal expansion mismatch stress between silicon and diamond is expected to be compressive in the deposition temperature range of CVD diamond (less than 1200°C), and can become tensile at temperatures greater than 1220°C [10] which is outside the temperature range for CVD diamond deposition. Thermal compressive stresses in diamond films on silicon substrates are smaller in magnitude compared to intrinsic stresses (less than 0.3 GPa at 1000°C deposition temperature) [10]. The sign and magnitude of the total residual stress in diamond films is therefore determined by the intrinsic stress. Tensile stresses in films are undesirable because crack propagation is promoted under a tensile stress state. Conversely, compressive stresses are desirable because they strengthen the films by hindering the propagation of cracks [13]. High compressive stress can however cause buckling in the film and induces wrinkles [12,14].

The sign and magnitude of total film stresses can be controlled via variation of the parameters affecting the intrinsic stress namely the deposition parameters.

2- PROPERTIES AND DEPOSITION OF DIAMOND FILMS

2.1 Properties of natural diamond

Natural Diamond has a unique combination of physical, optical and electrical properties that may perhaps be exploited in application of diamonds as a thin films [15,16]. Table 1 lists the properties of bulk diamond.

Carbon can be amorphous or crystalline. When carbon crystallizes in the cubic A4 structure (named after diamond [17]), diamond is formed [18]. The structure of diamond belongs to the space group Fd3 m-O_h^7. Diamond has a lattice constant a = 3.567 Angstroms at room temperature. The diamond structure has eight atoms per unit cell with each atom covalently bonded to another carbon atom (sp^3 tetrahedral bonds) [19]. The atomic distance (distance of closest approach) in diamond is 1.544 Angstroms [17]. Diamond usually crystallizes in octahedra crystallites whose faces are {111} planes. Less commonly, diamond might crystallize in dodecahedra crystallites in thin plates, with the crystals having {110} planes as their faces [18]. Compared to other hard materials, diamond has a low density, (3.52 g cm^{-3}) due to the small size of carbon atoms whose atomic radius is equal to 0.77 Angstroms. (Carbon has an atomic number of six and an electronic configuration of { $1s^2$ $2sp^3$ } [17]).

When carbon crystallizes in the hexagonal structure, graphite is formed. The lattice parameters are a = 2.461 Angstroms, and c = 6.708 Angstroms. Graphite has a lower density than diamond, (2.3 gcm^{-3} [18]). Graphite is formed in layers with strong trigonal bonds (sp^2), and an interatomic distance equal to 1.415 Angstroms in the basal plane of the hexagonal lattice. The fourth electron in the outer shell forms a weak bond of the Van Der Waals type, between the layers of trigonal carbon. This weak electrostatic Van Der Waals force is responsible for the low interplaner strength of graphite [19].

Amorphous carbon can be characterized as imperfect graphite structure; the sp^2 bonded carbon clusters have crystallographic layer planes which are not oriented with respect to a common axis. The orientation of the planes is random and the layers overlap on one another [19].

Diamond has some excellent mechanical properties. Diamond's hardness is the highest known (up to 100 GPa) [19], due specifically to its strong covalent bonds (high atomic bond energy) and carbon's small atomic radius. Diamond's high atom number density coupled with strong covalent bonds result in a very high elastic modulus (1160 GPa for single crystal diamond. Silicon, which has the same crystal structure as diamond's, has a elastic modulus of only 180 GPa [20]).

While diamond's room temperature thermal conductivity of 1100 W/mK is five times that of copper, diamond is a strong dielectric material (dielectric constant equal to 5.7) with electrical resistivity higher than

10^{16} ohm-cm. Diamond's thermal conductivity is much higher at room temperature than other hard materials [18]. The thermal conductivity of diamond at room temperature is one order of magnitude higher than that of silicon, which has the same crystal structure as diamond [18].

The optical properties of diamond are equally impressive with the rest of its properties, justifying diamond's use as optical windows for x-ray lithography due to a unique combination of high stiffness and high x-ray transmission [21]. Diamond has a high refractive index (2.47 at 5890 Angstroms electromagnetic wavelength [18,10]), resulting in a low angle of total internal reflection [18]. The optical band gap is 5.4 eV making diamond electrically insulating at room temperature. Diamond's absorption spectrum is quite complex, and resulted in classifying diamonds as type I or type II, depending on each type's absorption in the infrared, visible and ultra violet spectrum [18]. Type II diamonds transmit well in the ultra violet range down to an absorption edge at 2200 Angstroms. Type I diamond however shows absorption starting at 3300 Angstroms and increases rather steeply at shorter wavelengths [18].

Some type II diamonds are semiconductors. Therefore, type II diamonds were further classified as type IIa and type IIb, where type IIa are not semiconductors and type IIb are semiconductors. The type IIb semiconductor diamonds are usually blue p-type (boron doped) semiconductors [18]. The resistivity of type II diamonds ranges from 5 x

10^{14} Ohm cm to a low value of 100 Ohm cm for some type IIb semiconductors at room temperature [18]. Table 2 compares some optical and thermal properties of type I versus type II diamonds.

2.2 Properties of synthetic diamond

Interest in depositing thin diamond films is motivated by diamond's unique combination of properties, extreme hardness, chemical inertness, high electrical resistivity, high dielectric strength, optical transparency, and high thermal conductivity.

In the time interval following the development of techniques for depositing diamond films at reasonable rates by various subatmospheric pressure plasma techniques, diamond synthesis has become a rapidly developing area. The properties of synthetic diamond are usually different from those of natural diamond [22]. Synthetic diamond's properties vary with the deposition method and depend heavily on the deposition parameters. The variation in film properties arises from defects in the diamond lattice or from non diamond carbon phases like graphite [22]. Chemical-vapor-deposited-crystalline diamond films have high density, high abrasion, wear resistance, and corrosion resistance [23] making CVD diamonds useful for applications such as coating of twist drills and wire dies. The adhesion of diamond films to their substrates and the internal stresses arising from the deposition process are among the limiting factors for diamond's extensive use.

Table 1. Physical properties of bulk diamond

PROPERTY	VALUE / RANGE	ref
Structure	Cubic (diamond structure)	17
Stuckurberich symbol	A4	17
Space group	Fd3 m-O_h^7	24
Lattice constant (at 25°C)	3.5597 Angstroms	17
Melting point	4300°C	18
Energy gap (25°C)	5.4 eV	25
Thermal conductivity k ($W\,cm^{-1}\,K^{-1}$)	9.0-26	25
Density	3.51 gcm^{-3}	20
Refractive index		
at 656.3 µm	2.41	18
at 226.5 µm	2.72	
Transparency (See table 2)	IR, visible, UV	18
Resistivity	> 10^{16} ohm-cm	18
Dielectric constant	5.7	19
Dielectric strength	> 10^2-10^7 V/cm	
Hardness (Vickers)	70-100 GPa	19
Young's modulus (single crystal)	1150 GPa	18
Heat of formation	161 cal/mole	25

Table 2 Properties of various types of diamonds [after table 23, page 295 in [18] and [25] p. E-11].

Property	Type I	Type IIa	Type IIb
IR Absorption	absorption at 6-13μm	no absorption at 6-13 μm	
UV Absorption	strong absorption at wavelength less than 3000 Angstroms	strong absorption at wavelength less than 2250 Angstroms	
coefficient of Thermal conduc-tivity at 298 K (W /cm K)	9.90	23.2	13.6

Diamond is also becoming a popular choice for applications such as semiconductors, infrared-transmitting membranes, and X-ray transparent films for x-ray lithography [21,26].

2.3 Diamond deposition techniques

Several techniques have been developed to deposit carbon thin film. These techniques include microwave-plasma-assisted-chemica-vapor-deposition (MPCVD) [10,21,27,28], hot filament assisted CVD [22,29], ion beam sputtering [11], and low pressure CVD [16] as well as other methods. Diamond deposition methods can classified in one of three categories. The first category is ion beam deposition techniques which might use a single ion beam or dual ion beams. Ion beam techniques are used to deposit primarily diamond like carbon (DLC). The second category is the chemical vapor deposition techniques (CVD). Finally, the third group which has more use than the other two groups is the plasma assisted chemical vapor deposition (PACVD). Many deposition setups now use microwave plasma assisted chemical vapor deposition (MPCVD). The major advantage of the MPCVD is that transparent films are obtained with the appropriate deposition parameters.

Diamond must be formed under extreme conditions of pressure and temperature. Temperature and pressure spikes on the deposition surface at the moment of ion bombardment have been proposed [19]. Temperature spikes estimated to at least 3823 degree K and pressure

spikes to 1.3 x 10^{10} Pa (1.2 x 10^{5} atm) resulted from bombardment of the substrate by ions with 100 eV energy. The thermal agitation and the shock wave resulting from the impacts are enough to form a diamond nucleus 1 nm wide [19].

The proposed model [19] asserts that at room temperature, the diamond formed is thermodynamically unstable. Diamond is however, preserved at room temperature by the very high quenching rates following the collapse of the temperature spikes, thus preventing the transformation of the newly formed unstable diamond into more stable graphitic phases [19]. However atomic hydrogen or argon [19], present in the deposition atmosphere, used to bombard the substrate cause etching, which is the preferential removal of the weakly bonded sp^2 carbon atoms and other non carbon ions resulting in much purer diamonds [19]. Only diamond with strong C-C or C-H tetrahedral bonds is allowed to grow.

2.4 Mechanical properties of diamond thin films

The high abrasion, high hardness, wear resistance and corrosion resistance of polycrystalline CVD diamond justify CVD diamond's use for coatings of twist drills, machine tools, wire dies and nozzles. Several attempts have been made to deposit diamonds with hardness close to that of natural diamond (70 to 100 GPa [19]).

In a review on diamond properties, Tsai and Boggy [19] reported that

for DLC films deposited by ion beam with various carbon sources (carbon in rf plasma, carbon in arc, carbon in plasma), hardness up to 18 GPa were obtained, when the ion beam energy is in the range of 40 to 100 eV. Higher hardness up to 24 GPa were obtained with sputter orientation). A third material with <100> texture can be grown [31]. Clausing [31] has shown, through transmission electron microscopy and x-ray texture analysis, that stacking faults and twinning are necessary deposition technique by dc Magneton sputtering of a graphite target [19]. As the sputtering power density increased from 0.25 to 25 W cm^{-2}, the hardness value decreased from 24 to 7.4 GPa [19].

The hardness value was also dependent on other parameters. For instance, the hardness value of *i*-C diamond films increased with substrate potential up to 700 V [19]. Films deposited in an atmosphere containing hydrocarbons have higher hardness than films deposited in atmospheres not containing hydrogen. While diamond deposited by methods not including hydrogen had hardness values up to 24 GPa, the hardness values of diamonds deposited by the decomposition of hydrocarbons were as high as 100 GPa [19]. Diamond films deposited by electron assisted CVD with a mixture of methane and oxygen (2 percent by volume methane) with no hydrogen have hardness values approaching that of natural diamond [19].

Surface roughness of deposited diamond films vary with methane fraction in the deposition chamber. Diamond films deposited by MPCVD with methane fraction in hydrogen as 0.2 to 3.0 percent, had peak to

peak roughness of 10 to 15 nm [10]. The surface roughness was measured with a Dektak II stylus type profilometer with a submicron tip radius and by a an atomic force microscope [10]. The 10 to 15 nm roughness value seems low for polycrystalline diamond. However, Windischmann found the roughness to decrease with increasing methane fraction which was as high as 3 percent, possibly explaining the low roughness values. In films deposited by MPCVD at 0.7 percent methane in hydrogen, the surface roughness was measured as 35 nm, with a submicrometer stylus type profilometer [21]. Windischmann and Epps observed that surface roughness of deposited diamond films by MPCVD decreased with increasing methane fraction. They observed that as the methane fraction increased, the surface of the films became smoother, due to finer microstructure [21].

Windischmann and Epps Showed that the grain size in the diamond films is also a function of the methane fraction in the deposition atmosphere [10,21,31]. Figure 1 shows an obvious decrease in the grain size with methane fraction. The data in figure 1 were fitted by non linear regression analysis (Marquardt approximation) to the function $y = 112.25 \exp (1.631 x) + 14.115$, with a correlation factor $R=0.983$. Impurities can in general inhibit grain growth. The non-diamond components in the films are thought to be the grain growth inhibitors in diamond [10,21]. Raman studies of diamond films have shown that the non-diamond phase fraction increases with increasing methane concentration [10,21] (figure 2). Grain sizes were measured by

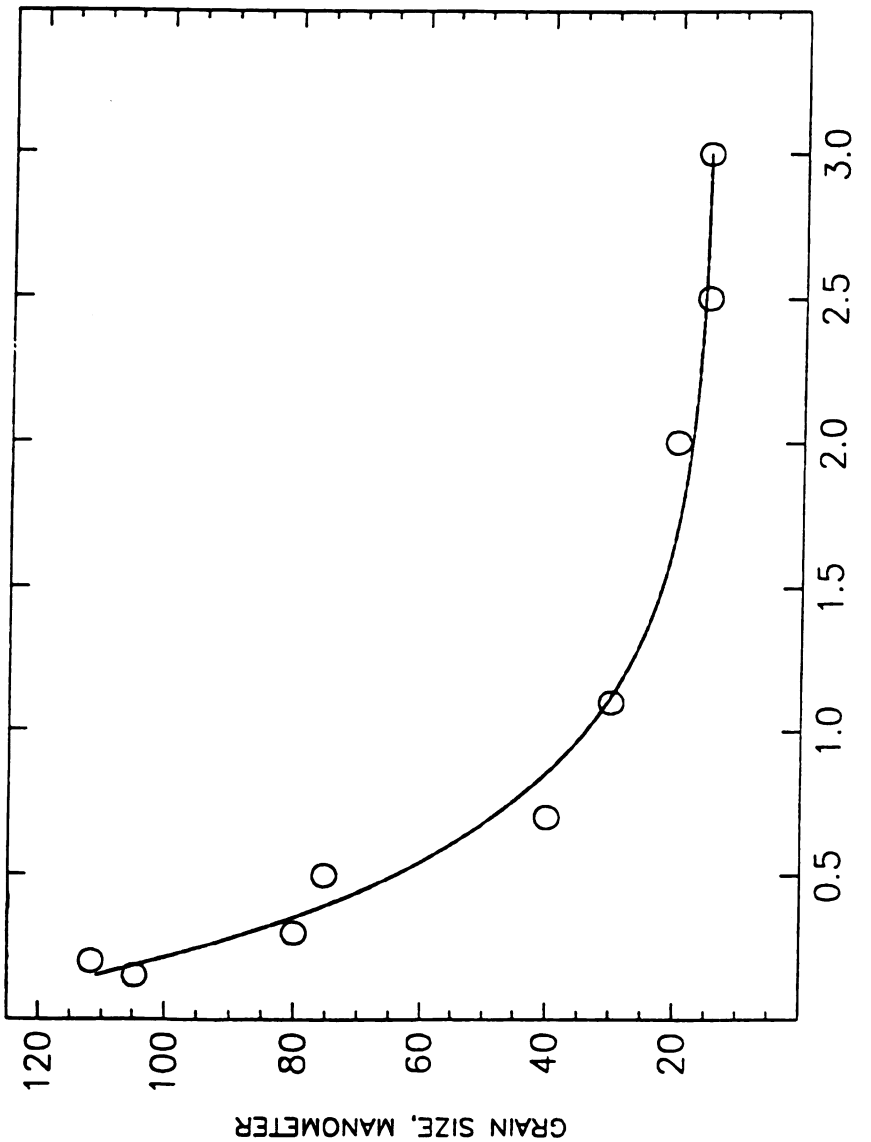

Figure 1. **Average grain size in diamond films versus methane fraction in hydrogen. After Windischmann [21].**

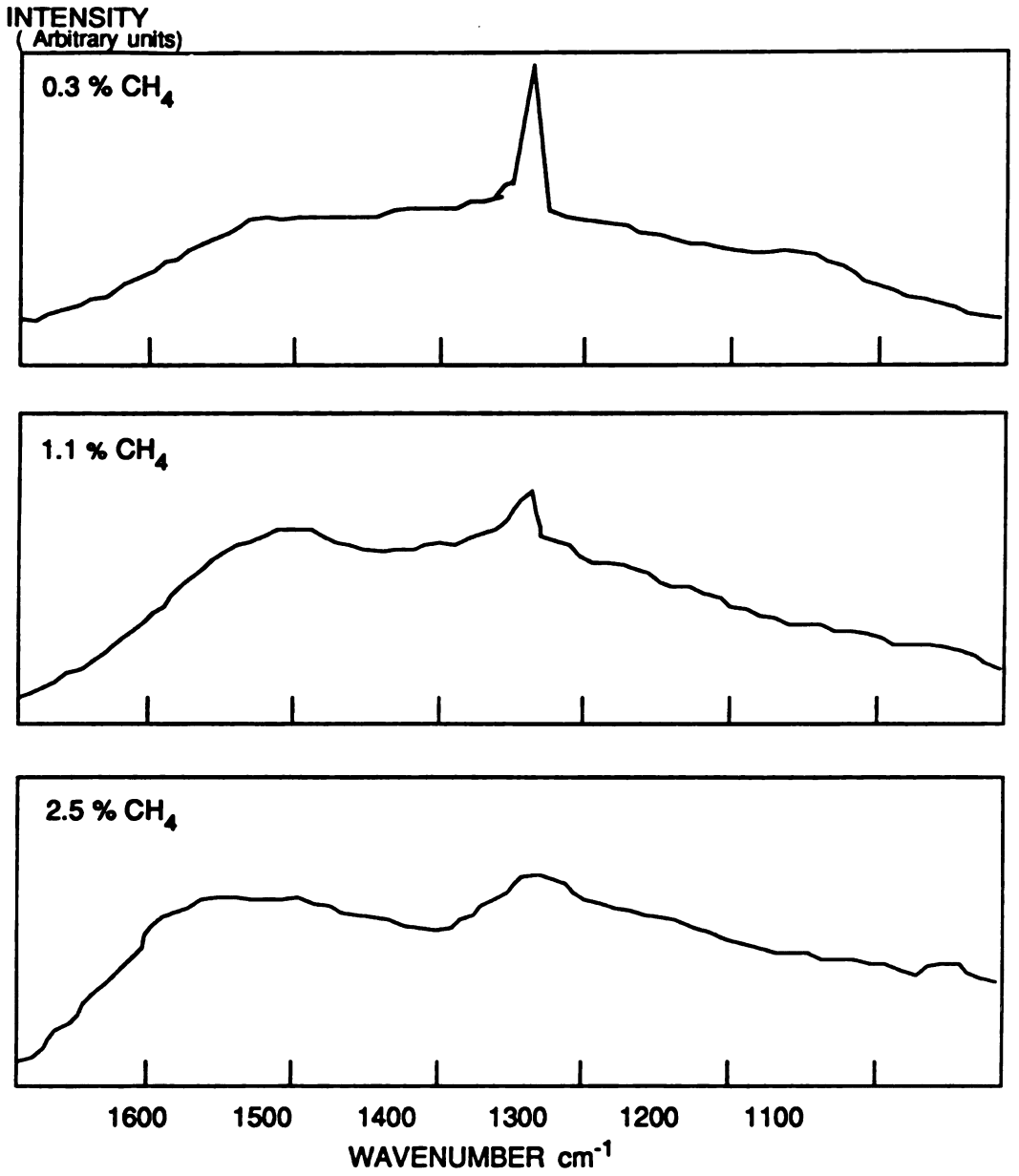

Figure 2. Raman spectra of diamond films prepared at a) 0.3 percent CH_4, b) 2.5 percent CH_4 and c) 7.5 percent CH_4. After Windischmann [10].

x-ray diffraction. The grain size was calculated from the FWHM of the reflection peak corresponding to diamond. The specimens used were deposited by MPCVD at 790°C with methane fraction ranging from 0.2 to 3.0 percent in hydrogen. The grain size decreased from 110 nm, at 0.2 percent methane to 15 nm at 3.0 percent methane [21].

The elastic properties of diamond films were not investigated as much as other properties. In most of the studies on diamonds, the value of the Young's modulus used was that of single crystal diamond, 1345 GPa [18]. The Young's modulus of diamond films was measured by Davidson et al. [16]. Davidson et al. used a cantilever beam of free standing diamond, deposited by microwave plasma assisted CVD, to measure the deflection δ of the beam, as a function of a static, manually applied load P. The deflection δ is relate to the load P by [16].

$$\delta = PL^3/3\ E_f\ I \qquad (1)$$

where L is the beam length, and I is the moment of inertia of the beam. A plot of δ versus P was made and the slope was measured. The value of the Young's modulus was determined from the slope. Several trials were carried, the value of Young's modulus was in the range of 1170 GPa to 1225 GPa, which is very close to the value of Young's modulus for single crystal of diamond, 1130 GPa [16]. A vibrating membrane method [20] was used to measure the Young's modulus of diamond

membranes. The biaxial elastic modulus was found to range from 730 to 850 GPa, which is only 0.61 to 0.71 of that of natural diamond [20].

The properties of deposited diamond films depends strongly on the deposition parameters. Deposition pressure, temperature and atmosphere affect the final properties of diamond films. While almost every deposition parameter affect some film property, the effect of deposition temperature, pressure and methane fraction in the deposition atmosphere can affect the properties more than any other. These effects will be discussed in the following sections.

2.5 Effect of deposition parameters

During deposition, carbon atoms can combine in one of many ways to form graphite plates, crystalline diamond or amorphous carbon. Hexagonal graphite is formed with planar sp^2 bonds, while tetrahedral sp^3 bonding results in cubic diamond.

Chemical vapor deposited polycrystalline diamond has two common morphologies, the {111} material and the microcrystalline material [31]. Both of these morphologies lead to <110> texture (preferred to the formation of the {111} and microcrystalline diamonds [31]. The third type exhibiting {100} facets are grown free of stacking faults and twinning if no oxygen or boron is present in the deposition atmosphere [31]. The author did not mention the minimum value of oxygen of boron's partial pressure to obtain a {111} material. Windischmann and Glen [10]

reported that the texture in MPCVD diamond deposited on (100) silicon depends on the deposition temperature and methane fraction in the deposition atmosphere [10]. At lower temperature and methane fraction, the texture was [11], however as the temperature and methane fraction increased, the texture changed quite frequently, then became predominately a <220> texture [10].

2.6 Effect of deposition pressure

At low temperature and pressure, the growth of diamond is not thermodynamically favored, a high density of defects exist in the diamond component of a CVD carbon films deposited under such conditions [22]. During film growth, there is a competition between diamond and graphite formation. Diamond growth dominates if hydrogen is used in the deposition atmosphere. The etching rate of graphite by atomic hydrogen is much higher than the rate for diamond since the sp^3 bond in diamond are stronger than the sp^2 bonds in graphite and amorphous carbon. Buckley et al. used Raman spectroscopy to investigate the characteristics of filament assisted CVD (FACVD) diamond [22]. The principal conclusion of Buckley's investigation was that in FACVD carbon films, the carbon type in the film (diamond, graphite or amorphous carbon) strongly depends on the total gas pressure in the deposition chamber. As the total gas pressure is lowered, more disordered carbon type is formed [22]. Buckley et al.

used constant methane concentration at 0.2 percent and deposition temperature of 950°C. Diamond films were deposited by FACVD on molybdenum substrates. The only parameter that was varied was the total gas pressure which ranged from 5 to 100 torr. Raman spectra were taken of all specimens. The results obtained are listed as follows:

1) at low total gas pressure, (about 5 torr), the diamond peak at 1330 cm^{-1} was obscure, indicating a very small fraction of diamond in the film. The film deposited at 5 torr was found to be predominately amorphous carbon, and displays a ball-like morphology which is not typical of diamond.

2) at total gas pressures between 5 and 30 torr, Raman spectra displayed two broad peaks centered around 1550 cm^{-1} and 1360 cm^{-1} indicating the presence on both graphite and amorphous carbon component in the film.

3) at total gas pressures higher than 30 torr, the broad peak around 1550 cm^{-1} sharpened and shifted to 1578 cm^{-1}, corresponding to crystalline graphite.

In all specimens, except for the specimen deposited at 5 torr, the position of the diamond peak at 1332 cm^{-1} was independent of the applied total gas pressure [22]. There is evidence that the diamond line does shift with externally applied pressure [32] (section 4.4). The spectroscopic resolution for the infrared devices used in this study possibly may not allow detection of the usually small shift in the diamond line with pressure. The line width, however, for both diamond

and graphite components vary with deposition pressure. The diamond line broadening with decreasing total gas pressure indicates an increasing defect density in the diamond component. The broadening in the graphite line with decreasing total gas pressure indicates that the amount of crystalline graphite is reduced, and eventually becomes amorphous carbon at low pressures [22]. Decreasing total gas pressure increases the disorder in both the diamond and graphite components. Increasing the total gas pressure tends to favor the formation of more defect free diamond component. Liou et al. found no significant changes in the growth rate of MPCVD diamond films with increasing total gas pressure from 6 to 50 torr [33].

2.7 Effect of deposition temperature & substrate temperature

Film growth rate depends on the deposition temperature. Grill et al. [34] found that in presence of a substrate voltage bias of 80 volts, the growth rate decreased with substrate temperature. The growth rate was 105 Å/min at 100°C and 65 Å/min at 250°C [34]. The films studied by Grill et al. [34] were diamond like carbon films deposited on silicon substrates by rf plasma decomposition of acetylene. The range of substrate temperature studied was 100 to 250°C. In agreement with Grill et al. [34], Liou et al. found that the deposition rate of diamond, at constant methane and total gas pressure, decreased rapidly as the substrate temperature increased (figure 3).

The

func

R=C

ther

are

tem

thre

tem

Wir

the

the

in t

and

with

Har

dia

MP

dep

at t

dis

of r

gra

The data in figure 3 were fitted (this thesis) by linear regression to the function $y = 1.212 - 74710^{-4} x + 0.15\ 10^{-5}\ x^2$, with a correlation factor R=0.995.

Liou [33], Windischmann [21] and Harshavarhan [35] all agreed that there is a temperature interval in which optimum deposition conditions are obtained and crystalline diamond is formed. The limits of the temperature interval, where conditions are optimum, varied between the three authors mentioned above [21,33,35]. In Harshavarhan's study, the temperature interval for optimum deposition was 900 to 950°C. In Windischmann's study, this interval reported was not clearly stated, but the study implies that this interval is roughly 500 to 850°C. Liou found the interval of optimum conditions to be 500 to 1000°C. The differences in the intervals might arise from the difference in deposition methods and parameters. The deposition method used by Liou [33] is MPCVD with a methane fractions ranging from 0.5 to 5 percent in hydrogen gas. Harshavarhan [35] used an oxyacetylene welding torch to deposit diamond on silicon. Finally, Windischmann deposited diamond films by MPCVD also with varying methane concentrations. For instance, films deposited at 550°C had three times as much methane as films deposited at 825°C [21]. The role of methane in the deposition process will be discussed in section 2.8. One should note at this stage that the amount of methane significantly affects the amount and crystallinity of diamond, graphite and amorphous carbon.

In spite of the slight differences among the reported temperature

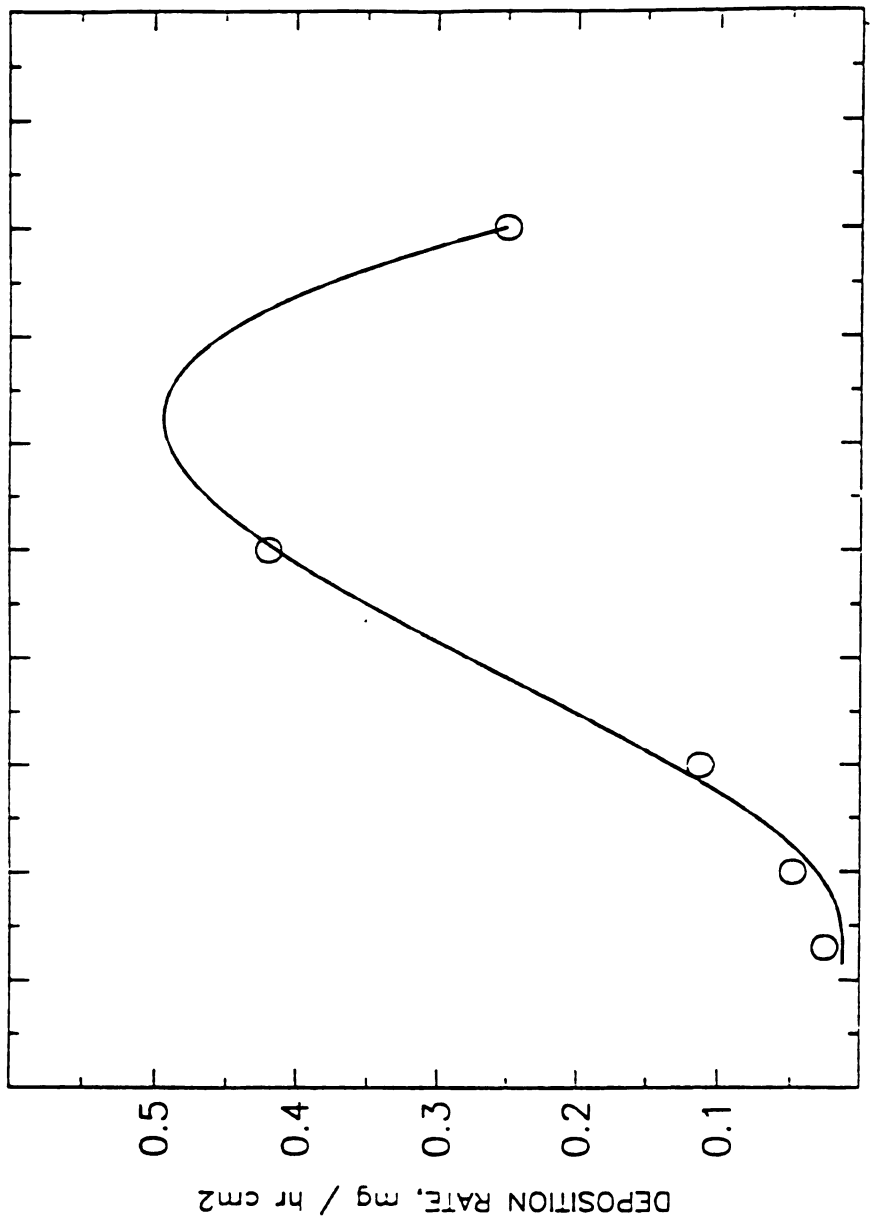

Figure 3. Deposition rate of diamond films versus substrate temperature. After Liou [33].

intervals

observa

authors

an inves

quality.

tempera

were co

1) At

describe

around

(figure

arise fro

disorder

centered

line widt

example

Raman s

centered

cm^{-1} [35

950°C),

practical

and grap

range, th

intervals at which optimum diamond deposition occurs, the general observations in the three studies [21,33,35] are similar. All three authors [21,33,35] used Raman spectroscopy of the deposited films as an investigative tool of the carbon components and their crystalline quality. All Raman spectra of diamond films were taken at room temperature in the three studies [21,33,35]. The following observations were common to the three studies:

1) At temperatures outside the interval of optimum conditions described earlier, Raman spectra show two broad peaks centered around 1560 to 1580 cm^{-1} and 1350 to 1355 cm^{-1}, respectively (figure 4). The broad peak around 1350 to 1355 cm^{-1} is believed to arise from small graphitic crystallites less than 20 nm in size, and / or disorder in tetrahedrally coordinated carbon network [21]. The peak centered around 1350 to 1380 cm^{-1} arises from crystalline graphite, the line width is proportional to the crystallinity of the graphite. For example, at temperatures less than 900°C or above 950°C [35], the Raman spectra shows two broad peaks; the amorphous carbon peak centered about 1350 cm^{-1} and the graphite peak centered around 1580 cm^{-1} [35]. In the same temperature range (below 900°C or above 950°C), the crystalline diamond peak centered around 1332 cm^{-1} is practically absent, indicating a dominance of the amorphous carbon and graphite to a lesser extent [35]. At temperatures in the 300 to 400°C range, the deposited films are mostly amorphous carbon.

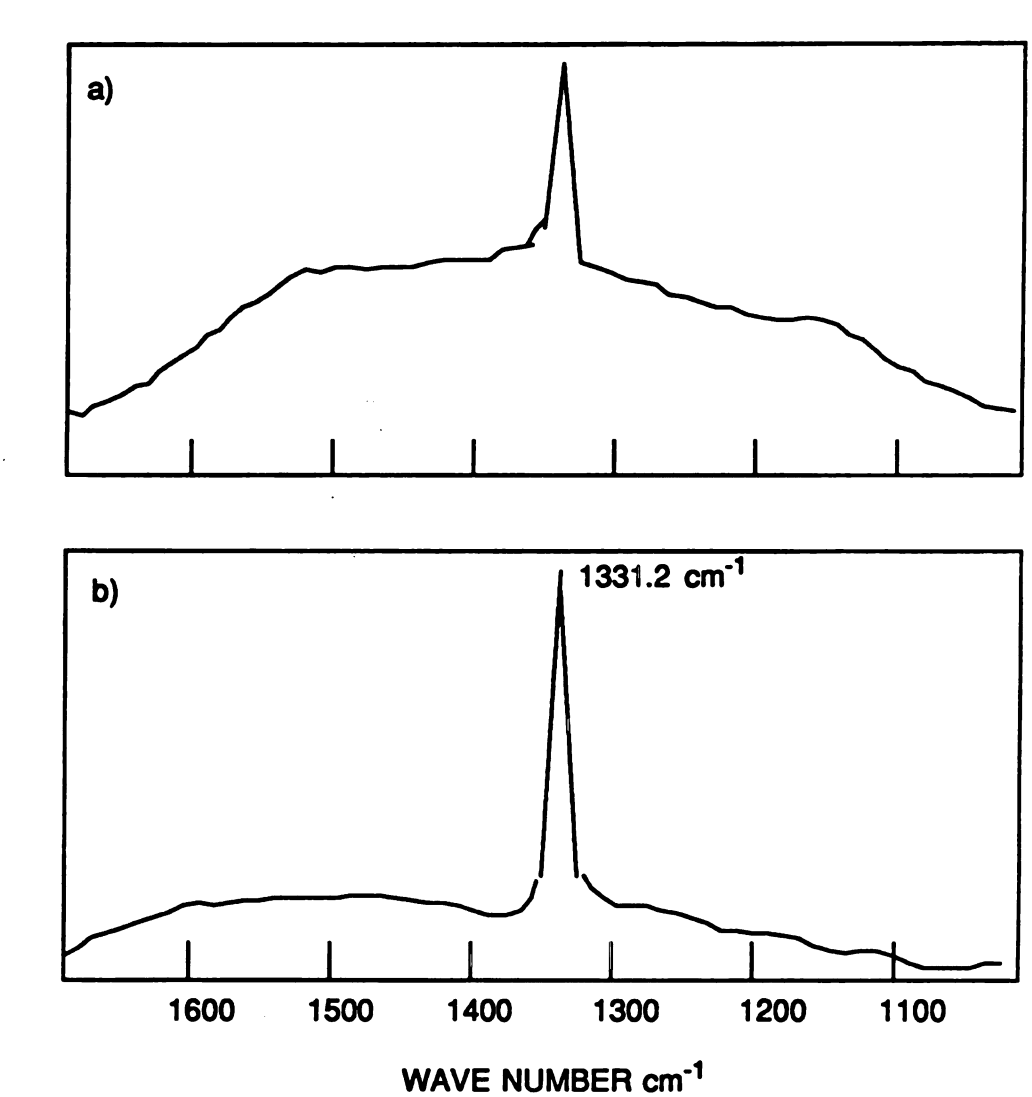

Figure 4. Raman spectra of deposited diamond films at a) 825°C and b) 550°C. After Windischmann [21].

On the other side of the temperature interval, at 980°C, the deposited films are mainly graphitic [35].

2) At temperatures within the interval of optimum conditions, there is a sharp peak around 1330 to 1332 cm^{-1} in the Raman spectra of the films. The peak centered about 1332 cm^{-1} is due to crystalline diamond [10,21]. In the same temperature range, the peaks centered around 1355 and 1550 cm^{-1} almost disappeared indicating a much smaller presence of non diamond carbon. For example, at 550°C, the non diamond components are virtually non existent as can be deduced from the lone and sharp peak around 1332 cm^{-1} in figue 4 [21]. Figures 2 and 4 are manually reproduced in this thesis from original curves; the precision of the data is therefore lost.

At temperatures in the range of 800 to 1000°C, diamond grains are several micrometers wide and well faceted [21]. Outside the temperature range of 800 to 1000°C, the grains are finer and unfaceted [36]. At lower temperatures, films have coarser microstructures in the range of 2 to 5 microns. Larger grains have lower grain boundary area. And since non diamond carbon and graphite tend to precipitate at the grain boundaries, they inhibit grain growth. Finer grains contain larger non diamond component at 825°C than grains deposited at 550°C [21]. One should note that the grain size is also a function of the nucleation condition through abration and seeding of the substrate surface.

2.8 Effect of methane and hydrogen gas on film properties

When methane is used in the gas mixture in the deposition chamber, the deposited diamond film properties depend on the fraction of methane in the deposition gas. Mechanical properties[27], optical properties [10,21,27,37] and the morphology [9,10,26,29,31] of the film vary with methane fraction.

The most important effect of methane fraction on diamond films is on the type and amount of the carbon component in the film that forms during deposition. Many researchers using various deposition method have concluded that the amount of non diamond phases in deposited diamond film is a function of the methane fraction in the deposition atmosphere [9,10,21,29,31]. Raman spectroscopy and x-ray diffraction are commonly used tools for investigating the carbon type (amorphous carbon, graphite or crystalline diamond) in carbon films. Raman spectroscopy is especially powerful in detecting the non diamond content in the films. The sensitivity of Raman signal from the sp^2 bond (unsaturated C=C) in graphite is about two orders of magnitude higher than the Raman signal from the sp^3 bond (saturated C-C) in the tetrahedrally coordinated diamond [29].

Raman spectra of diamonds from various studies have some common features. At low methane concentrations, there is a sharp narrow peak around 1332 cm^{-1}, indicating the presence of a large fraction of crystalline diamond [10,21,26,38]. At low methane fractions, the

relative

(relativ

1332 cr

demons

crystall

temper

diamon

in the f

fraction

carbon

relative

[10,21]

Spe

bonds

numbe

fractio

linear

factor

which

various

graphi

deposi

mixture

relative peak intensity at 1560 cm^{-1} due to absorption from graphite (relative to the diamond peak at 1332 cm^{-1}) is weak. The sharp peak at 1332 cm^{-1} combined with the relatively low peak at 1560 cm^{-1} demonstrate that at low methane fractions, the films obtained are mostly crystalline diamond, provided that other parameters such as optimum temperature and pressure are chosen. A small fraction of small non diamond carbon (graphite and/or amorphous carbon) inevitably exists in the film, even at low methane fractions [10,38]. As the methane fraction in the deposition atmosphere is increased, the non diamond carbon content increases as can be deduced from the increase in the relative intensity of the 1560 cm^{-1} peak at higher methane fractions [10,21].

Spectroscopic ellipsometry was used to measure the number of sp^2 bonds (proportional to the non diamond fraction in the film). The number of unsaturated sp^2 bond in the film increased with methane fraction (figure 5). The data in figure 5 were fitted (this thesis) by linear regression to the function $y = 1.76 + 2.53\ x$, with a correlation factor R=0.95. The same conclusion could be drawn from figure 2 which represents the change in Raman spectra of diamond films at various methane fractions; the relative intensity of the 1560 cm^{-1} graphite line increases with increasing methane fraction [10]. Films deposited by hot filament CVD [38], using hydrogen and methane gas mixture, showed differences based on the methane fraction used.

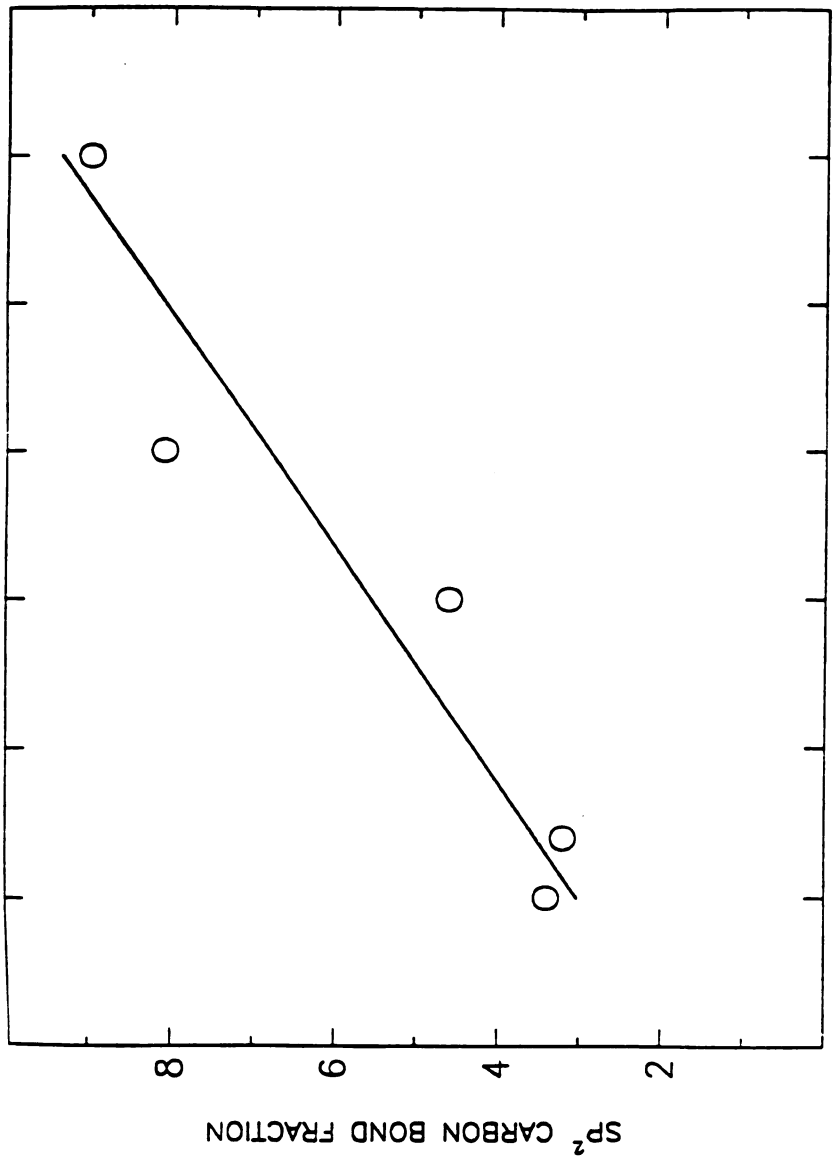

Figure 5. sp^2 carbon fraction in diamond versus methane fraction in hydrogen.
After Windischmann [10].

With all other conditions kept constant, two methane fractions were used in deposition; 0.5 percent and 1.0 percent methane fraction [38]. Under both conditions (0.5 and 1.0 percent methane), Raman spectra had a sharp peak around 1332 cm^{-1}, indicating the presence of crystalline diamond. However, in the Raman spectrum of the specimen deposited with the lower methane fraction (0.5 percent), a relative increase occurred in the peak around 1500 cm^{-1} representing absorption from amorphous carbon [38]. Consequently, just like graphite, amorphous carbon production is favored in films deposited at higher fraction of methane.

Films deposited by MPECVD (microwave plasma enhanced CVD) [c2], with methane fractions at 0.5 percent and at 4.0 percent, showed similar results to those in reference [38]. Indeed, specimens prepared at 0.5 percent methane fraction contained less non diamond carbon than specimen prepared at 4.0 percent methane. The Raman intensity of the 1550 cm^{-1} line was lower in the film deposited at the lower methane fraction. In another study, the Raman spectrum of a film deposited at 2 percent methane fraction was dominated by the graphite peak [26]. As the methane fraction was reduced, the diamond line gradually come to dominate the Raman spectrum [26].

When ethanol was used in the gas mixture along with hydrogen, the Raman intensity of the broad peak assigned to graphite increased with ethanol fraction. The specimens were deposited by HFCVD at two different ethanol fractions [9]. Both films contained line defects

consisting of twins, stacking fault, and dislocations, as well as highly disordered regions at the crossing points of twin boundaries [38]. The specimen deposited at the higher methane fraction contained more of these defects [38]. The above observations may indicate that stresses formed during film growth are partially relaxed by the formations of these defects. The defect density increased with methane fraction [38], thus increasing the methane fraction may allow stresses in the film to relax by the formation of defects. However, the trade off to stress relaxation is the loss in diamond purity, since non diamond content increases with increasing methane fraction.

In another study, three samples were deposited by HFCVD in a hydrogen and methane mixture, with three different methane fractions [29]. Films labeled A, B and C were respectively deposited at 1.0, 4.0 and 7.0 percent methane. Films A and B were identified as diamond by X-ray diffraction. The x-ray diffraction of sample C showed a sharp line only for the silicon substrate. Raman spectra of specimens A and B revealed sharp lines at 1333 cm^{-1} attributed to sp^3 bonds, thus supporting finding x-ray diffraction findings. The Raman spectra of films C however showed a broad peak around 1330 cm^{-1}. All three samples showed a peak around 1550 cm^{-1} that increased with methane fraction [29].

The growth rate of diamond films grown in an atmosphere containing methane increases with methane fraction [21,29]. As the methane fraction increases, the diamond film growth rate increases, then

decreases [29]. The diamond cluster size simultaneously becomes smaller with methane fraction [29]. TEM observations showed that at a 1.0 percent methane fraction, the diamond crystals are clearly defined and triangular [29]. At 4.0 percent methane, diamond grains are smaller. At 7.0 percent methane, the particles' morphology is ball-like without habit planes [29]. A different study [38] revealed that diamond films deposited at 0.5% methane were crystalline consisting of (111) planes forming triangle shapes. At 1.0 percent methane, the diamond consists of particles with a mixture of (111) and (110) planes [38].

To explain the decrease in grain size with simultaneous increase in the growth rate, a model was proposed [29] in which hydrogen is the determining factor. The model assumes that the diamond cluster size depends on the hydrogen to methane fraction (or on the number of available atomic hydrogen per carbon atom) [29]. At a low methane fraction, all the carbon atoms supplied by the decomposition of methane builds up on the rapidly growing film. There is enough atomic hydrogen around the substrate to ensure high etching rates of the non diamond phases. At this stage, the growth rate increases with increasing methane fraction. At higher methane fraction, too many carbon atoms are supplied. Only small clusters of low molecular weight are formed, most of which cannot survive at the high substrate temperature. The decomposition of the low molecular weight clusters may be one reason behind the slowing down of the growth rate [29]. Atomic hydrogen also brakes up the network of weakly bonded amorphous carbon between

diamond clusters, allowing diamond clusters to grow. At high methane fraction (assuming the gas is a mixture of hydrogen and methane), less atomic hydrogen is available to etch away the amorphous carbon network that forms between diamond clusters. The reduced etching power of atomic hydrogen at higher methane fractions might be a second reason why the growth rate of diamond slows down. The reduced etching power of hydrogen could also explain the increase in the non diamond content of films deposited at higher methane fractions.

The hydrogen content in diamond films increases linearly with methane fraction (figure 6). The data in figure 6 were fitted (this thesis) by linear regression to the function $y = -0.623 + 2.66\ x$ with a correlation factor $R=0.975$. The amount of hydrogen in the films is to be differentiated from the hydrogen fraction in the deposition atmosphere. The hydrogen concentration was measured by ^{15}N nuclear reaction (NR) analysis and by elastic recoil detection (ERD) spectroscopy. A hydrogen content of 7 to 8 percent [21] and up to 50 percent [39] was found in many films. The presence of hydrogen in the film is necessary to obtain good mechanical properties and infrared transparency [39]. Hydrogen stabilizes the diamond phase, films produced by decomposition of hydrocarbons are more stable and have better mechanical properties [22,39]. X-ray absorption fine structure (EXAFS) measurement showed that two thirds of the carbon in diamond films have sp^3 coordination. Most carbons attached to hydrogen atoms also have tetrahedral diamond like bonding [39].

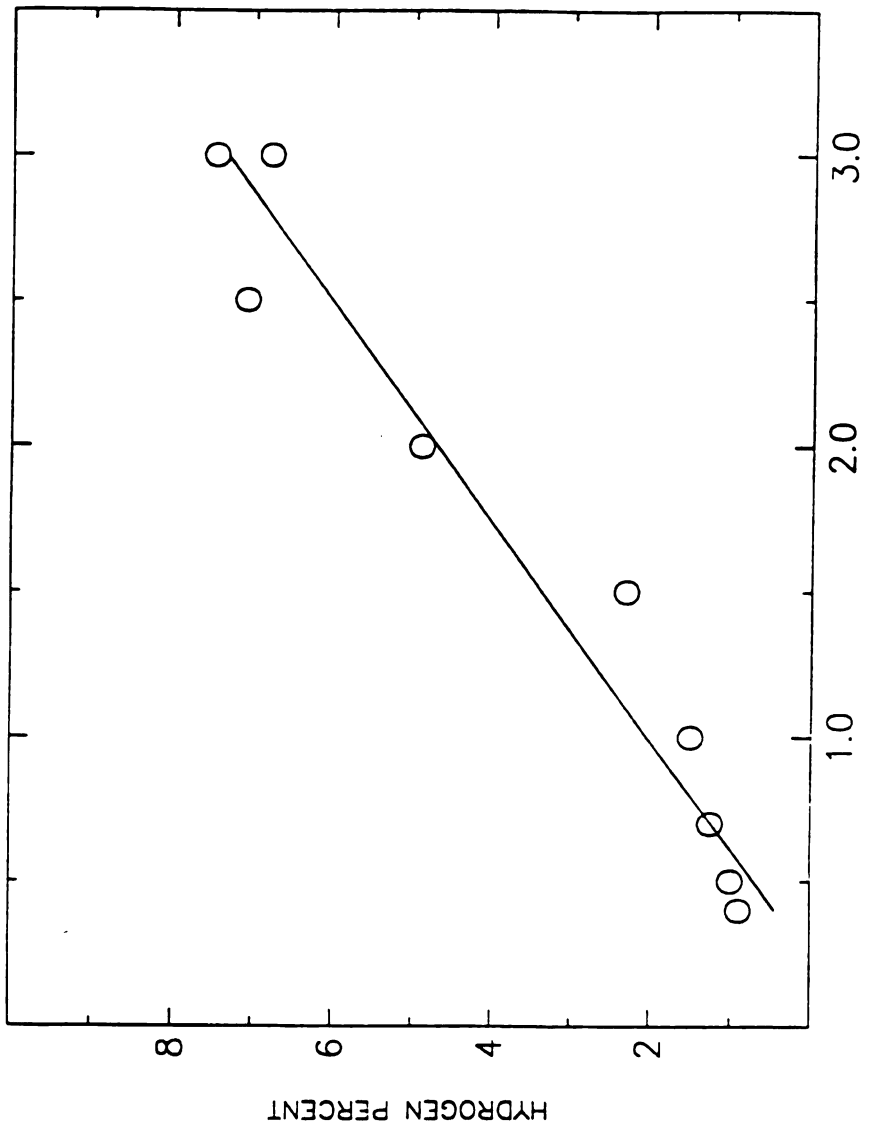

Figure 6. Hydrogen content in daimond films versus methane fraction. After Windischmann [10].

One third of the carbon atoms in the studied specimens have sp^2 trigonal bonds [39]. Hydrogen initially attached to carbon in sp^3 bonds may later detach at high temperature thus altering both mechanical and optical properties of diamond films. If hydrogen is lost upon annealing, film decomposition could result [39]. Loss of hydrogen and eventual decomposition or transformation to graphite occurred upon annealing at temperatures greater that 400°C [39]. A 100 percent transformation to graphite resulted from a 1000°C anneal [39]. While increasing the methane fraction in the deposition gas results in film defects which relax the stress, the hydrogen content also rises with the methane fraction[10]. An increase in hydrogen concentration in turn causes a greater degree of atomic misfit in the lattice. The misfit strain induces higher residual stress, giving rise even to spontaneous delamination [27]. Films deposited with a methane fraction greater that 15 percent delaminated spontaneously from silicon substrates, when film thickness was greater than 3000 Å [27].

3- PARAMETERS AFFECTING RESIDUAL STRESS

Several parameters affect the sign and magnitude of residual stress. Some of these parameters are discussed next.

3.1 Effect of film thickness on residual stress

Hoffman [8] reported that in metallic thin films the average intrinsic stress decreased with increasing film thickness. However, the average intrinsic stress is independent of thickness for thick films. For example, at film thicknesses greater than 2000 Å, silver [40] and gold [41] films showed practically no increase in stress, while no stress existed in copper and silver films until a threshold thickness of 200 to 300 Angstroms is reached [40,42]. Similar results were obtained for antimony [43] and gold film grown on quartz substrate [44] where the stress was zero until a threshold film thickness of few hundred angstroms, followed by a rapid rise in stress in a narrow thickness region of about 1000 Angstroms. A constant stress value is then reached for thicknesses greater than 1000 angstroms [44].

The trends for residual stress as a function of film thickness in dielectric films are not as clear as those for metal films [8]. ZnS films evaporated at the rate of 20 Å/sec have compressive residual stresses that decrease with increasing film thickness, up to about 2 μm [45] (figure 7).

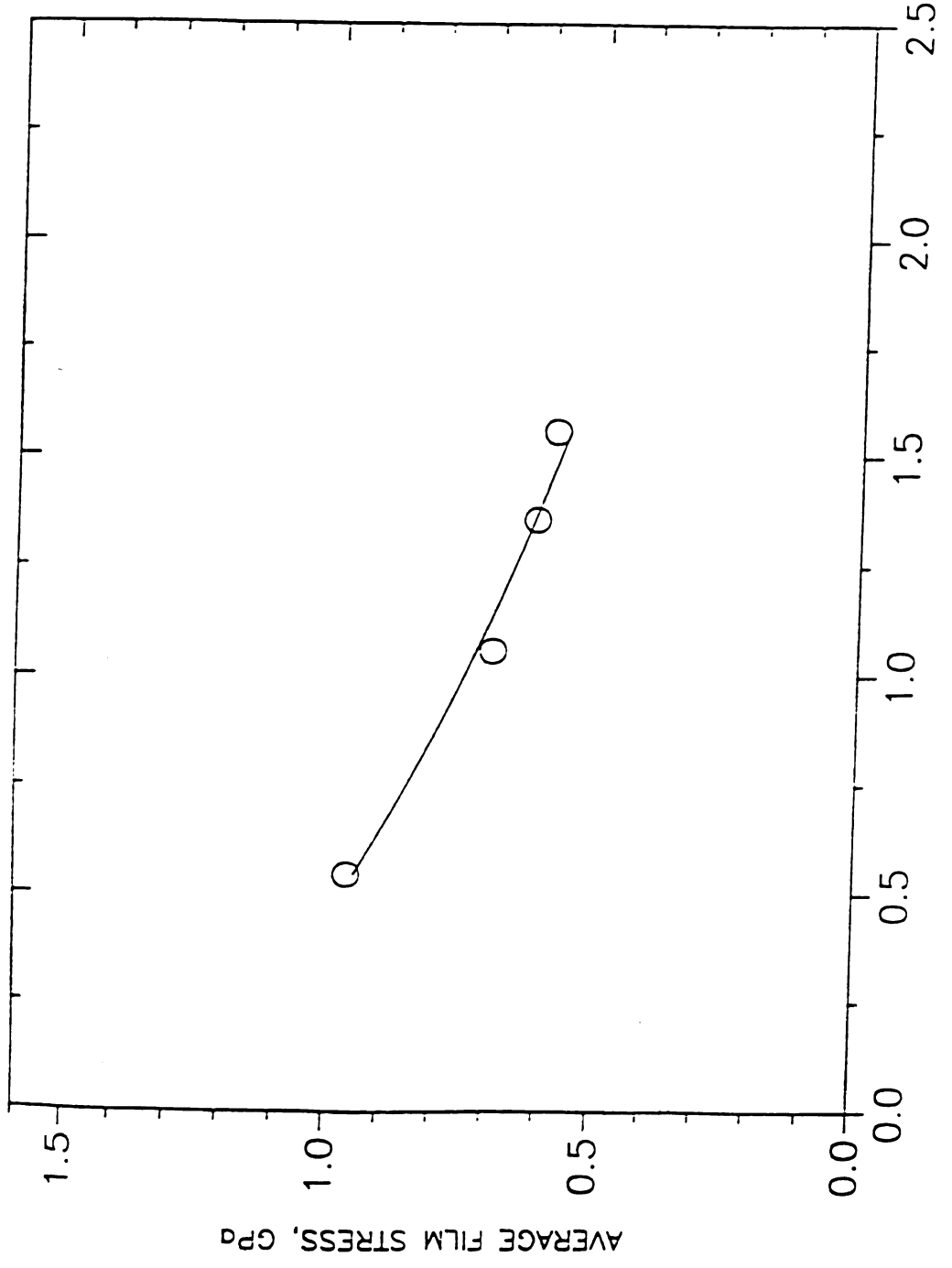

Figure 7. Average stress versus film thickness. After Blackburn [45].

Howe

to a c

tricky

this

the fu

Th

paral

silico

great

chang

in the

syste

was f

indep

an an

the ch

equa

Jus

films

create

depos

Tagni

the be

at 500

However, film stresses in carbon films on glass substrates increased up to a carbon film thickness of 1000 Å, then become independent of film thickness at higher thicknesses [46]. The data in figure 7 were fitted (this thesis) by non linear regression (Marquardt approximation) to the function $y = 1.237 \exp(-0.506 x)$ with a correlation factor R=0.99.

The sign of residual stress can also be thickness dependent. Strains parallel to the interface in GaP, GaAs and InP semiconductors grown on silicon substrates changed from compressive to tensile at film thickness greater than about 1.5 μm [4]. The tensile strains measured from the change in the radius of curvature were however thickness independent in the range of 1.5 to 5 μm film thickness in the semiconductor-silicon systems mentioned [4]. Stress in SiC films grown on silicon substrates was found to be large (2 GPa), compressive and thickness independent [3]. However, stresses in the SiC film became tensile after an anneal at 600°C, for 30 minutes [3]. Stresses were measured from the change in radius of curvature due to stress induced bending (equation 25) [3].

Just like in other dielectric films, internal stresses in thin diamond films quickly rises with film thickness, then decreases and reaches a plateau at higher film thicknesses [46,47]. For instance, in DLC films deposited at 300°C by electron bombardment of a carbon rod, the magnitude of the compressive stress measured during deposition from the beam deflection increased from 0 to -2.5 GPa when a film thickness of 500 Å was reached, then the stress deceased and remained constant

at film thicknesses up to 2000 Å [46] (figure 8).

Stress contributions in diamond films on silicon substrates include lattice mismatch stress and thermal expansion difference stress. At very low film thickness of few angstroms, the tensile lattice mismatch stress in the film balanced by the compressive thermal expansion stress such that the over all stress in the film is low and compressive. As the diamond film thickness increases up to about 1000 A, the magnitude of the tensile lattice mismatch stress decreases away from the interface. Consequently, the compressive thermal expansion stress becomes more dominant and the stress in the film becomes increasingly compressive up to about 1000 Å. The grains of diamonds start touching at about 1000 Å causing a tensile stresses to increase again (see discussion on grain boundary relaxation model section 8.2). As the tensile stress increases opposite to the compressive thermal expansion stress, the magnitude of the total compressive stress decreases and reaches a plateau when diamond grain growth in stopped.

3.2 Effect of ion beam energy on stress

Plasma-assisted-chemical-vapor-deposited silicon carbide films on silicon substrates have biaxial compressive stresses that increase with increasing ion beam energy; stress in the silicon carbide film increased from -0.5 to -2.0 GPa as the ion beam energy increased from 100 to 140 eV [3].

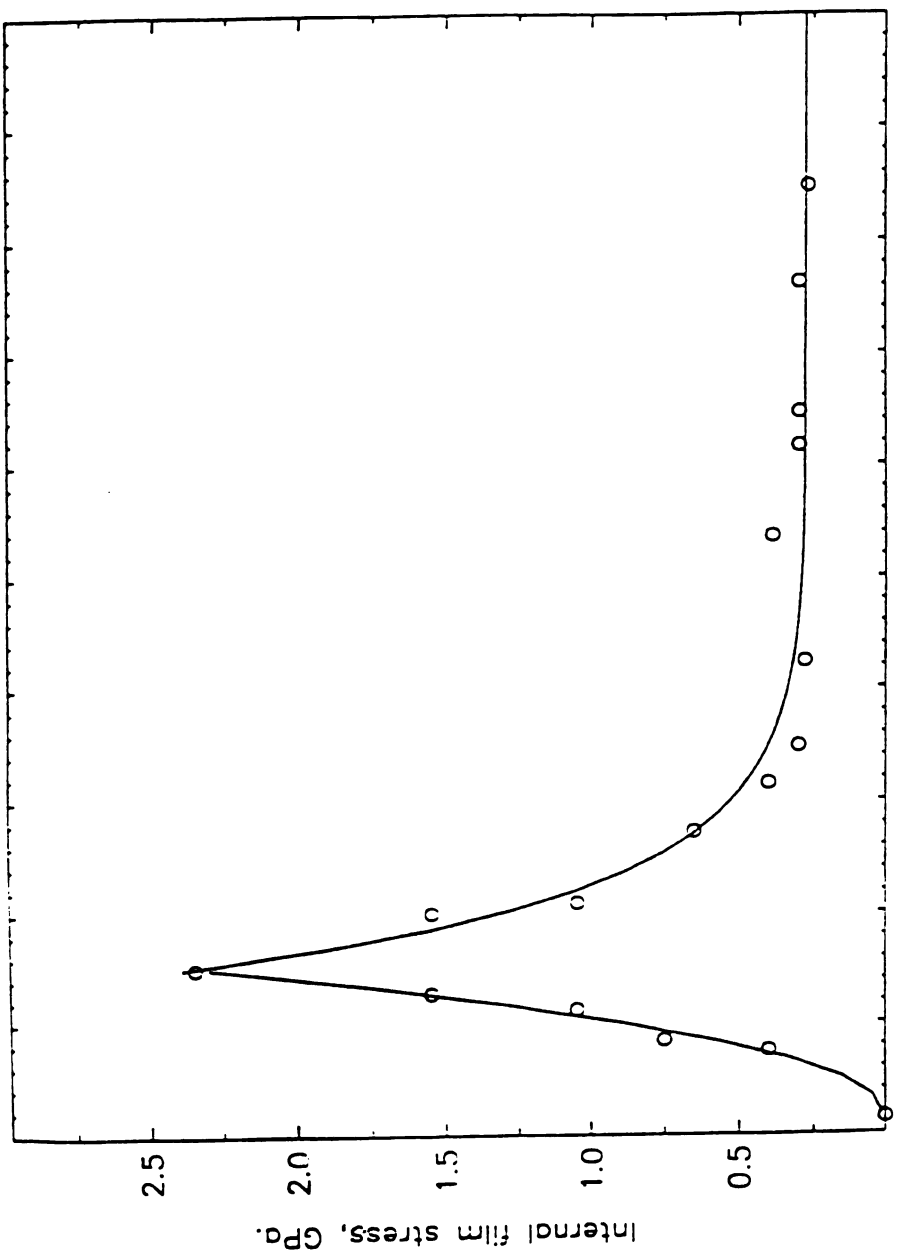

Figure 8. Dependence of growth stress on diamond film thickness. After [46].

Compressive stress is partially due to the presence of hydrogen in the film [3]. Removal of the hydrogen by a degassing treatment which consisted of an anneal at 600°C for 30 minutes, resulted in transition of stress from compressive to tensile (figure 9). The magnitude of the tensile stress in the film was as high as 2 GPa at an ion beam energy of 140 eV [3].

3.3 Effect of deposition rate on residual stress

Intrinsic stresses depend on deposition rate. Hoffman [8] reported that for the dielectric films he surveyed, internal stresses could either increase or decrease with increasing deposition rate. Compressive stresses in ZnS films increased linearly from -0.04 GPa at a deposition rate of 9 Å/sec, to a value of -0.06 GPa at a deposition rate of 22 Å/sec [45]. Compressive stresses in SiO decreased non linearly with deposition rate from -0.15 GPa at a deposition rate of 9 Å/sec, to a value of -0.06 GPa at a deposition rate of 40 Å/sec [45] (figure 10). The data for ZnS in figure10 were fitted (this thesis) by linear regression to the function $y = 0.231 + 0.174\ x$ with a correlation factor R=0.995, while the data for SiO were fitted by non linear regression analysis (Marquardt approximation) to the function $y = 0.056 + x^{4.33} + 0.0456$, with a correlation factor R=0.951. Magneton ion beam sputtered chromium films on Corning cover-glass substrates had high compressive stresses that decreased linearly with deposition rate [48].

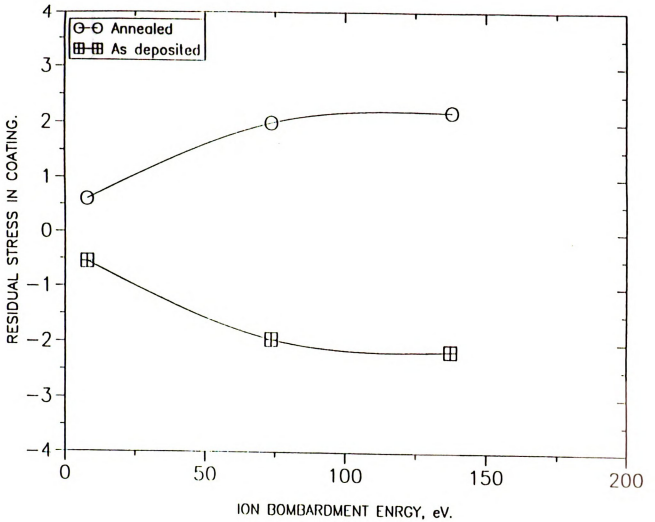

Figure 9. Residual stress versus ion bombardment energy. After Argon [3].

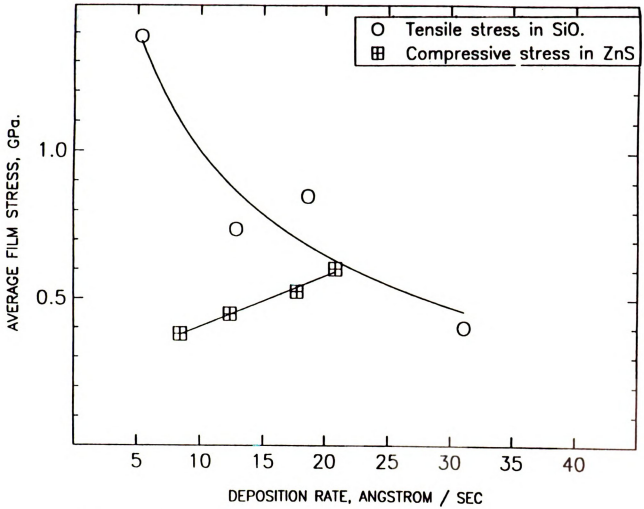

Figure 10. Average film stress versus deposition rate. After Blackburn [45].

Indeed, the integrated stresses (integrated over the thickness) in the chromium films decreased linearly from -350 N/m at a deposition rate of 0.13 nm/sec, to a value of -200 N/m at a deposition rate of 1 nm/sec [48].

3.4 Effects of deposition pressure on residual stress

Magneton ion beam sputtered chromium films deposited at the rate of 1.0 nm/sec, in an argon gas atmosphere, had stresses that varied dramatically with deposition pressure [48]. Indeed, for a film thickness of 0.25 microns, a compressive stress measuring -1.5 GPa, at 0.05 Pa argon pressure, decreased to -1.0 GPa at 0.1 Pa, then increased and switched to a tensile stress 0.8 GPa at 1.5 Pa then again decreased to zero at 7 Pa. Stresses were measured from the observed center deflection of the substrate bowing under stress. (Equation 25). No considerable change in the magnitude or sign of the stresses, as a function of the deposition pressure was realized when argon was replaced with krypton [48]. Blachman [49] argued that compressive stress in copper films on molybdenum substrates are due to atomic argon entrapped in the film. Hoffman however argued that the change in stress from tension to compression with increasing deposition pressure cannot be correlated to entrapped argon, since no appreciable quantities of argon was found in the copper films.

3.5 Effects of deposition incidence angle on residual stress

When dielectric films are evaporated at an incidence angle other than normal incidence, the films mechanical properties may become unstable when exposed to air after deposition [8]. Priest et al. [50] found that the stress in SiO films changed from 0.1 GPa tension to -0.1 GPa compression, and the films partially delaminated from the substrate after only three minutes exposure to air. The author attributed the change in the stress sign and the delamination of the film with exposure time to the partial pressure of water vapor, since no stress sign change or delamination were observed when samples were exposed to dry nitrogen at atmospheric pressure [50].

Evaporation at higher angles can also result in anisotopic stresses [8]. For iron films deposited at 36.5 degree incidence, the difference in the magnitude of the stresses in the X and Y directions (figure 11), increased with increasing film thickness. At a 0.1 microns thickness, the ratio of the stresses in the X and Y directions σ_X/σ_Y was approximately 4/3 indicating a larger stress in the X direction [50]. However, while for iron [50], σ_X/σ_Y increased from 1 to 1.2 as the incidence angle increased from 0 to 40 degrees, σ_X/σ_Y for SiO [51] deceased to 0.7 at 20 degrees then rapidly increased to 5.5 at 60 degrees. Stress anisotropy can be estimated by the interference fringes method (section 4.3). Interference fringes are formed when the film is

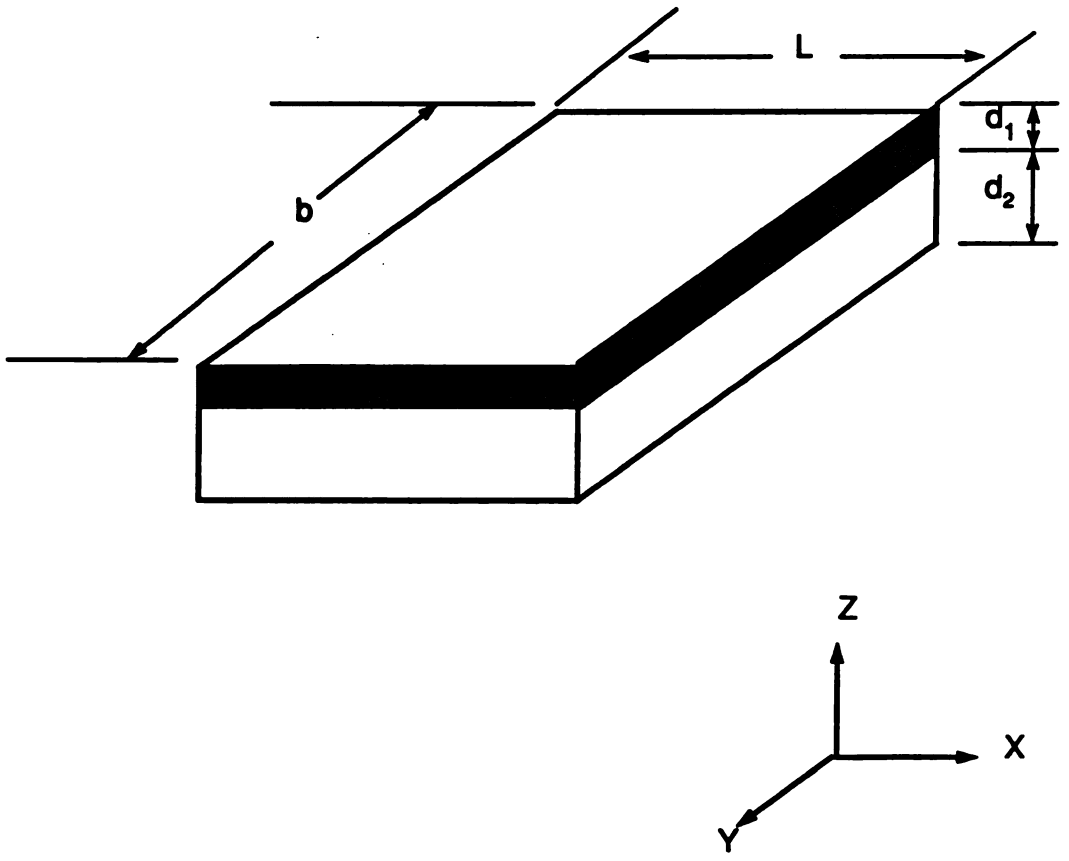

Figure 11. Three dimensional two layer system

illuminated with a monochromatic light. The Fringes are circular if the stresses in the X and Y directions (figure 11) are equal. Otherwise, the stress anisotropy causes the fringes to become elliptical. The ratio of the two ellipse radii is proportional to σ_X / σ_Y [8].

3.6 Effect of crystallite size on stress

Blackburn [52] has shown that in very thin LiF films (less than 100 Å), deposited at 12 Å/sec on carbon coated glass substrates, stress is dependent on the crystallite size. Measured stress on the LiF films were tensile and increased in a parabolic way from 0 to 0.9 GPa as the crystallite size (average cross sectional area) increased from 0 to 10^4 $Å^2$ [52] (figure 12). The data for LiF film in figure 12 were fitted by non linear regression analysis (Marquardt approximation) to the function $y = 0.0403 \exp (0.467 x)$, with a correlation factor R=0.95. Both Halliday [53] and Blackburn [52] measured a stress value of 5 GPa for a LiF film thickness of 100Å. Stress was not dependent on crystallite size for film thicknesses greater than 250 Å [52,53]. Blackburn's and Halliday's findings agree with the results obtained by Fleet [54] who found that the average crystallite size in nickel films increased with films thickness only up to a thickness of 250 Å and was constant thereafter. This would explain the stress dependence on crystallite size which is in turn is dependent on film thickness when the film thickness is less than 250 Å.

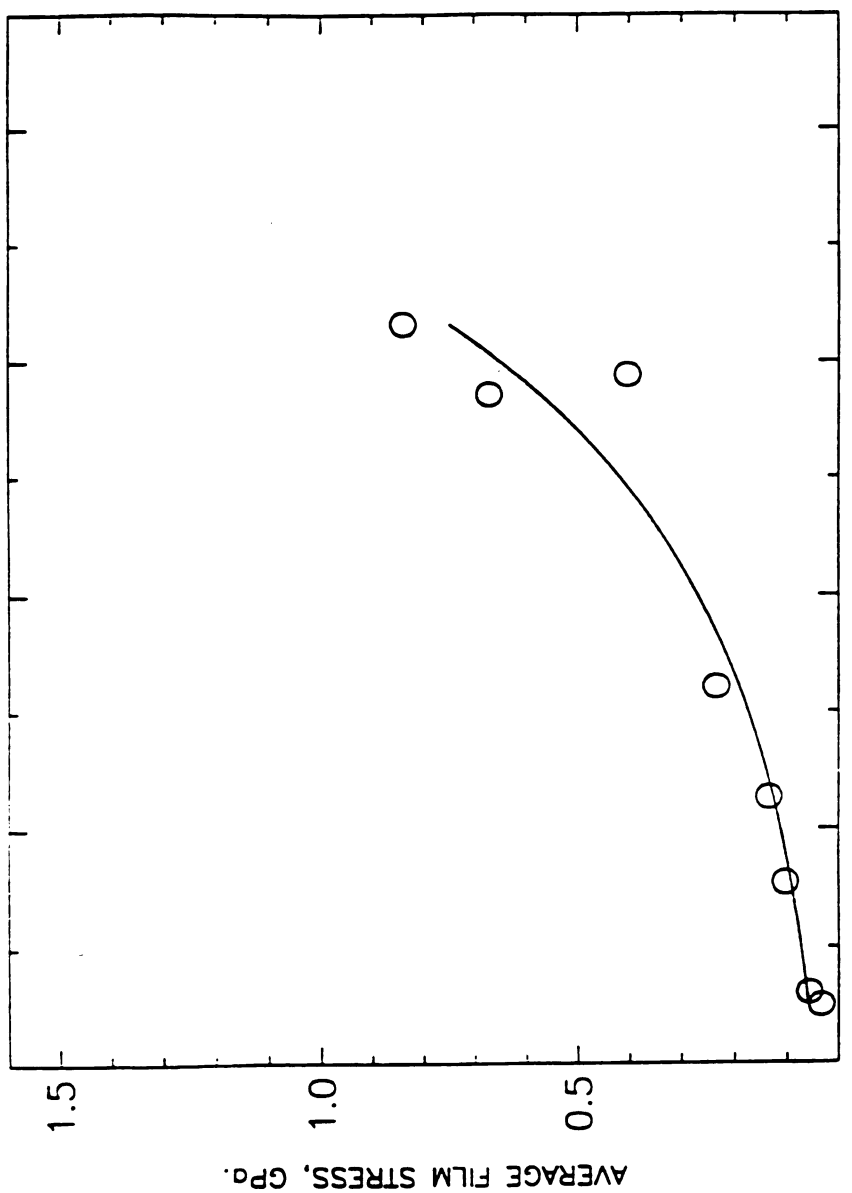

Figure 12. Average stress in LiF films vrsus crystallite size. After Blackburn [45].

4- STRESS MEASUREMENT METHODS

4.1 X-ray stress measurement

The change in the crystal lattice parameter due to residual strain is a measure of stress in thin films [4,8]. X-ray diffraction can be used to measure changes in the lattice parameter. Haraki and Mitsuru [4] have measured the lattice constant in various isotropic materials in a direction perpendicular to the interface. The strain in the z direction (perpendicular to the interface is given by [4]

$$\varepsilon_z = (a - a_o) / a_o \qquad (2)$$

where

a_o = known lattice parameter, and

a = the measured lattice parameter of the strained film.

The stress resulting from the strain described by equation 2 is [8]

$$\sigma_z = (E_f / 2\nu_f)[(a - a_o) / a_o] \qquad (3)$$

The biaxial elastic strain parallel to the interface (in the XY plane) is obtained by using the elastic stiffness constants C_{ij} of the films, to

obtain the following relationship [4]:

$$\varepsilon_x = \varepsilon_y = (2\,C_{12}/C_{11})\;\varepsilon_z \qquad (4)$$

where ε_z is given by equation 2 and 1 and 2 subscripts denote the X and Y direction. The biaxial stress in the X and Y directions is then

$$\sigma_R = (E_f / 2\nu_f)\,(C_{12}/C_{11})\;[(a-a_o) / a_o] \qquad (5)$$

4.2 Stress measurement with the energy gap method

Using a deformation potential model [4], the strain in the film is estimated from the photoluminescence peak shift, in the photoluminescence spectra performed at some temperature T. T is a temperature where the photoluminescence intensity is high. The calculated energy gap change due to straining in the film is then [4]

$$\Delta E(T) = [\,2\,\lambda 1(C_{11}-C_{12}) / C_{11} + \lambda_2(C_{11}+2C_{12}) / C_{11}]\,\varepsilon\,(T) \qquad (24)$$

where

$\Delta E(T)$ = the change in the energy gap of the film at temperature T and due the stress in the film.

$\varepsilon(T)$ = the biaxial strain measured at a temperature T.

λ_1 = the hydrostatic deformation potential,

λ_2 = the shear deformation potential, and

The strain $\varepsilon_0(T_0)$ at the measurement temperature T_0, is obtained from the temperature dependence of the strain given by

$$\varepsilon_0(T_0) = \varepsilon(T) + \Delta\alpha(T)\ (T - T_0) \tag{7}$$

where $\Delta\alpha(T)$ is the difference in thermal expansion coefficient between the substrate and the film. The biaxial stress in the film (parallel to the interface), at the measurement temperature T_0, can be obtained by combining equations 6 and 7 to yield

$$\sigma_R = [\,E_s/(1-\nu_s)]/[\,\Delta E(T)/\{2\lambda_1 (C_{11}-C_{12})/C_{11} + \lambda_2 (C_{11}+2C_{12})/C_{11}\}] \tag{8}$$

4.3 Stress calculation from the curvature change of the substrate

When dissimilar isotropic materials are joined together, stresses arise at the interface as well as within the layers. These stresses can arise from holding one member under stress at the time of joining, by an expansion in one member after joining, or by joining materials with different expansion coefficients as is the case for diamond-silicon composite system.

To measure the total internal stress (thermal and intrinsic) in thin films, many authors have used a stress calculation method based on measuring the change in curvature of the substrate before and after the deposition of the film. Windischmann [10,55], Gehan [27], Rossingnon and Evans [56], and Nir [8] used Stoney's equation (equation 9) to measure stresses in thin films

$$\sigma_R = E_s \, t_s^2 \, / [6 (1 - \nu_s) \, t_f \, \rho] \qquad (9)$$

where the terms are defined after equation 23.

Oel and Frechette [57] derived equation 9 through a minimization of elastic strain energy in the composite system. A similar derivation was used by Argon and Gupta [3] to obtain a stress curvature for a circular substrate-film composite.

Consider a two layer system as shown in figure 11. Under equilibrium, the stresses in the system can be resolved in an X,Y and Z

coordinate system as shown in figure 11. The strains within a layer in the XY plane are given in terms of the stresses by Hook's law for elastic deformation by [57]

$$\varepsilon_x = [\sigma_x - \nu\sigma_y - \nu\sigma_z] / E \quad (10)$$

$$\varepsilon_y = [\sigma_y - \nu\sigma_x - \nu\sigma_z] / E. \quad (11)$$

E is the Young's modulus of the layer and ν is the Poisson's ratio of the layer. ε_x and ε_y are the strain in the X and Y directions. σ_y and σ_x are stresses in the X and Y directions. ν is the layer's Poisson's ratio. The magnitude of a biaxial stress σ_i within the ith layer is then given by [57]

$$\sigma_i = E_i \varepsilon_i / (1 - \nu_i). \quad (12)$$

ε_i, σ_i and ν_i are respectively the strain, the stress and the Poisson's ratio in the ith layer. Equilibrium requires that the sum of all forces in the multi-layer body be equal to zero or [57]

$$\Sigma \sigma_i d_i = 0, \quad (13)$$

where d_i is the thickness of the ith layer (figure 5). If we use equation (6) for the stress, then equation13 becomes

$$\Sigma \; E_i \varepsilon_i / (1 - \nu_i) = 0. \qquad (14)$$

At the interface, the strain differential $a_{1\text{-}2}$, between the two layers is given by

$$a_{1\text{-}2} = \varepsilon_1 - \varepsilon_2. \qquad (15)$$

Generally, the interface between two stressed layers is spherically curved (figure 13). If the radius of curvature ρ is not small, the strain within a layer perpendicular to the interface is linearly proportional to the distance η_i separating the neutral axis of the ith layer from the interface. If a point is at a distance z from the interface, then the strain in the ith layer at that point is given by [57]

$$\varepsilon_i = (\eta_i - z) / \rho. \qquad (16)$$

Equation 15 for the strain differential $a_{1\text{-}2}$ can now be rewritten with the help of equation 16 as follows:

$$a_{1\text{-}2} = (\eta_1 - \eta_2) / \rho. \qquad (17)$$

At any point X, Y, Z in the system, the energy density is given by

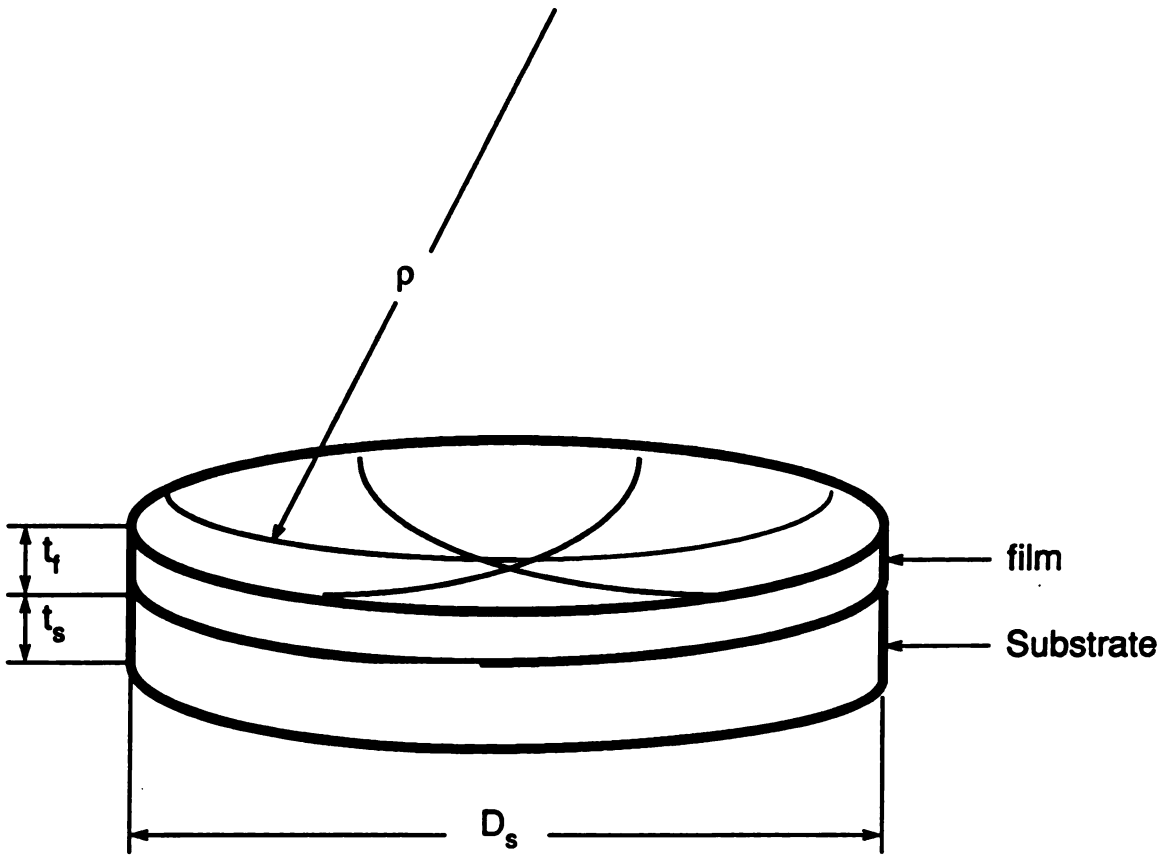

Figure 13. Substrate and film bowing to radius of curvature ρ, D_s is the substrate diameter. t_f and t_s are respectively the thickness of the film and the substrate.

$$\int \sigma \, d\varepsilon = (1/2)\, \sigma_x \varepsilon_x + (1/2)\sigma_y \varepsilon = \sigma\varepsilon. \tag{18}$$

The strain energy per unit area ϕ for the entire system is [57]

$$\phi = (E_1 / 1-\nu_1) \int \varepsilon_1^2 dz + (E_2 / 1-\nu_2) \int \varepsilon_2^2 dz. \tag{19}$$

Using equation 16 for ε and (11) for η_2, the strain energy is then

$$\phi = (E_1 / 1-\nu_1) \int (\eta_1 - z)^2 / \rho^2 \, dz + (E_2 / 1-\nu_2) \int (\eta_1 - a_{1\text{-}2}\rho - z)^2 / \rho^2 \, dz. \tag{20}$$

The requirement for minimal strain energy is satified by setting the partial derivative of the strain energy with respect to η and ρ respectively to zero. This leads to an expression for the neutral axis distance and another one for the radius of curvature, given by [57]

$$\rho = [\, S_1^2 d_1^2 + S_2^2 d_2^2 + 4\, S_1 S_2 d_1^2 + 4\, S_1 S_2 d_2^2 + 4\, S_1 S_2 d_1^2 + 6\, S_1 S_2 d_1 d_2] \,/\, [\, 6\, a_{1\text{-}2} S_1 S_2\, (d_1 + d_2)\,], \tag{21}$$

Where d_1 and d_2 are layer thicknesses as shown in figure 7, and

$$S_1 = E_1 d_1/(1-\nu_1)$$

$$S_2 = E_2 d_2/(1-\nu_2) \qquad (22)$$

are the stiffness of both layers. A similar equation to equation 21 was given [4] in term of the strains ε parallel to the interface:

$$1/\rho = [\, 6\ E_1E_2d_1d_2\,(d_1+d_2)\,\varepsilon\,] \,/\, [\ E_1d_1 + E_2d_2\,)\,(\,E_1d_1^3 + E_2d_2^3\,) + 3E_1E_2d_1d_2(d_1+d_2)^2]. \qquad (23)$$

If for the two layer system, shown in figure 7, we treat layer number one as the thin film and the second layer as the thicker substrate, then we can do the following substitutions

$d_1 = t_f$ = film thickness

$d_2 = t_s$ = Substrate thickness

$E_1 = E_f$ = Young's modulus of film material

$E_2 = E_s$ = Young's modulus of substrate material

$\nu_1 = \nu_f$ = Poisson's ratio of film material

$\nu_2 = \nu_s$ = Poisson's ratio of substrate material.

With the help of equation 12, Rossignon and Evans derived the relationship of the stress to the radius of curvature from equation15

$$\sigma_R = [E_s\ t_s^2 / 6(1-\nu_s)\, t_f \rho\,]\ [(1 + t_f / t_s)(1 - 4\, t_f / t_s)] \qquad (24)$$

This equaion can be further simplified if $t_f << t_s$, yielding to what is known as the Stoney equation [8]

$$\sigma_R = [E_s\ t_s^2 / 6(1-\nu_s)\, t_f \rho\,]. \qquad (9)$$

Equation 9 is therefore applicable only for film thickness much smaller than substrate thickness and for the central deflection of the wafer much smaller than its diameter.

Rubin et al. [58] calculated the residual stress based on the center deflection δ of a beam of length L. The expression Rubin used is

$$\sigma_R = 4\, E_s\, t_s^2\, \delta\ /\ 3(1-\nu_s)\, t_f\, L^2 \qquad (25)$$

Stress measurement according to Stoney's equation is more straight forward than Raman spectroscopy use for stress measurement. The parameters needed for the a measurement are the wafer properties, which in case of the silicon wafer, are well known, the film thickness and the curvature. The major assumptions made are the isotropy of the

film and substrate [57]and that no stress develop in the substrate [4]; the substrate behaves rigidly since it is much thicker than the film, elastic changes occur only in the film [20]. The stress measured must be the elastic range. It is also assumed that the interface bonding is strong enough not to allow slippage or spalling and that the substrate is initially flat, otherwise, the difference in deflection before and after the film is deposited must be used instead.

4.3.1 Importance of the film thickness

What the radius of curvature method measures is the force per unit thickness rather than a stress value. If the film thickness is uniform, the uniform stress (equal to the average stress) is simply obtained by dividing the force per unit thickness by the thickness value. However the above scenario represent the best possible conditions which are: the film thickness is uniform and the force per unit width has a constant value (a direct result of the assumption of film thickness uniformity). Unfortunately, neither assumption holds. In the case of MPCVD diamond films the film thickness is not uniformly distributed [10,21]. The force per unit with is not constant; Hoffman [48] carried an *in situ* measurement of the force per unit width in Cr films by interferometric observation (section 4.3.2) of the resulting deflection during film deposition. The force per unit width was calculated from the quantity $[E_s t_s^2 / (1 - \nu_s^2)] (k_x + \nu k_y)$ where k_x and k_y are experimentally measured

constants. Hoffmann found the force per unit width to decrease linearly with film thickness [48]. Consequently, even the value of the force per unit width measured by the radius of curvature change reflects the average force per unit width in the film. The obtained stress value in Stoney's equation is therefore the average force per unit width divided by the average film thickness. A more accurate stress measurement with Stoney's equation would involve the following steps; first an *in situ* method (Hoffman's methods described above or in section 4.3.2 for instance) has to be used to map the curvature change during deposition as a function of the instantaneous film thickness. The value of the force per unit thickness as function of the film thickness is then obtained as did Hoffmann with Cr films [48]. Second, the film thickness distribution along the radial direction of the film must be mapped. At a given point of the film surface where the thickness is some value t_o, the instantaneous stress is given by the ratio of the force per unit thickness evaluated at t_o, divided by the thickness layer dt at the height t_o. The total stress is thus the sum of the contributions of all dt layers from zero to the maximum height. One can conclude from the above discussion that the value of the stress as given by Stoney's equation reflects a stress value that averages both the force per unit width and the film thickness over the entire film thickness range which differs from Raman stress measurement giving the stress value within the skin depth. An interesting case occurs when the film thickness is less than the skin depth as is the case for a diamond film few microns thick. In this case,

the laser beam samples the entire thickness, thus both the interfacial stress and bulk stress are measured, and possibly the an average stress is obtained.

The most important consequence of stress measurement by measuring the curvature of the film is that the measured stress is the average stress in the film; including the interfacial, bulk and surface stresses. The stress obtained in a film from the change in the radius of curvature measurement gives an average stress while the Raman and x-ray stress measurement gives the near surface or interfacial stress [59]. Stress values can be very different at the interface from average values, since the thickness dependence of stress is a well established fact [8]. According to the derivation of Stoney's equation, the average stress obtained assumes a uniform film thickness distribution over the measured area. In MPCVD deposition, the film thickness does vary from the center towards the edges of a circular film. Windischmann deposited films by MPCVD where the film thickness was 3.0 microns at the wafer center and dropped to 50 percent of the center value at a radial distance of 25 mm, and 1.25 microns at 37 mm, the average thickness was 2 microns [10,21]. The area of measurement had to be reduced to decrease the effect of the thickness gradient [10,21]. Since the stress is assumed to be inversely proportional to the film thickness, even small variation in the film thickness result in resolved stress variation over the area of measurement. For instance, in ZnO films the stress was 0.73 GPa at 5 microns film thickness and 0.58 GPa at 10

microns [56]. Thus, a 50 percent decrease in film thickness resulted in 26 percent increase in stress. Measurement of an average value of the film thickness becomes critical to accurate average stress measurement in the film.

Given a film with a non uniform film thickness distribution, the measured stress value from the change in curvature does not give a reliable representation of the film stress since only an average value is obtained, the upper and lower limits of stress values are thus unknown.

4.3.2 Errors and resolution

Film thickness measurement with 2.5 to 10 nm accuracy is routinely obtainable with a profilometer stylus [3]. The process involves thickness measured by masking the substrate during deposition and creating a step at various edges of the film. The steps are measured with a profilometer and an average value of the thickness is taken [3,12]. Other thickness measurement methods are SEM and light interference methods which offer a similar error range to the profilometer step measurement. All of the thickness measurement techniques should take into account the film thickness variation; the spatial distribution and number of measurements on the film thickness affect the measured average value of the thickness. Perhaps the best method for measuring the average film thickness is the differential weight analysis; the film

and substrate are precision weighted, the substrate is then chemically etched out and the film is weighted again. Alternatively, the substrate is weighted first, then weighted again after the film is deposited. Assuming a diamond density of 3.515 g/cm3 , the volume of the film is estimated and divided by the base area of the film resulting in an average value of the film thickness, a preferred value for Stoney's method [60].

The measurement of the film thickness from a created step is not convenient for a real application because it must have an area where no film is deposited. SEM observation involves destroying part of the samples and differential weight analysis results in complete removal of the film from the dissolved substrate. Film thickness measurement with a light interference method is a nondestructive method that can be used to measure the film thickness.

Many authors have reported the use of a profilometer to measure the radius of curvature of the substrate bowing under stress [3,27]. A commercially available Dektak II was often used [3]. However the method for radius of curvature measurement most frequently used is the light interference fringes method. Interference fringes are formed by placing the film-substrate composite against an optical flat which is a specially ground surface that is often glass. Then the specimen is illuminated with a monochromatic light through the glass. Bending of the sample causes the formation of set of closely spaced interference fringes [8,56]. The radius of curvature is then given by [56]

$$\rho = x_n^2 / n\lambda \qquad (26)$$

where $2x_n$ is the diameter of the nth dark fringe, and λ is the wavelength of the illuminating monochromatic light. For a circular film-substrate system (figure 13), if the fringes are circular then the stresses in the X and Y directions have the same magnitude. However if the fringes are elliptical, then stresses in the two directions are unequal [56]. Some authors measured the stress from the curvature of the stressed film compared to a perfectly flat surface [4], however the net curvature change [55] before and after the film deposition results from the film stress. For instance, the curvature is measured before and after a silicon film is chemically etched out, the net change in the curvature is then attributed to film stress [59]. For the measurement of the beam deflection with a stylus, the deflection of the stylus under a 25 mg load is assumed negligible [3]. The error in measuring the deflection with Stoney's equation was found to be less than 20 percent compared to measured deflections on a simply supported circular plate under load. The relative error in repeated measurements is less than 10 percent [3]. The deflection of a beam measured with optical microscope with a point-to-point focus technique has an accuracy of 0.1 microns [16]. Many authors approximated the radius of curvature by $z^2/ (8 w)$, where z is the measured bow height and w is the distance over which

the bow is measured given that z/w << 1 [59]. Given the accuracy of the film thickness and curvature measurement stated above, the stress is measured from radius of curvature to an accuracy within 0.09 GPa [56], and 0.05 GPa [34]. The reported stress resolutions for the stress measurement from the radius of curvature is 0.01 GPa [10].

Hoffman reported on the minimum detectable force per unit width for a variety of deflection measurement techniques [8]. To convert the force per unit width to a stress resolution, the force per unit width are divided by a typical 1 micron film thickness, the obtained resolution ranges from 10^{-5} GPa for mechanical and interferometric techniques to about 10^{-3} GPa for optical and x-ray techniques. Thus very high stress resolution can be obtained with the curvature measurement methods. The stress resolution can be improved by using thinner substrates.

The measurement of the beam or wafer deflection as an *in situ.* method during the deposition is at a disadvantage compared to Raman spectroscopy because there is a difficulty in isolating the stress transducer from the energetic deposition environment, it can be can be costly and difficult to use [15]. Raman spectroscopy would only require a window for the laser beam to pass through the deposition chamber wall. The advantage of *in situ* measurement over conventional methods is that one can measure curvature of films as thin as 30nm and directly measure the intrinsic growths stress [15], since thermal stresses do not develop until the film and substrate are actually cooled to room temperature. Hoffman [15] measured the insitu stress in molybdenum

film by the incremental voltage change of the capacitive film with incremental deposited film.

The maximum difference in the elastic modulus of (100)silicon is 16 percent, but no important variation in curvature were observed for any orientation of the stylus with respect to the wafer when the film is uniform [3]. The Young's modulus in Stoney's equation representing the substrate should be average in-plane modulus [3]. Using a single crystal for the substrate thus introduced an error in the stress value as calculated from Stoney's equation, since the elastic constant are not isotropic; they depend on the crystallographic orientation. The assumption of isotropic materials, for Stoney's equation to be applicable, should hold; the condition for isotropy is [60]

$$2\,C_{44} / (C_{11}-C_{12}) = 1 \qquad (27)$$

the ratio is equal to 1.21 for diamond and 1.56 for silicon. The applicability of Stoney's equation can be argued in the case of diamond and silicon since they are essentially isotropic but not truly isotropic. One should note however that the elastic constants ratio as a condition for isotropy is dependent on the reported value of elastic constants and thus can get closer or farther from 1 depending on the scatter in the values of the elastic constants. It would be also a problem to interpret stress results if the magnitude of the stress is beyond the elastic deformation of diamond. Clausing measured stresses in diamond films

that approach the stress at fracture, the magnitude of the stress was as high as 6.1 GPa, while the stress at fracture is about 11 to 20 GPa the measurement method was x-ray diffraction [31]. Clearly, such measurement would not be reliable by radius of curvature method because the stress value is in the plastic deformation range. Further errors in the measured stress according to Stoney's equation would arise if the films are delaminated, bowing of the substrate due to film stress can no longer be measured by Stoney's equation [27], the interface is assumed to be strong enough to avoid debonding.

If a reliable nondestructive technique can be used for film thickness measurement, the radius of curvature method becomes a nondestructive method for stress measurement. Measurement of the curvature with a stylus can be destructive though; the surface can be scratched with the stylus [59].

4.3.3 Advantages of the curvature methods

Some of the advantages of stress measurement from the change in the radius of curvature over the Raman shift and X-ray measurement have already been discussed earlier. Other advantages include stress measurement in films of any morphology (amorphous or crystalline) while Raman method measures stress only in single or polycrystalline materials, the same is true for x-ray stress measurement [59]. The radius of curvature is a direct and easy mechanical measurement of

stress [59], while Raman and x-ray techniques involve various assumptions and are rather lengthy. Raman spectroscopy requires a lengthy set up time and careful calibration, and thus is a lot costlier than curvature measurements.

The only systematic stress measurement study that used x-ray, Raman and curvature methods was done by Trimble et al. [59]. Polycrystalline silicon films with an oxide layer were used. X-ray (400) peak shift from the change in the inter planar spacing in the 50 microns thick polycrystalline silicon films through the oxide layer yielded a stress of 0.037 GPa within 0.01 GPa, the skin depth is 5 microns at the at 40 KeV x-ray line. Raman measurement yielded no shift with a 0.2 cm^{-1} resolution corresponding to stress resolution of 0.05 GPa. The conclusion was that the stress was less than 0.05 GPa which is higher than the stress value measured by X-ray, the sampling depth in the silicon was 3 microns at 647 nm Ar laser line. These measurements represent stress only within 3 to 5 microns from the interface. Using the radius of curvature method, the stress was found to be about an order of magnitude smaller; about 0.004 to 0.006 GPa depending on the orientation of the measurement direction across the wafer, stress anisotropy is thus observed with this method [59]. From the fact that the stress measured by the change in the radius of curvature is much smaller than the stress measured by the x-ray technique, one can conclude that Stoney's equation provides an average value of the stress over the entire thickness x-ray diffraction samples stress only at

the interface where the stress is expected to be higher than in the bulk of the film.

4.4 Stress measurement from the Raman peak shift

In materials with the diamond crystal structure, the triply degenerate zone-center phonon mode is known to split and shift under stress [61]. The degeneracy of phonon mode is lifted by lowering the crystal symmetry due to an applied or residual strain [62]. The shift of the zone center mode with stress can therefore be used a measure of stress in diamond film as well as a pressure sensor as a diamond anvil cell DAC [63]. In the following paragraphs, a derivation of the phonon frequency shift due to stress is reported for single crystals with application to diamond under a biaxial stress state in the XY plane.

In presence of strain, two atoms in a unit cell are assumed to behave according to the dynamical equations describing the zone-center phonon modes and have the form [61]

$$m\,\partial^2 u_i / \partial t^2 = -\Sigma K_{ij} u_j$$

$$= -\left(K^0_{ij} u_j + \Sigma \left(\partial K_{ij} / \partial \varepsilon_{kl} \right) \varepsilon_{kl} u_j \right) \qquad (28)$$

where u_i is the ith component of the relative displacement of the two atoms in the unit cell, m is the reduced mass of the two atoms in the unit

cell and K_{ij} are atomic force constants. $K^{o}_{ij} = m \nu_0^2$ is the effective spring constant of the F_{2g} triply degenerate diamond mode in the absence of strain. $(\partial K_{ij} / \partial \varepsilon_{kl}) \varepsilon_{kl} = K'_{ijkl}$ is the change in the spring constant due to the strain ε_{kl}. i, j, k and l are crystallographic axis [61].

Since diamond has a cubic symmetry, there exist only three independent K' components, namely

$$K'_{iiii} = m\ p$$

$$K'_{iijj} = m\ q$$

$$K'_{ijij} = m\ r\ (i \neq j).$$

p, q and r are independent deformation potentials (strain derivatives) [61]. With the assumption of harmonic motion, the phonon frequencies for the strained lattice can be deduced from equation 28 which results in a 3 X 3 secular determinant with eigenvalues λ [64]. The eigenvalues are given by [64]

$$\lambda = \nu_{st}^2 - \nu_o^2 \qquad (29)$$

where ν_{st} is the line frequency of the stressed film and ν_o is the frequency of the unstressed film. Equation 29 can be approximately

rewritten as

$$\nu_{st} \approx \nu_o + \lambda / 2\nu_o \qquad (30)$$

The solution to the 3 X 3 secular equation is a cubic in λ therefore, it has three solutions. Depending on the stress state, the three eigenvalues can be all equal under a hydrostatic stress to completely independent under a uniaxial stress parallel to one the <110> directions of the sample [61,65].

Equation 28 can be solved for the strains in the film as a function of the frequency change. In the case of a non hydrostatic stress state, two eigenvalues are equal and thus only two eigenvalues are independent. The corresponding phonon frequencies according to equation 30 are the doublet and the singlet which are respectively given by [61,64,66]

$$\nu_d = \nu_0 + 2\nu_h + \nu_u/3$$
$$\nu_s = \nu_0 + 2\nu_h - 2\nu_u/3 \qquad (31)$$

where ν_h and ν_u are respectively the shifts due to hydrostatic and shear component of the strain [67]. The hydrostatic component of the stress does not cause splitting of the zone center phonon [62], but contributes to the total observed frequency shift [62].

The stresses in the film can be determined from the strains using the

following equation [9]

$$\varepsilon_{ij} = S_{ijkl}\,\sigma_k \tag{32}$$

Considering that the Z axis is perpendicular to the surface of the film, that X = [100], Y = [010] and Z = [001] and that the stress at the surface is zero, the biaxial stress $\sigma_{xx} = \sigma_{yy} = \sigma$ in the film is non zero and [64]

$$\varepsilon_{xx} = \varepsilon_{yy} = (S_{11} + S_{12})\,\sigma$$

$$\varepsilon_{zz} = 2\,S12\;\sigma$$

$$\varepsilon_{ij} = 0 \quad \text{for } i \neq j. \tag{33}$$

For a biaxial stress state ν_h and ν_u are given by [66]

$$\nu_h = \sigma\;(p+2q)\,(S_{11}+S_{12})/6\,\nu_0$$

$$\nu_u = \sigma\;(p-q)\,S_{12}/2\nu_0 \tag{35}$$

From the above equations, the shift of both the singlet and the doublet due to a biaxial stress state is determined to be

$$\Delta\nu_s = \nu_s - \nu_0 = \sigma/\,2\nu_0\,[\,2p\,S_{12} + 2q\,(\,S_{11} + S_{12}\,)]$$

$$\Delta\nu_d = \nu_d - \nu_0 = \sigma/\,2\nu_0\,[\,p\,(S_{11} + S_{12}) + q(\,S_{11} + 3\,S_{12}) \tag{36}$$

Equations 36 are identical to those used for the singlet and doublet shift due to a biaxial stress in thin films given by Engler [68] and Nishioka [64] and differ from the equations given by Ceideira et al. [61] for a uniaxially applied stress.

Usually, the Raman spectra are given in terms of the scattered intensity as a function of the wave number w (cm^{-1}) rather than the frequency. The relationship between the wave number w, the frequency ν and the speed of light c is given by

$$\nu = 2 \pi c w \tag{36}$$

where $c = 3 \times 10^{10}$ cm/sec. Equation 36 can be rewritten as

$$\nu = 6 \pi 10^{10} w \ (cm^{-1}) \tag{37}$$

Given the above relationship then

$$\nu_0 \ (1/sec) = 6 \pi 10^{10} \ w_o \ (cm^{-1})$$

$$\Delta\nu \ (1/sec) = 6 \pi 10^{10} \Delta w \ (cm^{-1}) \tag{38}$$

The values of S_{ij}, p, q are reported for diamond and silicon are given in table 3. Using these values, the relationship between the biaxial

stress in the diamond film and the diamond line shift of both the singlet and the doublet are calculated in this work to be

$$\sigma_s\,(\mathrm{GPa}) = -8.11672\ 10^{-4}\ w_o\ \Delta w\ (\mathrm{cm}^{-2})$$

$$\sigma_d\,(\mathrm{GPa}) = -16.3014\ 10^{-4}\ w_o\ \Delta w\ (\mathrm{cm}^{-2}) \qquad (39)$$

taking w_o = 1332.5 cm-1 [69], then

$$\sigma_s\,(\mathrm{GPa}) = -1.08\ \Delta w_s\ (\mathrm{cm}^{-2})$$

$$\sigma_d\,(\mathrm{GPa}) = -2.17\ \Delta w_d\ (\mathrm{cm}^{-2}) \qquad (40)$$

From the above linear relationship of the stress with line shift, the diamond pressure coefficient for a single crystal under a biaxial stress are 0.93 cm^{-1}/GPa for the singlet line shift and 0.46cm^{-1}/GPa for the doublet line shift. Equation 40 are derived for diamond single crystals with an homogenous biaxial stress parallel to the surface of the diamond film.

It is interesting to note that the coefficient 1.08 GPa/cm^{-1} calculated here for a biaxial stress in the XY plane is equal to the coefficient given by Yoshikawa [9] for a tensile uniaxial stress along [001]. The above similarity is to be expected since in the configuration used in this thesis, the compressive stress in the XY plane of the film is going to

induce a tensile stress in the Z direction which corresponds to the [001] direction of applied stress in Yoshikawa's calculation [9]. From the above observation one is allowed to compare the calculated coefficient in equation 40 for a biaxial compressive stress state with experimentally measured values of the same coefficient for tensile stress in the <100> direction given that there are no published results to the author's knowledge) for frequency shift under a biaxial stress for diamond. The survey of the reported values for the diamond frequency shifts under various stress distributions is summarized in table 4. According to table 4, the experimentally determined shift coefficient for uniaxial stress along the <100> is 1.37 GPa/cm^{-1} [70] which is close to the 1.08 GPa/cm^{-1} calculated here. Gezan et al. [62] reported that the estimated calculated stress value to cause a 1 cm-1 shift is 1.081 GPa which is in very close agreement with the value calculated here (1.08 GPa). One should note that even though the calculation is simple, no calculated shift coefficient under biaxial stress was reported in the literature for either single crystals or polycrystalline diamond. One would conclude here that the calculated value of shift coefficient 1.08 GPa/cm^{-1} is a reasonable value to use for further stress calculation assuming a (100) orientation.

Table 3. Elastic constants and deformation potentials of silicon and diamond.

Property	Diamond	silicon
S_{11} (GPa^{-1})	$9.5240\ 10^{-4}$	$76.8\ 10^{-4}$
S_{12} (GPa^{-1})	$-0.9913\ 10^{-4}$	$-21.4\ 10^{-4}$
p (sec^{-2})	$-1.0710\ 10^{28}$	$-1.43\ 10^{28}$
q (sec^{-2})	$-5.2620\ 10^{28}$	$-1.89\ 10^{28}$
W_o (cm^{-1})	1332.5	525.7

Table 4. Reported diamond shifts under stress.

Ref.	Stress state	Measured pressure coeff. cm^{-1}/GPa	Calculated Pressure coeff. cm^{-1}/GPa	Pressure range (GPa)	Diamond sample
63	hydrostatic	2.37	N/A	0-25	DAC*
72	isotropic	2.90	N/A	0-18	(100) plate
9	// [100]	N/A	0.93	N/A	Single crystal
73	hydrostatic	2.87	N/A	0-30	(100) plate
71	// [110]	0.73	0.66	12.1	(110) disk
70	// [001]	0.73	N/A	0-1	(100) plate
70	// [111]	2.20	N/A	0-1	(111) plate
70	Hydrostatic	3.20	N/A	0-1	(100) plates
69	Hydrostatic	2.64	N/A	0-15	Natural diamond
74	Hydrostatic	2.90	N/A	15-40	(100) PCD**
65	Hydrostatic	2.33	N/A	0-30	DAC*
75	hydrostatic	2.96	N/A	0-2.3	Single crystal

* Diamond anvil cell
** Polycrystalline diamond

4.4.1 Nature of the dependence of stress on the frequency shift

The phonon frequency shift with stress depends on many factor. The crystallographic orientation of the single crystal, the orientation with respect to the single crystal of the incident laser beam as well as that of the scattered beam, the polarization of the laser beam, and the stress distribution are the key elements in correctly measuring the stress in a single crystal from the measured frequency shift.

The stress in single crystals was found theoretically [61] and experimentally [64,71] to vary linearly with frequency shift. The stress varied linearly with shift for Ge, GaSb, GaAs [61] and diamond under a variety of stress distributions [9,65,69,70,71,72,74]. Furthermore, the linear dependence of the stress on frequency shift holds for both the singlet and doublet splits as well as in the no-split case [32,61,65]. However, the dependence of the stress on the frequency shift is linear only to about 40 to 70 GPa [74]. The stress range of interest in this work is less than 10 GPa, therefore the assumption of linearity is solid for the purpose of measuring stress in thin films.

For diamond and silicon, the stress measurement is made easier due to their cubic diamond structure which reduces the number of parameters necessary for stress calculation, namely the elastic constants S_{ij} (C_{ij}) and deformation potentials p, q, r. The elastic constants for diamond are available in the literature [9], however, there is a considerable scatter in the reported values due to various

measurement methods. For instance, the value of C_{11} was found to be 151 GPa by Brillouin scattering measurement and 390 GPa by the ultrasonic wedge method [76], which is more than twice the value of 151 GPa. The same kind of scatter exists for the deformation potential constants. Furthermore, the deformation potentials are derived for uniaxial and hydrostatic stress conditions and not a biaxial stress state. Therefore, until precise deformation potentials are measured under a biaxial stress state, it remains unknown how much of an error is being made by using already published deformation potential constants. Accurate values of the deformation potential constants are critical to the precise measurement of the strains from which the stresses are calculated. To avoid errors due to scattering in the elastic constants, one might look at the strain values instead of the stresses for various stress measurement techniques.

Unlike other phonon frequencies, the F_{2g} frequency (at 1332.5cm^{-1} for diamond [69] and 520.7 cm^{-1} for silicon [59]) shift primarily under stress (from its unstressed position) and does not shift from other effects. For instance, the characteristic line of graphite is known to shift with incident laser frequency [77].

The F_{2g} band in diamond crystals is known to shift with stress, but more critical to stress measurement is the splitting of the band under stress. Under a hydrostatic stress state, the F_{2g} band does shift but does not split [70]. However, Under a non-hydrostatic stress state, the

triply degenerate phonon line of the diamond structure splits into non degenerate (singlet) and doubly degenerate phonons (doublet) or into three singlets [61]. For instance, in Ge film under biaxial stress parallel to the film surface, the triply degenerate line split into a singlet and a doublet under a uniaxial stress parallel to either a <100> or <111> crystallographic directions, the triply degenerate line in diamond single crystals splits into a singlet arising from bonds parallel to the stress direction and a doublet perpendicular to the stress direction, but split into three singlets under a uniaxial stress parallel to the <110> crystallographic directions [61,62,65]. Under a biaxial stress, the F_{2g} line also splits into a singlet and a doublet [68]. The magnitude of the frequency shift differs with the stress state; the shift from the singlet in a uniaxial stress state is different from the magnitude of the shift of the singlet in a biaxial stress state. For instance, the estimated stress to cause 1 cm^{-1} shift under hydrostatic stress is1.081 GPa for diamond and 0.609 GPa for silicon which is lower than under uniaxial stress, namely 1.9435 GPa for diamond and 0.825 for silicon [62]. Furthermore, the magnitudes of the shift of the split bands also differ, in all cases the highest frequency is that of the singlet [63]. The ratio of the intensities of the singlet to the doublet is 4 to 1 for Ge single crystal under uniaxial stress [61]. Since the singlet has the highest frequency [63] and corresponds to bond deformation in a direction parallel to the stress direction[61], one can conclude that the highest frequency shifts occurs from deformation in the plane or direction of stress.

The magnitude of the shift also depends on the polarization of the laser beam. If the laser beam is polarized such that the electric field is directed parallel to the stress direction [32], the shift of the line is about 3.5 times as compared to the case where the electric field is perpendicular to the stress direction [32]. If the laser light is polarized such that the electric field forms an angle with the stress direction, the shift is a linear combination of the two shifts parallel and perpendicular to the stress [32]. For a completely random polarization, the observed shift is half the sum of the two shifts, and the line width reflect the contribution of both shifts [32].

The magnitude of the shift is also dependent on the assumed value of the diamond phonon frequency in the unstrained state. Most authors assume the value of 1332.5 cm^{-1} [59,73], but other values have been used, 1333 cm^{-1} for instance [72]. In the case of small stresses, a 0.5 cm^{-1} error in the above assumption will result in a stress error of the order of 0.1 GPa, which is a considerable error.

Once it is known whether or not the F_{2g} band split and what it splits into, according to the stress distribution and sample-laser orientation, it becomes important to identify the band or bands being observed in the Raman spectra. The scattering geometry is the determining factor. In back scattering geometry, only the singlet is observed [9,74], the doublet may exist but is not observed. For example, in back scattering geometry with Z=[001] along the laser beam direction, only the singlet is observed the doublet is preserved but not observed [68].

As can be seen from table 4, the highest frequency is observed under a hydrostatic stress state. In the case of a planar homogenous stress applied to a flat sample, there is an extra uniaxial compressive stress that will drive the shift coefficient towards a truly hydrostatic condition [74]. For diamond, if the shift coefficient under the biaxial compressive stress is used as in equation 40, a possible systematic error is the contribution of the uniaxial tensile stress parallel to the surface of the film [74]. For instance, an homogenous stress applied by a flat solid included a uniaxial compressive stress along [001] perpendicular to the surface, the shift coefficient was experimentally found to be 2.90 cm^{-1} / GPa. Furthermore, the samples used were polycrystalline [74]. The condition used in reference 74 are very close to those used in the present work. Knight [26] interpreted shift in PCD films as due to stress and calculated the stress from the pressure dependence of the shift in diamond of Sharma [63], the shift coefficient Knight used was 2.33 cm^{-1} /GPa or 0.42 GPa/cm^{-1}. From the above discussion, its seems that the shift coefficient that fits the stress measurement in films under biaxial (homogenous) stress (and a stress perpendicular to the film surface), is 0.35 to 0.45 rather than 1.08 GPa/cm^{-1} calculated from the secular equation. The rationing behind the above choice is that the calculated value from the secular equation considers only the contribution to the shift from the biaxial stress and not the stress in the z axis of the film. Furthermore, the model is for a single crystal and thus cannot be used for a polycrystalline material.

4.4.2 What causes Raman shifts

In order to interpret shifts as stress, it critical that there are no other effects causing shift that can be mistaken for stress.

The F_{2g} phonon frequency of diamond at 1332.5 cm^{-1} was found to down shift with the fraction of ^{13}C isotope of carbon [24]. The normal isotopic 13C concentration is 1.1 percent. Increasing the amount of ^{13}C up to 91 percent, resulted in negative band shifts down to 1288.7 cm^{-1} [24]. Diamond band position is independent of excitation wavelength [9] and also independent of the laser excitation source type (i.e. argon, krypton. The electric field effect on the diamond frequency position was investigated [62]; the electric field necessary to cause a 1 cm-1 shift is high about 10^6 V/cm, dielectric breakdown is expected to occur at such applied field. Thus no contribution to the frequency shift from the electric field is expected [62]. The next source of frequency shift that must be considered is the temperature rise due to laser heating. The diamond was found to change very weakly with temperature, a net shift of about 2 cm^{-1} resulted from about 400 °C temperature increase [69]. Thus, the effect of laser beam heating on the shift can be ignored, especially that diamond has a very high heat conductivity (5 time that of copper at room temperature); the heat will dissipate quickly into the diamond bulk.

The only considerable frequency shifts of the diamond band reported

in the literature are due to deposition parameter, lattice mismatches and thermal stress (thermal expansion mismatch stress). A rather inconsistent shift with deposition pressure is reported throughout the literature [22,60]. There is a systematic shift of the diamond peak with methane fraction in MPCVD depositions. Positive shifts of about 1 cm^{-1} occurred for methane fraction up to 4.0 percent [26,29]. Larger shifts to 3 cm^{-1} are observed at 7.5 percent methane fraction [29]. Similar shift with methane fraction were observed with ethanol in the deposition gas. Unusually high shift of 13 cm^{-1} were observed at methane fraction less than 1 percent [26]. Lattice mismatches between the film and substrate are also a source of frequency shift. In diamond films deposited on hard substrates such as alumina and silicon carbide, shift of -5 to +13 cm^{-1} are observed [26]. The dependence of the shift on the deposition temperature is such that at the temperature range where crystalline diamond is formed the shifts are small . For deposition temperature such that non diamond phases are formed the shift are in the order of 1 to 3 cm^{-1}. At 1200°C, the diamond line completely disappeared [26]

The deposition parameters including gas pressure, temperature, methane fraction and hydrogen fraction (proportional to the methane fraction), were shown in previous sections to affect the degree of ordering by changing the sp^3 to sp^2 bond ratio and result in growth stresses. In graphite polycrystalline films, the stress was found to be dependent on the grain size. There is no evidence to support the same

argument for diamond; the grain size is linearly proportional to the methane fraction [10,21]. It is therefore difficult to separate the effects of grain size and methane fraction on the stress in the film and thus on the frequency shift. Deposition temperature variation also affect the degree of ordering as well as varying the degree of thermal expansion mismatch between the film and substrate and consequently affecting the magnitude of thermal stress during the cooling down from deposition. Lattice mismatch between the film and substrate induce interfacial stresses. The only parameter that is shown to significantly induce diamond band shifting that is not stress induced is the amount of isotopic ^{13}C in the film. There is no reason to believe that the ^{13}C fraction in deposited film is greater that the normal isotopic fraction. It is therefore evident that the shifts of the diamond band at 1332.5 cm^{-1} is stress induced. Indeed it is rather evident that the F2g mode of diamond shift with stress. There is long list of studies done on the pressure dependence of the diamond line [32,69,70,74]. In most cases however, the studies used single crystals and externally applied hydrostatic pressure with a gas medium or a uniaxial stress along a known crystallographic orientation. To the author's knowledge, no systematic study has been carried on the diamond line dependence on residual growth stress with polycrystalline samples. From the available data on the pressure coefficient of diamond under various stress distribution, on can only speculate on the magnitude of the shift coefficient with stress for polycrystalline films under biaxial stress in a plane parallel to the

interface.

Given the above arguments, one can cautiously assume that in the case of polycrystalline diamond films, the shift of the diamond peak is stress induced.

The laser skin depth of most ceramics is few microns. For graphite, the skin depth is 0.6 microns at 488 nm wavelength [32]. For silicon, the skin depth is about 3 microns at 644 nm [59]. The very small skin depth of the laser beam probing the sample implies that the observed shift are due to surface effects and may or may not reflect the stress state in the bulk of the sample. In the case of diamond the depth of focus is plus or minus 50 microns about the focal plane [72]. Given that the diamond film thickness hardly exceeds 10 microns, the diamond film is entirely on focus and thus the shift observed from stress do reflect the stress distribution over the entire film thickness in the volume being probed by the laser beam. The volume in consideration is a cylinder with the height being the film thickness and the base equal to the laser beam spot diameter (assuming a circular laser beam cross section). The residual stress distribution in the film is such that at the first few hundred Angstroms from the interface, the stress is high due the contribution of the lattice mismatch and thermal expansion mismatch. The stress then levels off towards the free surface of the film. Therefore it seems that the measured shifts reflect the contributions of both interfacial and bulk stress within the film thickness. Within the probed volume, the C-C bond distortion is going to decrease away from the

interface, there is going to be a spectrum of phonon frequencies corresponding to the various bond distortions from the interface to the free surface of the film. The spectrum of frequencies is reflected in the Raman spectra by a widening of the diamond line. The highest shift is going to be due to the greatest distortion which occurs at the interface. Broad diamond peak might indicate stress inhomogeneity within the scattering volume; a sharp line about 2 cm^{-1} wide results from homogenous stress [73]. Thus line width is an indication of stress homogeneity [73] but is not the only contributing factor line broadening.

Since the beam spot size is about 2 microns, the probed area is very small compared to the sample dimensions. The measured shift from the probed area would thus reflect the stress state from only the scattering volume in that area; the stress measures this way is then a local stress and does not reflect the macroscopic stress state of the film. If the stress is known to be homogenous over the volume of the film, then the local stress measurement would be a good representation of the stress in the film. However, if the macroscopic stress distribution is not uniform, the locally measured stress within the beam spot diameter cannot be taken as a representative of the stress in the film. The advantage to measuring stress in a micro-volume is the ability to actually map the stress distribution by taking point to point measurement across the surface of the film. The above method would be an excellent way to map stress anisotropy in a film. The derivation of the shifts due

to stress is based on a single crystal with known orientation with respect to the laser beam. In the case of a polycrystalline film as is the case in most diamond films investigated, the derived stress calculation equations cannot be directly used. However, the average grain size in diamond films deposited by MPCVD is about 1 micron. Given that the beam size at the sample surface usually about 1 to 5 microns which is about the same as grain size and given that the film thickness usually about a micron, smaller than the average grain size, it is likely that the laser beam is focused on a single crystal or the boundary between two grains. Because of the possible scattering from only one or two grains, the theory may be applied. The questions becomes whether the stress state within a single crystal represent the isotopic stress distribution in the diamond film.

It is usually assumed that growth stresses in diamond films are isotopic and thus uniform across the film in a plane parallel to the interface. Furthermore, the stress is a function of the film thickness. If the film thickness is not uniform, then the stress in the film cannot be homogenous in directions parallel to the interface. Windischmann reported that the thickness of MPCVD films decreased to 50 % of its value at the center of film at a radial distance of 25 mm [21]. The variation was attributed to the non uniformity of the plasma electric field [21]. The thickness variation across a film can be easily monitored by Raman spectroscopy since the intensity of the Raman line increases linearly with film thickness [26] because of increased scattering volume

with increasing film thickness. The ratio of the scattered intensities at two different point in the film is probably equal to the ratio of the film thicknesses at the same points, given that the exact same conditions are used for the measurement.

4.4.3 Advantages and weaknesses

The reported stress magnitudes in thin diamond films ranges from zero to about 2 GPa. The stresses measured are therefore small; the resolution of the frequency shift measurement and the errors due to experimental setup must be small enough so that small stress magnitudes can be detected trough small frequency shifts.

In Raman spectroscopy, the resolution is a function of the slit width, the number of slits per millimeter of the natural line width of the laser used. How precisely the stress is measured depends on how accurately one can define the position of the diamond band and determine its center. The center of the band is taken as the position of the band rather than the maxima of the band peak. If the diamond band is symmetric, then the maxima is obviously at the center of the peak which can be then easily measured. If the band is not symmetric, the center of the peak has to be determined by either a graphical method or a computational method where the peak is fitted with a function and the center is mathematically computed. The resolution is therefore dependent on natural and artificial line broadening. The line width

(usually taken as the full width at half maximum) is the sum of the contribution of instrumental line broadening ranging from 2.5 to 4.0 cm^{-1} and which depends directly on the slit width of the spectrometer, on the intrinsic broadening and non homogeneous stress effects. The natural line width of the diamond band is 1.65 cm^{-1} [74]. As explained earlier, there can be a broadening of the band due to non homogeneous stress distribution in the scattering volume, resulting in more then one displaced diamond phonon frequency. A small increase (less than 1 cm^{-1}) in line width over the natural line width indicates both homogenous stress distribution [74] and limited instrumental broadening. High resolution is obtained with a slit width of 75 microns when the line width represents true width without instrument broadening [26]. Slit widths of 150 to 400 microns will result in medium to low resolutions. At low resolution of 8 cm^{-1}, the line suffers from instrument broadening [9,22]. A 3 cm^{-1} resolution is considered high resolution[9]. A spectrometer slit width of 100 microns resulting in a spectral resolution of 1 cm^{-1} [75]. The lateral spatial resolution Raman spectroscopy was reported to be 2 microns within the optical skin depth [32], (more conventional characterization techniques have a spatial resolution about 1 mm) [32]. 1 micron lateral resolution and 6 microns depth resolution have also been reported for Raman spectroscopy [63].

Whalley [75] measured the diamond band center graphically by determining the mean frequency of the band as a function of intensity.

A best line fit is then drawn through the obtained points. The line is extrapolated to the band. The intersection with the band is taken as the band center and peak position [75].

Measuring the peak position by the line extrapolation method is accurate to within 0.1 cm^{-1}, the error was taken as the standard deviation for many repeated measurement [75]. The error in shift measurement taken as the standard deviation from repeated measurements was 1.3 cm^{-1} [74], 1.2 cm^{-1} [65]. The errors of 1.2 and 1.3 cm^{-1} in references [74] and [65] are higher than in reference 75 for the same measurement method. Errors as high as 1.3cm^{-1} are too high for stress measurement in diamond films, since the shifts observed are of the order of 1 to 3 cm^{-1}. A computer generated position measurement would reduce these errors. A computer software can be used to isolate and expand the peak of interest from the rest of the Raman spectrum. Errors in the order of 0.1 cm^{-1} can be achieved (See section on experimental procedure).

A critical element to precise measurement of the peak position is the calibration process with a Raman spectra having well known peak positions. Calibration can be accomplished with peak p0sition accuracy to within 0.05 cm^{-1} [66].

4.4.4 limitations and sensitivity

Stress measurement by Raman spectroscopy is a powerful tool for surface stress measurement, for diamond, the laser focal depth is 20 to 30 microns [65,74]. The skin depth is usually in the order of 2 microns for non transparent material. Thus the main limitation of the Raman stress measurement method is that only surface stress measurement can be achieved. However, for thin films of thickness equal or less than the skin depth at the laser wavelength used, all of the film is in focus, and thus stress over the entire film is averaged. Another limitation of the method is that the stress measured represent the area within the laser diameter and the skin depth. Thus, unless the stress is known to be uniform, the measurement is not only at the surface but also local. Measurement at various location of the surface is necessary to map the stress distribution. As explained earlier, the local stress measurement can be used as a means to measuring stress anisotropy. If the film thickness profile is known, the laser spot can be applied at point where the thickness is known; the dependence of stress on film thickness can for instance be evaluated. Conversely, the measured magnitudes of stress over a given area could be used to map the film thickness variation over the given area.

The Raman signal is not sensitive to cluster sizes about 50 Å in diameter. Raman spectrum of diamond film consisting mainly of diamond clusters 40 Å in diameter did not show a diamond line, so local stress

at those clusters cannot be measured from Raman shifts. For the same 40 Angstrom diamond clusters, X-ray absorption near edge structure (XANES) spectroscopy showed the same spectrum as for diamond with fully developed grains [29], thus proving to have a higher sensitivity to very small particles. Small amounts of diamond in graphite cannot be detected since scattering cross section of graphite is 50 times that of diamond [78]. The sensitivity of the Raman signal can be enhanced with surface enhanced Raman spectroscopy (SERS). With SERS, it is possible to analyze layers 20 nm in mean thickness by coating the diamond surface with a mono layer of silver [78]. SERS is thus an excellent way to measure stress in very thin films that are 20 to 50 nm thick and can be used as an in situ method for stress monitoring during film growth. In situ measurement allow to measure the intrinsic growth stresses separately since thermal mismatch stresses develop only upon cooling to room temperature from the deposition temperature.

Another limitation of Raman spectroscopy is that thermal decomposition of films can occur at high laser power, if the laser power is reduced to avoid thermal decomposition of the film, the signal can be weakened. In diamond films, thermal decomposition did not occur at low laser power of 60 mW [37].

The advantage of Raman spectroscopy over conventional methods is its sensitivity to very small perturbation to the crystal phonon frequencies. For instance X ray diffraction measurement of lattice constant ranging of 0.3562 nm to 0.3566 nm did not yield any

recognizable differences while well resolved shift up to 2.7 cm-1 from the same diamond samples with a 3 cm^{-1} resolution [9]. It is however difficult to resolve shifts less than 0.2 cm^{-1}. For a diamond film a 0.2 cm^{-1} correspond to a stress of 0.08 GPa which is less than the average error reported in the calculation of the stress in diamond films with the Raman shift.

Another advantage of Raman spectroscopy arises when there is more that one film layer on substrate. Peaks from the various layers can be obtained and the stress in every layer can be calculated. The absorption of the various film layer becomes critical since the laser light can be fully absorbed before it reaches a given layer. To measure stress by other methods, the layer are etched out one by one and net changes are attributed to the specific layer removed.

Stress measurement by Raman spectroscopy is a non destructive techniques [32]. Since, a simple optical microscope is used to focus the laser beam on the sample, the sample dimensions are often not a problem. An optical microscope can be designed to accommodate any specimen size.

5- DEPOSITION THERMAL STRESS

5.1 Effect of deposition temperature, thermal stress

Residual stress arising from thermal expansion mismatch between the film and the substrate depends on temperature difference ΔT, between the substrate temperature during film growth and the measurement temperature, usually room temperature. The thermal strain ε_{Th} is then [8]

$$\varepsilon_{Th} = \Delta\alpha(T)\ \Delta T. \tag{41}$$

$\Delta\alpha(T)$ is the difference of thermal expansion coefficients between the film and substrate. $\Delta\alpha(T)$ is a function of temperature since the thermal expansion coefficients of the film and substrate are each functions of temperature. As the deposition temperature increases, differential expansion stresses vary according to the temperature dependence of both the film and substrate's thermal expansion coefficients. Intrinsic stresses decreases with temperature [8]. The thermally induced stress, σ_{Th}, in the film can be calculated from the thermally induced strain in equation 41, and is given by

$$\sigma_{Th} = E_f\ (\alpha_f - \alpha_s)\ (T_s - T_0) \tag{42}$$

Where $E_f = E_f(T)$ is the Young's modulus of the film and $\alpha_f = \alpha_f(T)$ is the thermal expansion coefficient of the film, $\alpha_s = \alpha_s(T)$ is the thermal expansion coefficient of the substrate, T_s is the substrate temperature during deposition and T_0 is the measurement temperature. From the stress equation 42, stress dependence on the deposition temperature is evident.

5.2 Thermal stress modeling

Thermal stresses can be easily calculated for a thin film-substrate system. However, thermal stress in thin films is difficult to determine experimentally because the temperature of the film is not easily measured. Thermal stress arising from thermal expansion coefficient mismatch depends on the substrate temperature during deposition and the temperature at which the measurement of the stress is taking place and on the substrate material. If bending of the beam during heating is ignored (the substrate is much thicker than the film), the biaxial thermal stress is given by [55]

$$\sigma_{Th} = E_f \, (\alpha_f - \alpha_s) \, (T_s - T_0) \, / \, (1 - \nu_s) \qquad (43)$$

where $E_f = E_f(T)$ is the Young's modulus of the film, $\alpha_f = \alpha_f(T)$ is the

thermal expansion coefficient of the film, $\alpha_s = \alpha_s(T)$ is the thermal expansion coefficient of the substrate, T_s is the substrate temperature during deposition and T_0 is the measurement temperature. A positive stress usually exists in metal films over a glass substrate, while a compressive stress state develops in metal films deposited on alkali halide substrates [8]. In 0.25 microns thick chromium films, deposited on glass wafers by Magneton sputtering (current density of 25 to 300 Am^{-2}), the thermally induced tension (stress integrated over the thickness of the film) was measured as -21 Nm^{-1}. The total internal tension in the chromium film was -250 Nm^{-1} at the same thickness. The magnitude of thermal stress is therefore much smaller than that of the internal stress; less than on tenth in this case [55]. The stress was measured from the change in the substrate curvature. (Equation 25)

5.3 Variation of stress with deposition temperature

During the deposition period, the substrate will expand. When a film has a smaller thermal expansion coefficient than the substrate, the substrate shrink more than the film during the cooling down to room temperature. Compressive stresses develop in the film provided no slippage in the interface occurs between the film and substrate (figure 14) . A tensile stress will develop if the film has a higher thermal expansion coefficient than the substrate. For instance, GaP films

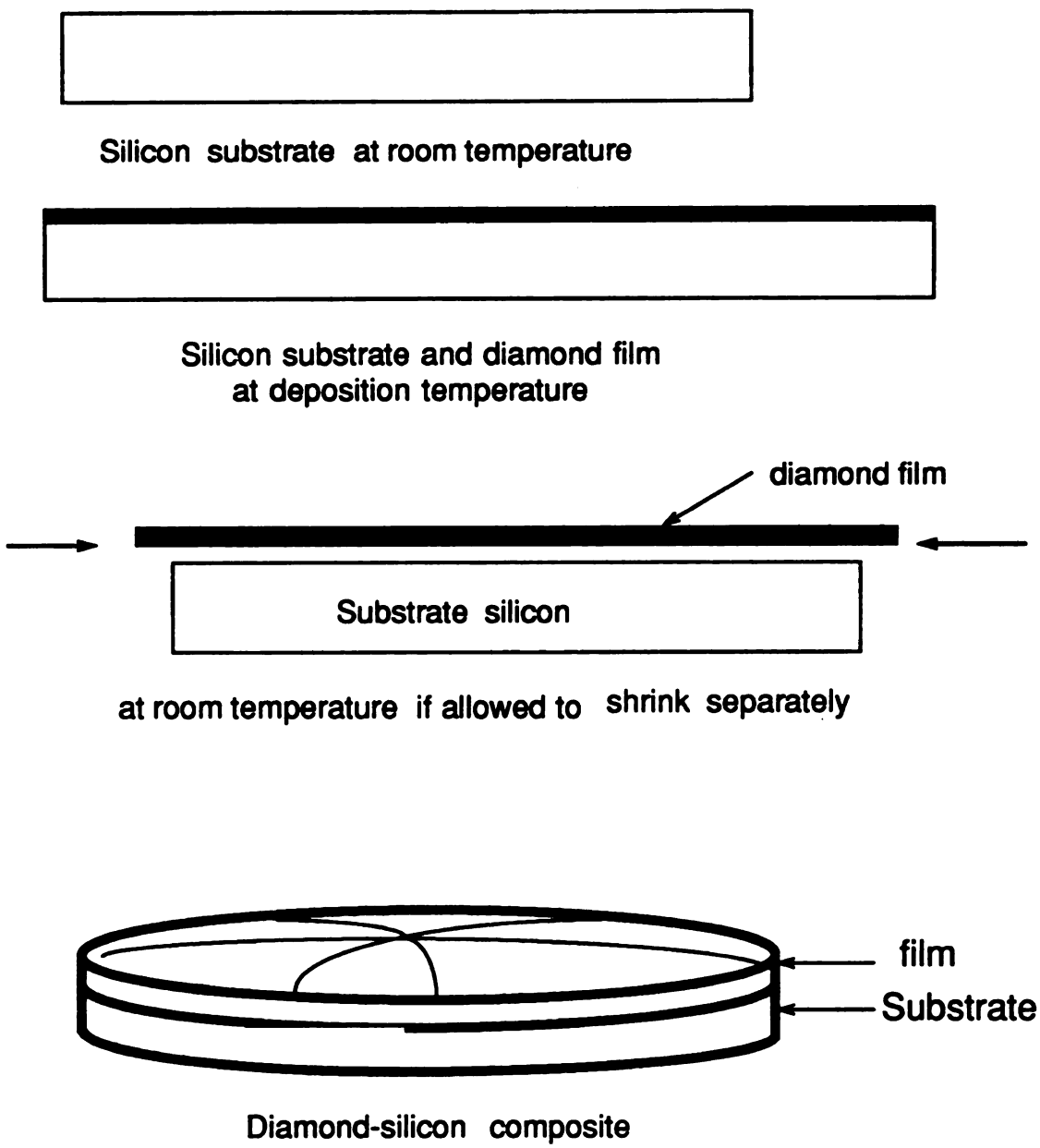

Figure 14. Graphical representation of thermal stress development in diamond films on a silicon substrate.

deposited on silicon substrates developed a tensile thermal strain equal to 0.9 x 10^{-3} , thermal expansion coefficient of GaP is greater than that of silicon [4].

Diamond films deposited on silicon substrates have differential thermal stresses that are compressive as long as they are deposited at a temperature less than 1220°C [10]. In most of the literature, thermal stress is calculated from

$$\sigma_{Th} = E_f \, (\alpha_f - \alpha_s) \, (T_s - T_0) \, / \, (1 - \nu_f) \qquad (43)$$

Generally a single average value of the thermal expansion coefficient is used for the entire temperature interval from deposition to room temperature [4]. Furthermore, the Young's modulus is treated as a temperature independent constant [10] which of course is not the case. For DLC films deposited at low temperature around 100°C the assumptions may be justified since the temperature interval is not as high as in CVD films where the temperature interval between deposition and room temperature can be as high as 1000°C. Windischmann used a better approach to calculate the thermal stress. Windischmann used an average value of $\alpha_f - \alpha_s$ for every 100°C temperature interval, then summed the individual contributions of all intervals [10].

A new model for thermal stress calculation is presented here and believed to be an improvement over the model presented by

Windischmann [10]. The Young's modulus of diamond and the thermal expansion mismatch between the film and the substrate are temperature dependent, consequently, an integration over the deposition to room temperature interval is used here instead of adding up stress contributions from a number of finite temperature intervals as proposed by Windischmann. The model is essentially not very different from the model used by Windischmann; by integrating over the temperature range, contribution to stress from an infinite number of intervals are added up instead of finite 100 degrees intervals, as used by Windischmann. The temperature dependence of the Young's modulus of diamond is taken into account while Windischmann treated the Young's modulus as temperature independent. The biaxial thermal stress will be recalculated in this work taking into account the temperature dependence of the expansion coefficients of the film and the substrate as well as the Young's modulus of the film .

The thermal strain in the films was given by

$$\varepsilon_{Th} = \Delta\alpha(T)\ \Delta T. \qquad (41)$$

The $\Delta\alpha(T)\ \Delta T$ term should be treated as the contributions of the thermal expansion difference $\Delta\alpha$ at a temperature interval dT summed over the entire temperature range. Therefore equation 41 should be

rewritten as

$$\varepsilon_{Th} = \int \alpha_f(T) - \alpha_s(T)\, dT \qquad (44)$$

from the deposition temperature to room temperature. The thermal expansion coefficients of silicon and diamond are functions of temperature (figure 15). The thermal expansion coefficient data in figure 15 was used to calculate the thermal expansion coefficients difference $\alpha_f - \alpha_s$ at regular temperature intervals.

The data for $(\alpha_f - \alpha_s)(T)$ as a function of temperature was fitted by linear regression analysis. The resulting fitted function is given by

$$(\alpha_s - \alpha_f)(T) = +1.64\,10^{-6} - 4.01\,10^{-9}\,T + 3.3\,10^{-12}\,T^2 - 1.88\,10^{-15}\,T^3 \qquad (45)$$

where T is in degree Celsius The above function (equation 44) was fitted with a correlation coefficients R =0.997 (figure 16). The above fit is a good as can be further seen in the plot of the residual (figure 17).

The Young's modulus of diamond is expected to decrease with temperature as is the case for many ceramics. For instance, the Young's modulus of alumina [79] was found to decrease with temperature according to Watchman's equation (equation 46) [79]. Anderson [80] argued that Watchman's equation is valid for many ceramic oxides as long as the Poisson's ratio is not a strong function of

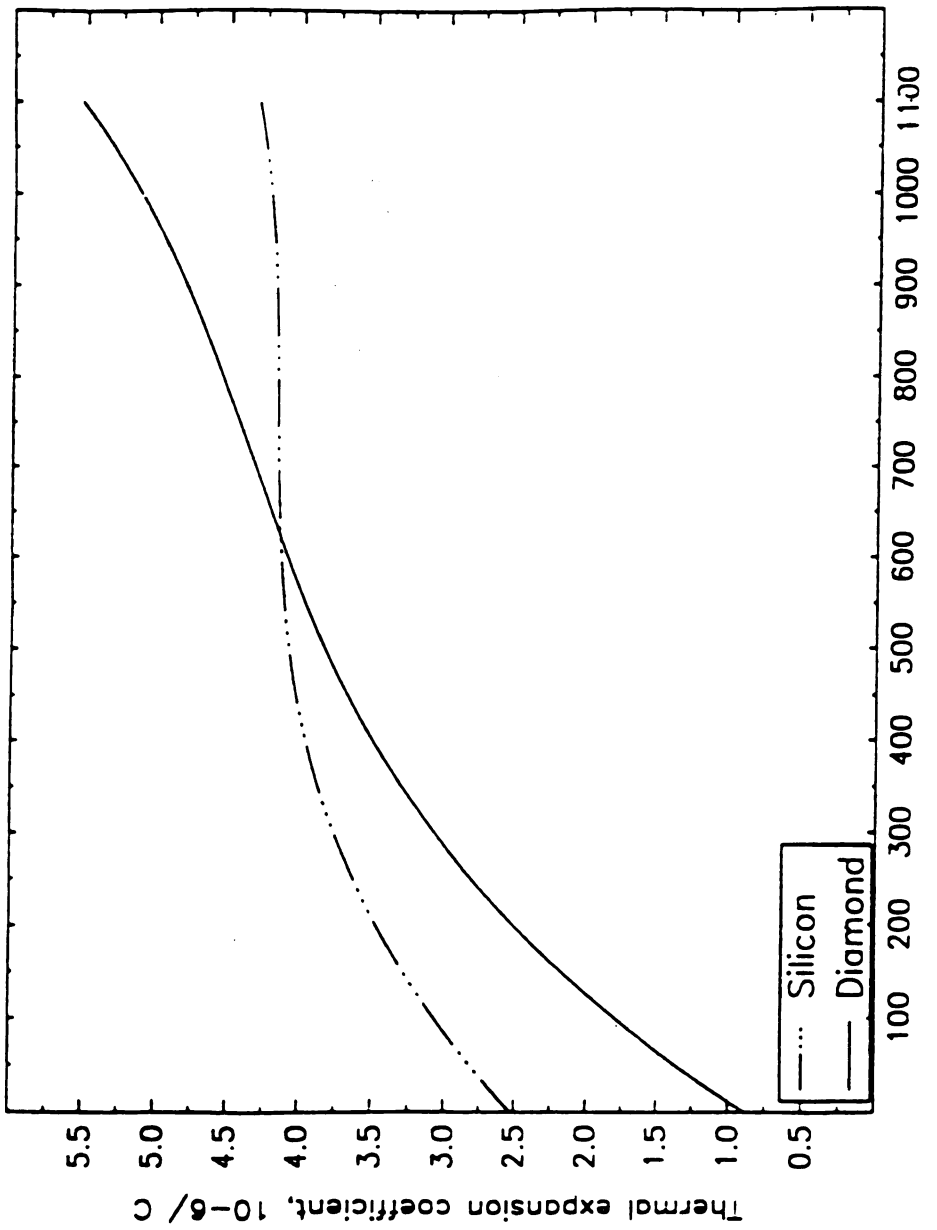

Figure 15. Temperature depndence of the thermal expansion coeffecients of silicon and diamond [81].

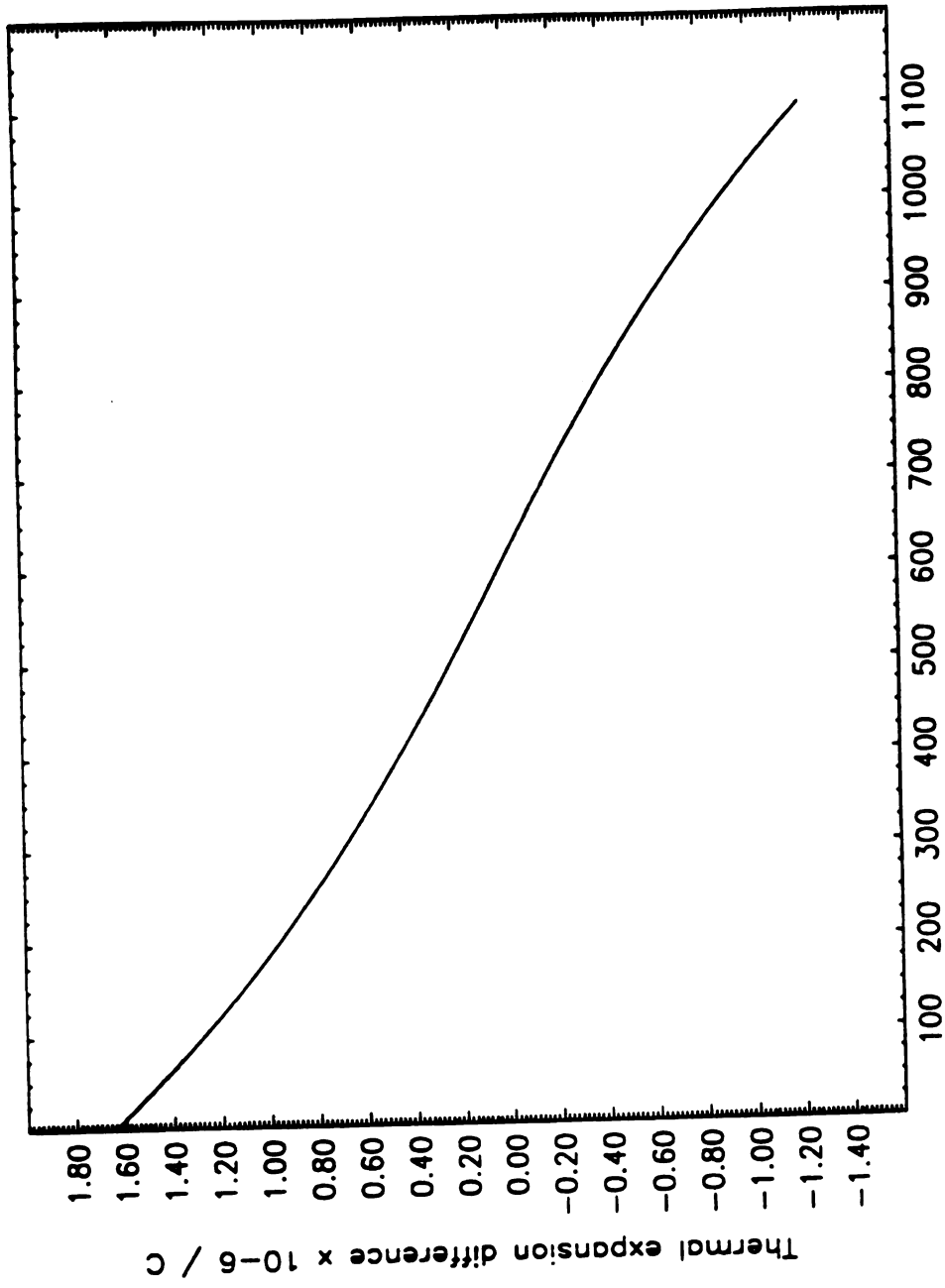

Figure 16. Difference of thermal expansion coefficient od diamond and silicon as function of temperature. R=0.997.

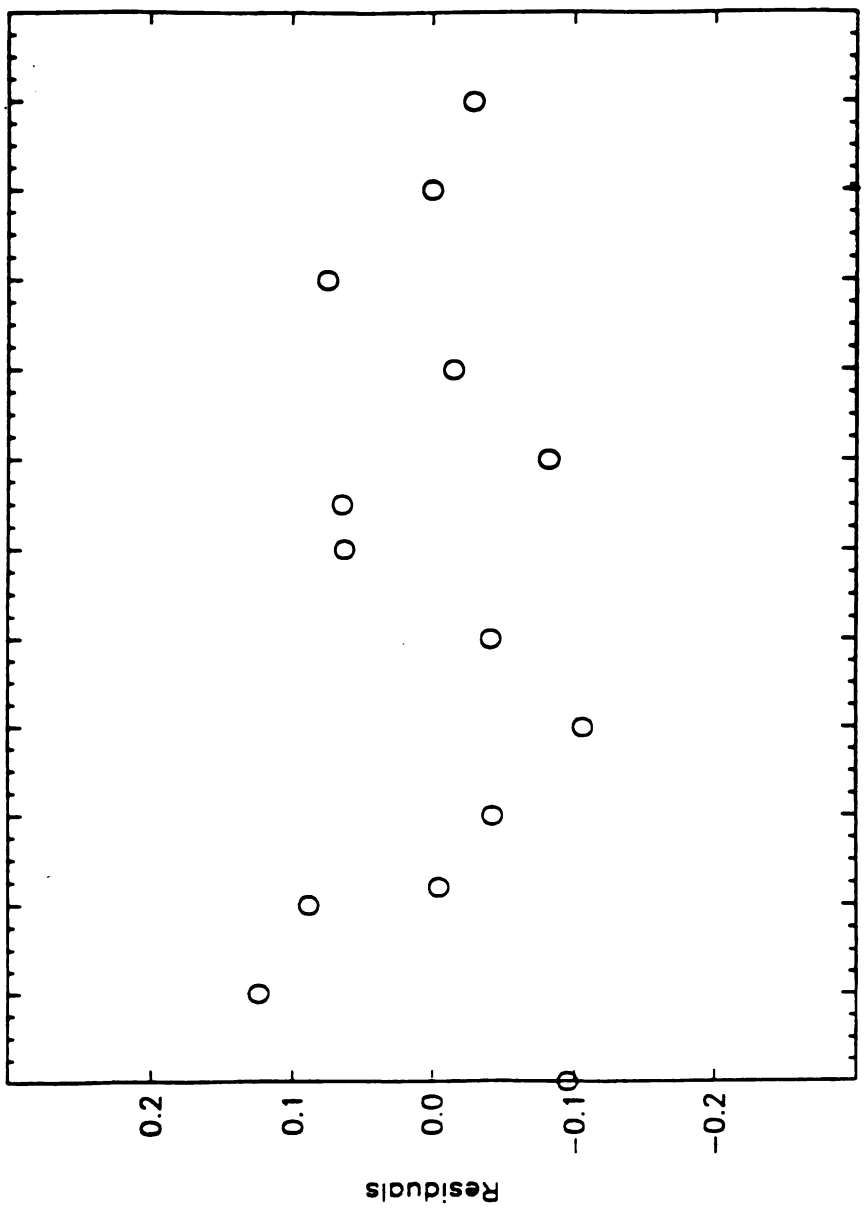

Figure 17. Residuals as a function of temperature for the cubic fit for the thermal expansion difference in figure 16.

temperature. Anderson [80] attempted to relate the empirical temperature independent constants of Watchman's equation to the Debye temperature and the Gruneisen constant [80].

Experimental data for the temperature dependence of the Young's modulus of diamond could not be located. Some elastic constant values of diamond are available [9], however, data for elastic constants from the same author at different temperatures were not available. Due to the scatter in the elastic constant data in the literature, Young's modulus of diamond at various temperatures cannot be calculated from published data either.

Alternatively, an estimate of the temperature dependence of the Young's modulus of diamond is attempted here. As is the case for many ceramic oxides, the temperature dependence of the Young's modulus of diamond is assumed to behave according to Watchman's equation. The latter assumption involves the assumption that the Poisson's ratio of diamond is not a strong function of temperature. Watchman's equation is given by

$$E(T) = E_o - b \exp (- T_o / T) \qquad (46)$$

where $E(T)$ is the Young's modulus at a temperature T, E_o is the Young's modulus at zero degree Kelvin and b and T_o are experimentally determined parameters. Anderson estimated T_o to be

equal to half the Debye temperature [79]. The Debye temperature of diamond is Θ=2248 degree Kelvin [81] such that T_o =1224 K. We assume that there is no fall off in the magnitude of Young's modulus from zero degrees Kelvin to room temperature, thus E_o can be estimated as1150 GPa which is the room temperature value of Young's modulus of diamond [82]. The last step would be to estimate the value of the b constant. For many ceramics, the magnitude of the Young's modulus is drops about 1 percent for every 100 degrees temperature increase. For instance, the drop off in the Young's modulus of alumina [79] and MgO [80] was about 1 percent per 100°C. The constant b is then calculated from the drop off of the Young's modulus. A value of 0.4 was calculated for b assuming a drop off in the Young's modulus of about 1 percent per 100°C for diamond. Watchman's equation for diamond's Young's modulus with the assumptions mentioned above is then given by

$$E(T) = 1145 - 0.4 \exp (- 1224 / T), \qquad (47)$$

where $E(T)$ is in GPa and is T in degree Kelvin. Figure 18a is a plot of $E(T)$ as a function of temperature according to equation 47.

The temperature range of interest for diamond deposition is 300 to 1300 K (0 to 1000°C). Since $(\alpha_f - \alpha_s)(T)\ E(T)$ needs to be integrated later a polynomial approximation of $E(T)$ makes the

integration easier. The E(T) curve over the 300 t0 1300 K was therefore fitted to a cubic with a correlation coefficient equal to R=1.0. The fit is clearly very good. The approximated function of over 0 to 1000°C (figure 18b) is then given by

$$E(T) = 1147.22 - 2.81\,10^{-2}\,T - 2.55\,10^{-4}\,T^2 + 8.410^{-8}\,T^3 \qquad (48)$$

where E(T) is in GPa and is T in degree Celsius.

Now that expressions as a function of temperature exist for both the Young's modulus and the thermal expansion difference, the thermal stress $\{(\alpha_f - \alpha_s) \times E\}\,(T)$ can thus be integrated over the deposition temperature range. Let

$$\Phi(T) = \int \{(\alpha_f - \alpha_s) \times E\}\,(T)\,dT \qquad (49)$$

Then the thermal stress is given by

$$\sigma_{Th}(T) = \Phi(T_s) - \Phi(T_0) \qquad (50)$$

Since the measurement temperature is usually room temperature, then T_0= 25°C and $\Phi(T_0)$ is treated as a constant. By substituting equations 47 and 48 into equation 49, and evaluating Φ(25°C), and substituting

the expression for $\Phi(T=T_s)$ and $\Phi(T_0=25°C)$ into equation 50, the following expression for $\sigma_{Th}(T)$ is obtained

$$\sigma_{Th}(T) = 4.58\,10^{-2} - 1.89\,10^{-3}\,T + 2.32\,10^{-6}\,T^2 - 1.18\,10^{-9}\,T^3 + 2.7\,10^{-13}\,T^4 - 2.3\,10^{-16}\,T^5 + 1.27\,10^{-19}\,T^6 - 2.3\,10^{-23}\,T^7 \qquad (51)$$

Figure 19 is a plot of the biaxial thermal stress as a function of the deposition temperature according to equation 51 corrected for the various values of Poisson's ratio of diamond reported in the literature [83,76,82,60]. One should note here that the Poisson's ratio value of 0.07 [82,60] has been reported in two recent studied on polycrystalline diamond films, which is the microstructure studied here.

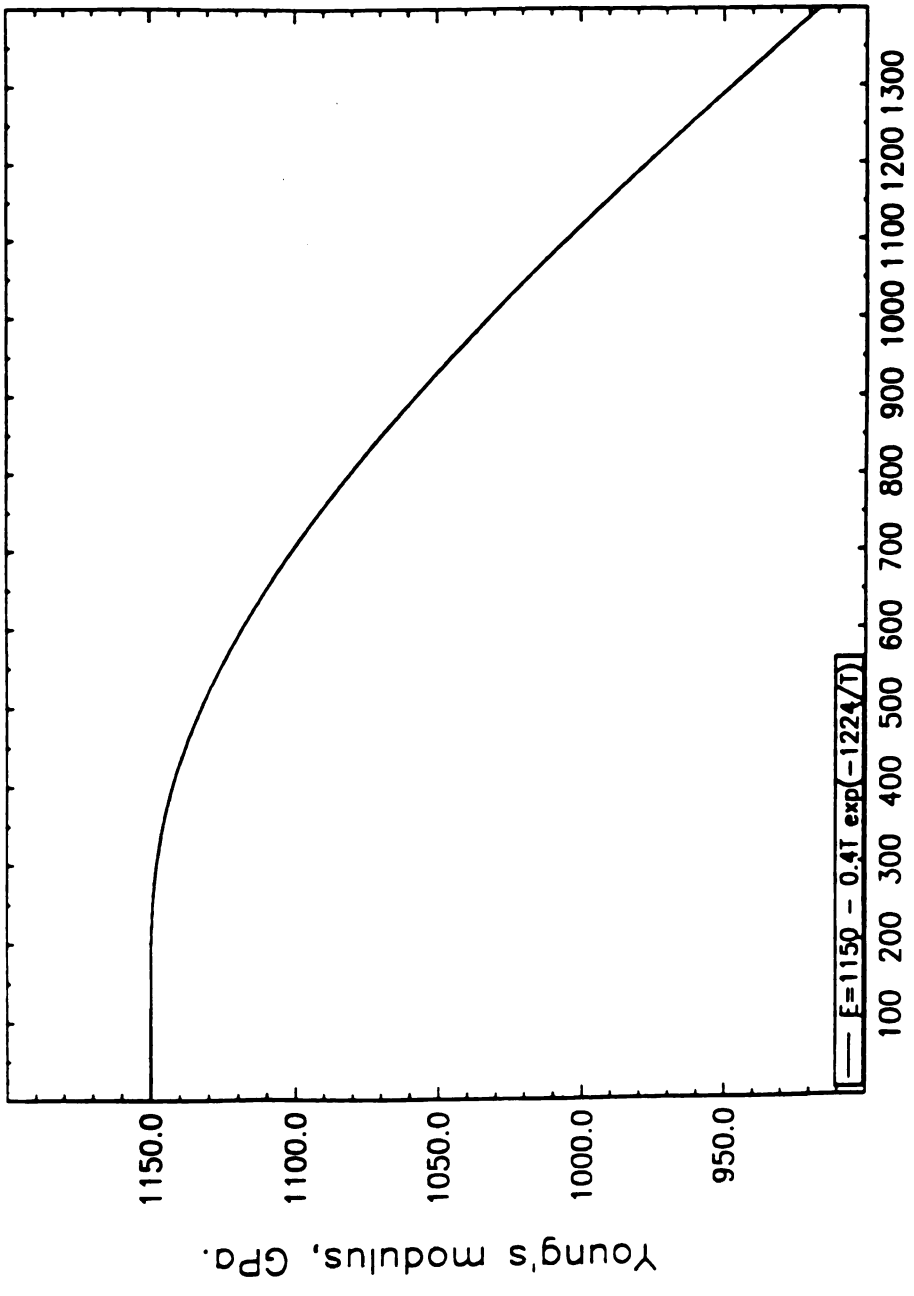

Figure 18a. Variation of Young's modulus with temperature accoeding to Wachtman's equation 47.

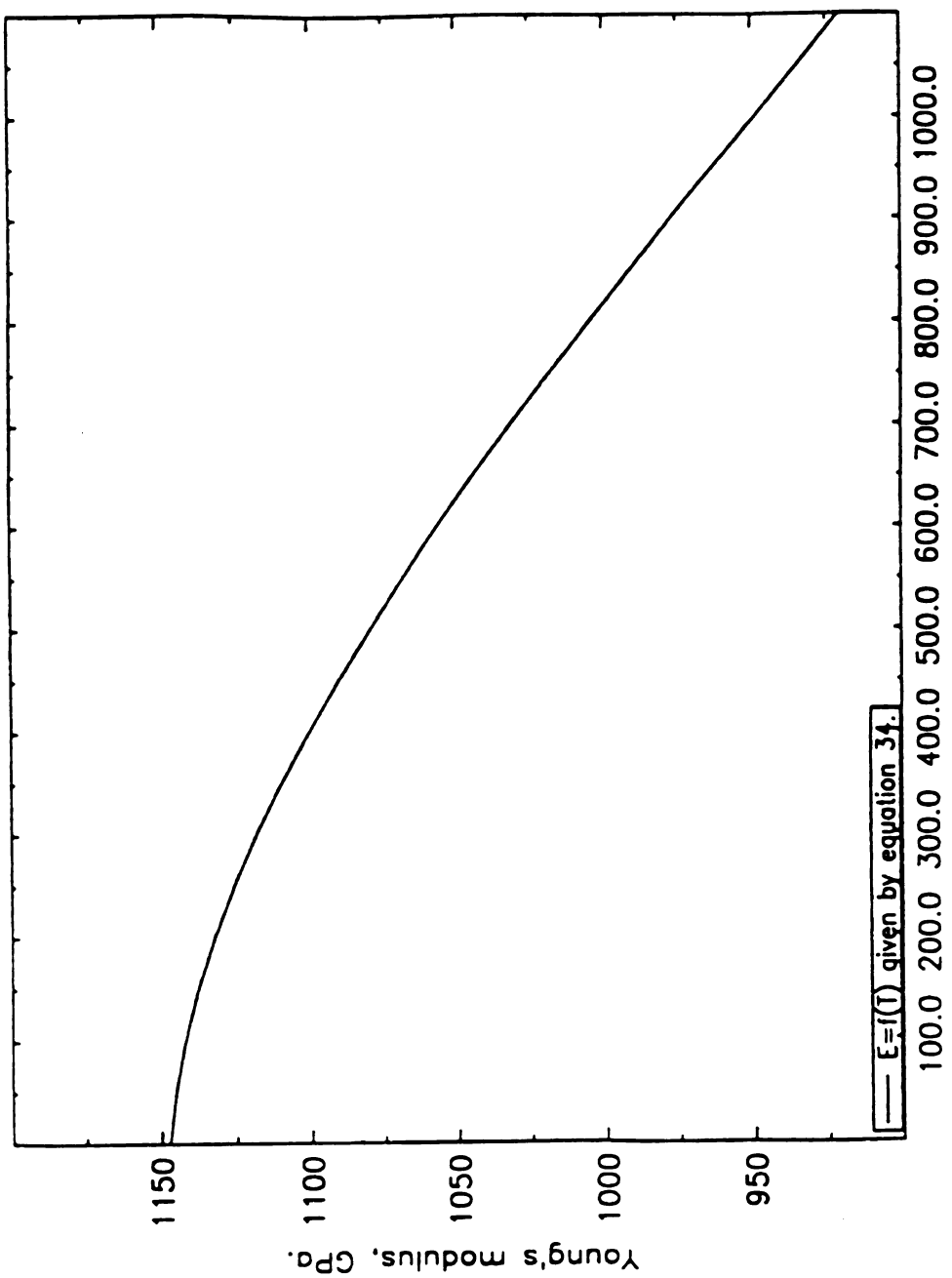

Figure 18b. Temperature depence of Young's modulus fitted to a cubic function in the CVD temperature deposition range with R=1.0.

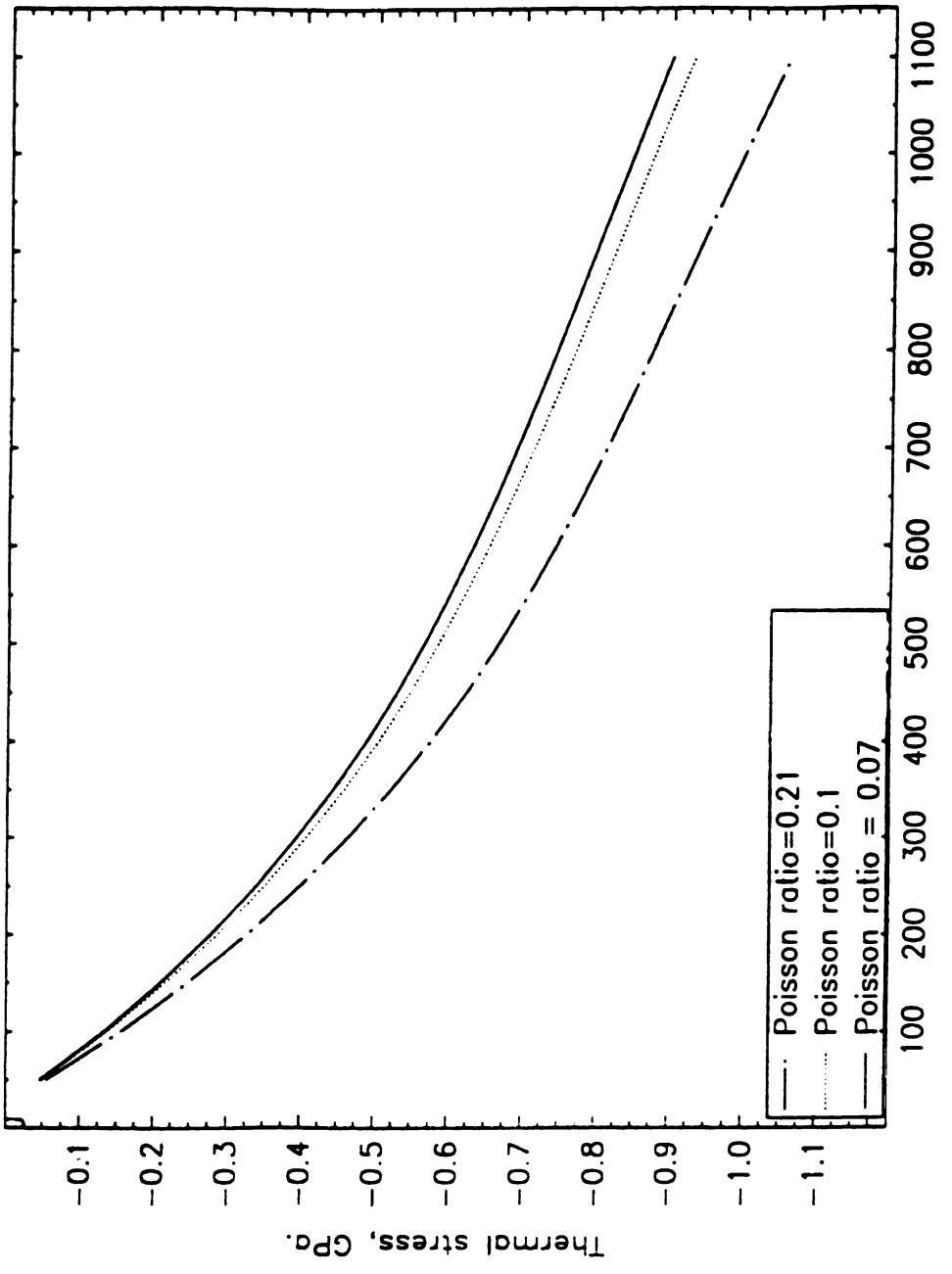

Figure 19. Temperature dendence of thermal stress calculated from equation 51.

6- EXPERIMENTAL PROCEDURE

6.1 Materials

The samples used are silicon wafers with the (100) crystallographic axis perpendicular to the surface of the wafer. One surface of the silicon wafer is polished and the backside is rough. Reference 84 provides the specification about the cutting, polishing, surface roughness as well as other information. Measurement on the silicon wafers were carried in the as provided state with no modification to the wafers except for an annealing treatment.

One (100) silicon wafer with diamond films deposited on the polished side was supplied by Jie Zhang, a Ph.D. student in the Electrical Engineering department at Michigan State University. The silicon wafers were two inches in diameter, including the wafer with the deposited diamond film.

6.2 Diamond deposition

Diamond films were deposited by Jie Zhang on (100) silicon wafers using the microwave plasma chemical vapor deposition (MPCVD) [85] method. The MPCVD deposition was carried at 2.45 GHz. The deposition temperature was 980C and the deposition plasma pressure was 70 torr, the microwave power was maintained at 750mW. The

deposition lasted less than four hours. The deposition atmosphere was a mixture of 1.0 percent methane in hydrogen. The deposition setup is illustrated in figure 2 of reference [85].

6.3 Curvature measurement

The curvature in the silicon wafer with and without the deposited diamond film was determined by measuring the center deflection (bow) in the silicon wafer. The bow was determined from the surface profile obtained with a DEKTAK IIA type surface profilometer.

To carry a measurement on the DEKTAK IIA, a sample is placed on a rotary stage (127 mm in diameter) that allows to rotate the sample 360 degrees about an axis perpendicular to the stage surface. The positioning of the sample is done with an X and Y thumb wheel that allows to move the rotary stage (thus the sample) in the X and Y horizontal directions. A rough leveling wheel allows the rotation of the sample about an axis running parallel to the rotary stage surface (thus parallel to the wafer surface); this rough leveling allows to position the sample so that its surfaces are as parallel as possible to the horizontal plane. The rotary stage does not move up and down. Instead, a focus knob allows to move in the Z direction an arm into which is connected the stylus, a camera and an optical microscope. The focus knob is used to put the sample surface in focus for either the optical microscope or the camera so that details to be measured are in focus. When a camera

is used, a video screen shows the stylus and the area around the contact between the sample surface and the stylus. All of the already described functions are manually operated.

When the DEKTAK IIA is turned on, the video screen shows various options that can programmed for the measurement. The parameter to be programmed and automatically executed later are the scan length from 50 microns to 30 millimeters, the scan speed ranging from low to high, the scan range with automatic or manual sample leveling, the scan profile type, a step or peak and valley type. An R cursor and M cursor stand for reference and measurement cursors can be moved on the video screen to obtain measurements at any point within the scan length.

The DEKTAK IIA has a vertical resolution of 0.5 nm. The stylus tip radius is 12.5 microns. The stylus tracking force is field adjustable from 10 to 50 mg. The maximum sample thickness allowed is 20 mm. The Dektak profilometer is connected to a thermal printer as the output device.

Once the parameters are programmed, a measurement can be done. The video camera focuses from the stage to about 20 mm above the rotary stage. The sample is positioned and put in focus with the camera. The scan mode is turned on. An initial scan is executed according to the stored parameters. The first profile of the surface is usually not leveled; the profile appear on the video screen such that the first contact point appear at Z=0 and the point at the end of the scan

appears at some point on either side of the Z=0 plane. The rough leveling thumb wheel is used to rotate the sample such that both the begin and end point of the scan are at the Z=0 plane. Two function are available for automatic improved leveling and Zeroing (setting the end point of the scans to Z=0) when the manual leveling is close to within few thousand Angstroms from leveling at Z=0). The profile is finally in its final form and a measurement can be obtained. The profile can be manipulated by moving the borders of the plot. A copy of the final plot is sent to the printer. A measurement of the height of a feature for instance can be either done on the printout, since it is properly scaled, or alternatively by moving the reference cursor which reads the horizontal position or the measurement cursor which reads the height of a given feature.

The above procedure was used to measure the center deflection of the silicon wafers in the as provided state, on annealed silicon wafer and on the silicon side of the diamond-silicon film before and after it was annealed. No measurement was carried directly on the film surface to avoid stylus tip scratching because of the very high hardness of diamond. The scan length was kept constant at 30 mm in all samples

6.4 Annealing heat treatment

Annealing of the diamond film on the silicon substrate and two silicon wafers was carried in a non oxidizing atmosphere. The furnace

used was an MRL Thermtec three-zone horizontal muffle tube. The temperature control is achieved by a Eurotherm type 812 controller toward the middle of the tube and type 810 Eurotherm controller at the two ends of the tube. The samples are placed in an alumina inner tube, on top of a tube dee that provides a flat surface. All the samples were placed on silicon scrap pieces to avoid contact and contamination from the alumina. The inner tube is sealed with a stainless steel sealant a plastic gasket. The seal allows for the constant flow of nitrogen gas during the annealing. The inner tube is heated inside the muffle tube. Two inconel tubes are connected to the inner alumina tube trough the stainless steel seal and to the nitrogen gas source. The gas flow arrangement consist of the tubes connecting the nitrogen source, a mechanical pump, two Nupro T valves and a flow meter.

Two silicon wafers and the silicon-diamond sample were placed inside the alumina tube, the temperature controller was programmed such that a temperature increase rake at 10°C per minute heats up the inner tube and the sample to 650°C, the temperature was then maintained at 650°C for one hour. Finally, a temperature decrease rake of 10°C per minute cools down the set up to room temperature, the samples were left in the furnace overnight to make sure they cool down slowly so that no thermal stresses develop during cooling.

During the heating rake, the inner tube chamber was first vacuum pumped to remove the air in it. The vacuum is then turned off and by using one of the valves, the inner tube chamber was flushed with

nitrogen. The nitrogen flow was increased until a flow rate of 2 liter per minute was set. The nitrogen gas was flowing during the heating, annealing and cooling stages. The nitrogen flowing out of the inner alumina tube through a plastic tube was released in an oil bath preventing air from flowing in the inner tube during annealing.

6.5 Raman spectroscopy

Raman spectra of all the samples were taken with a laser Raman microprobe available at the department of chemistry, and operated by Dr. Thomas Carter, chemistry specialist, department of chemistry at Michigan State University. The laser used is a Spectrophysics model 164 continuous argon ion laser operated through a cavity prism that isolates the laser wavelength used from the laser plasma lines. The laser is operated at 487.98 nm. An external prism further disperses the exciting laser light to isolate laser plasma from the 488 nm line. The sample is placed on the stage of the micro attachment of a Spex 1877 tipple spectrometer. The laser light is focused on the sample using a series of mirrors and a Zeiss (L. D-EPIPLAN) 40 times objective lens which is also used to collect the back scattered light from the sample. The scattered light is received by the tipple monochrometer-detector assembly with three dispersion stages that are essential to reducing the amount of stray radiation reaching the detector which otherwise can overshadow the much less intense Stokes scattered radiation. The

dispersion elements are ruled gratings. Raman spectra are then acquired with scanning monochrometers that allow to detect only the frequencies of interest. The output of the scanning is a plot of the scattered intensity as a function of the wavenumber. The output is sent to a minicomputer system that can record the data and plot it on a monitor. The stored data is then used to generate a plot with any of the conventional plotting computer software.

Throughout the various scans, the laser power was 850 mW, with only 85 mW reaching the sample surface. A slit width of 100 microns was used. The detector dispersion elements was set to 1800 grating per millimeter. The laser light was in normal incidence to the surface of the sample and was polarized such that the electric field is parallel to the sample and stage surfaces.

6.5.1 Calibration for Raman spectroscopy

The calibration is done with a toluene sample. Toluene has several sharp peaks the position of which are independent of the laser wavelength. Toluene fluid is inserted in a capillary tube and placed on the stage in contact with the laser beam. The laser light is focused on the toluene sample and a scan is taken. When all the toluene peaks are sharp and well resolved, the calibration is carried by first assigning the appropriate wavenumber to each known peak according to the standard toluene Raman spectrum. The actual positions of the toluene peaks from

the calibration sample are fitted with a cubic to match the assigned values to the various peaks. The peak positions in wavenumber are then checked. If all the peaks are at the correct wavenumber position within an acceptable error, the calibration is done and actual measurements on any sample can be carried. It was noticed during the calibration that the error in the position of the peaks in not constant from one peak to another. This is attributed to the cubic nature of the peak position fit. To reduce the effect of the variation in errors from peak to peak, the calibration with toluene was done differently depending on whether the sample scanned is silicon or diamond. When the sample scanned was diamond the calibration was done such that the center of the spectrum is at the diamond position of 1332 cm^{-1}. Similarly, the calibration spectrum is centered at the silicon position at 521 cm^{-1} when silicon samples were scanned. This procedures proved capable of reducing the errors of both silicon and diamond spectrum measurements.

6.6 Film thickness and grain size measurement

Micrographs taken with scanning electron microscopy SEM were used to measure the film thickness and the grain size in the diamond film on the silicon wafer.

Strips about 1 cm long and 3 mm wide were cut from the silicon-diamond wafer. The strips were mounted on cylindrical stand with an epoxy / araldite (Ciba-Geigy) glue that cures and hardens in a few

minutes after it is applied. One sample was glued flat on the stand such that the diamond film faces up, and was used to take micrographs of the grain size. Two other samples were mounted and glued on one edge to allow for the measurement of the diamond film and silicon substrate thicknesses. All three samples were then sputtered with gold with an EMSCOPE gold sputterer. The gold sputtering was done at a 0.1 torr vacuum at 20 mA. The sputtering rate was 7 nm per minute. After 3.5 minutes, the sputtered gold film thickness was about 24.5 nm. After the gold sputtering, the samples were scanned with a JOELJSN-35CF scanning electron microscope (SEM), operating at 15 KV accelerating voltage. The magnifications used for film thickness measurement ranged from 160 times for the silicon to1800 times for the thinner diamond film. The magnification used for grain size measurement on the diamond film was 6600 times.

The film thickness for the silicon and diamond was determined by taking several measurements on the micrographs. An average value of the film thickness was then calculated.

The grain size of the diamond film was determined by the linear intercept method, where the grain size G is given by $L / (n M)$, where L is the measured length on the micrograph n is the number of the line-grain boundary intersections and M is the micrograph magnification.

7- EXPERIMENTAL RESULTS

7.1 Curvature measurement

The results of the curvature measurements are summarized in table 5. The curvatures of the as provided silicon wafers was measured on three separate wafers respectively called silicon1, silicon 2, and silicon 3. Only silicon wafers 2 and 3 were later annealed. All three silicon wafer had two curvatures in opposite directions, probably from buckling to maintain the mechanical stability of the wafer. Figures 20, 21 and 22. The original deflection of the silicon wafers in the as provided state, was taken as the average of the two deflection measurements in silicon 2 and 3 and equal to $d_o = 19.15\ 10^3 \pm 500$ angstroms. Silicon1 wafer had two defections, almost symmetric about the center of the wafer. Thus it is not used for the reference deflection calculation.

There was no obvious change in the curvature of the annealed wafer silicon 2 and 3 (figures 23 and 24) as compared to the same silicon 2 and 3 wafers in the as provided state. The diamond deposition caused the positive deflection of 19,150 Å to be reversed to a negative -76,000 Å bow (figure 25), resulting in a net bow change of -95,150 Å. The annealing of the diamond film caused the center

deflection to decrease from -76,000 to -65,000 Å (figure 26). Thus a net change of -11,000 Å resulted from annealing the diamond film on the silicon wafer. Surface profiles taken on the rough side of the uncoated silicon wafers had high surface roughness. Therefore, accurate deflection measurements from the rough side of uncoated silicon wafers were not possible.

Table 5. Curvature measurement results.

Sample	State	Center defection / Error (1000 Angnstroms)	Measurement surface
Silicon* 1	as provided	+6.2 / 0.5	polished
Silicon* 2	as provided	+19.8 / 0.5	polished
Silicon* 3	as provided	+18.5 / 0.5	polished
Silicon* 2	annealed	+19.8 / 0.5	polished
Silicon* 3	annealed	+18.5 / 0.5	polished
Diamond	as deposited	-76.0 / 2.5	Si/rough
Diamond	annealed	-65.0 / 2.5	Si/rough

* uncoated wafer

Silicon 1, 2 and 3 refers to the three uncoated silicon wafers numbered 1, 2 and 3 used in the experimental procedure.

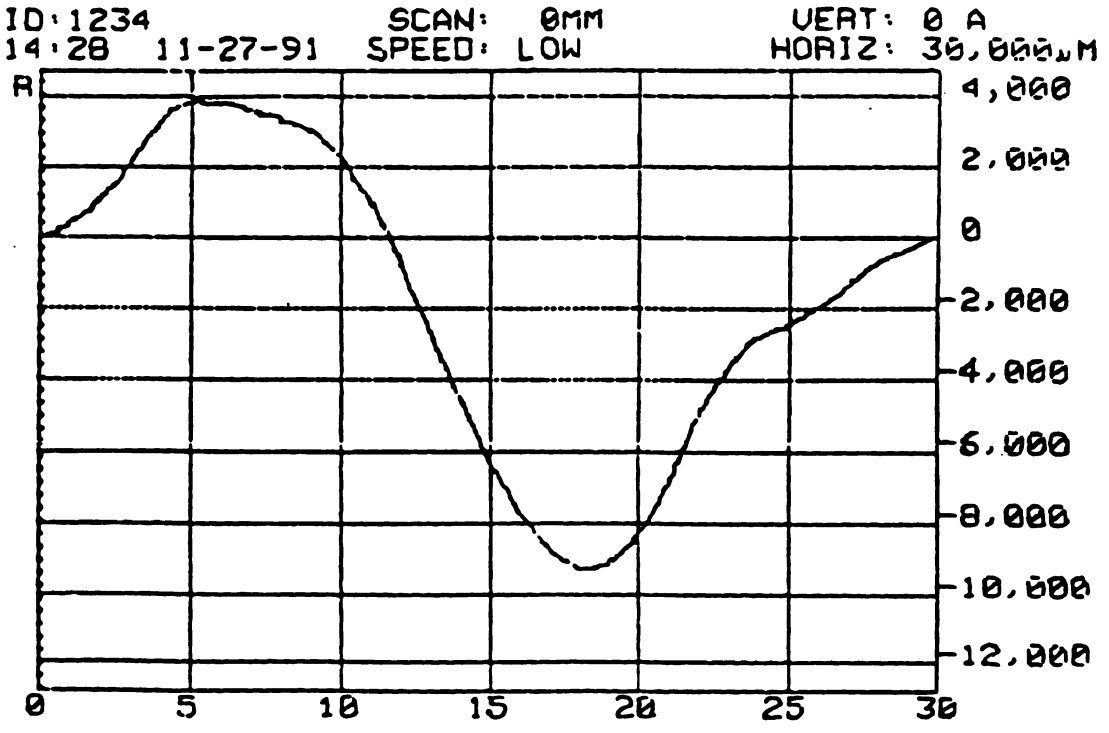

Figure 20. Surface profile of uncoated silicon 1 wafer taken with a dektak II on the polished side

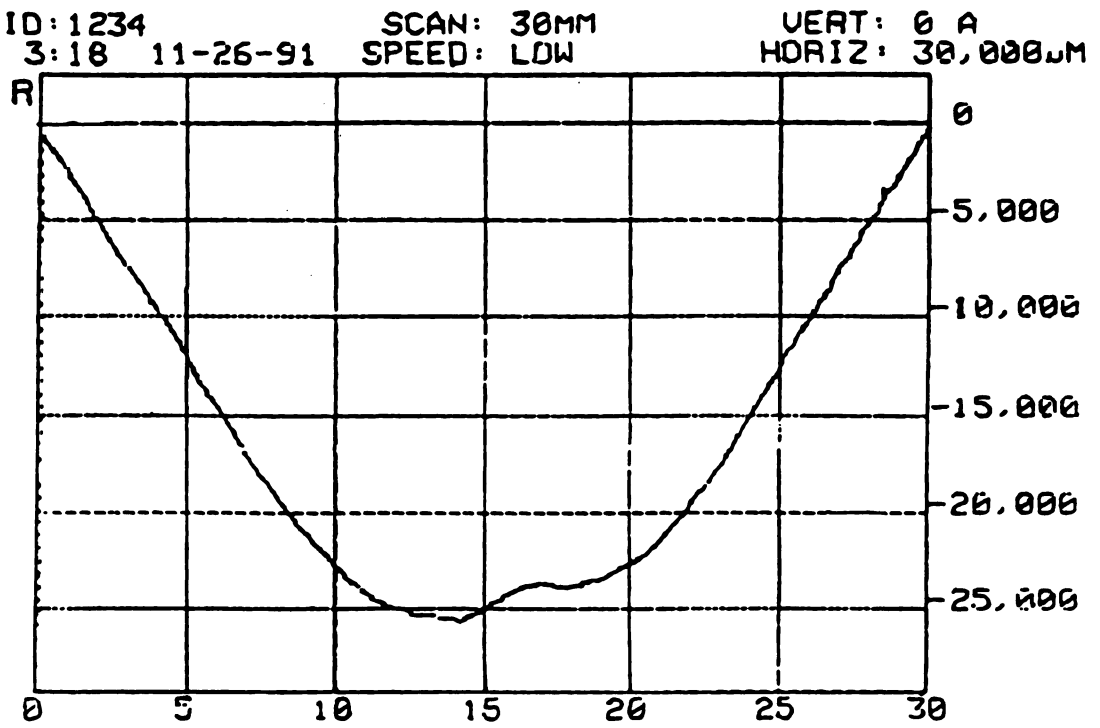

Figure 21. Surface profile of uncoated silicon 2 wafer taken with a dektakII on the polished side

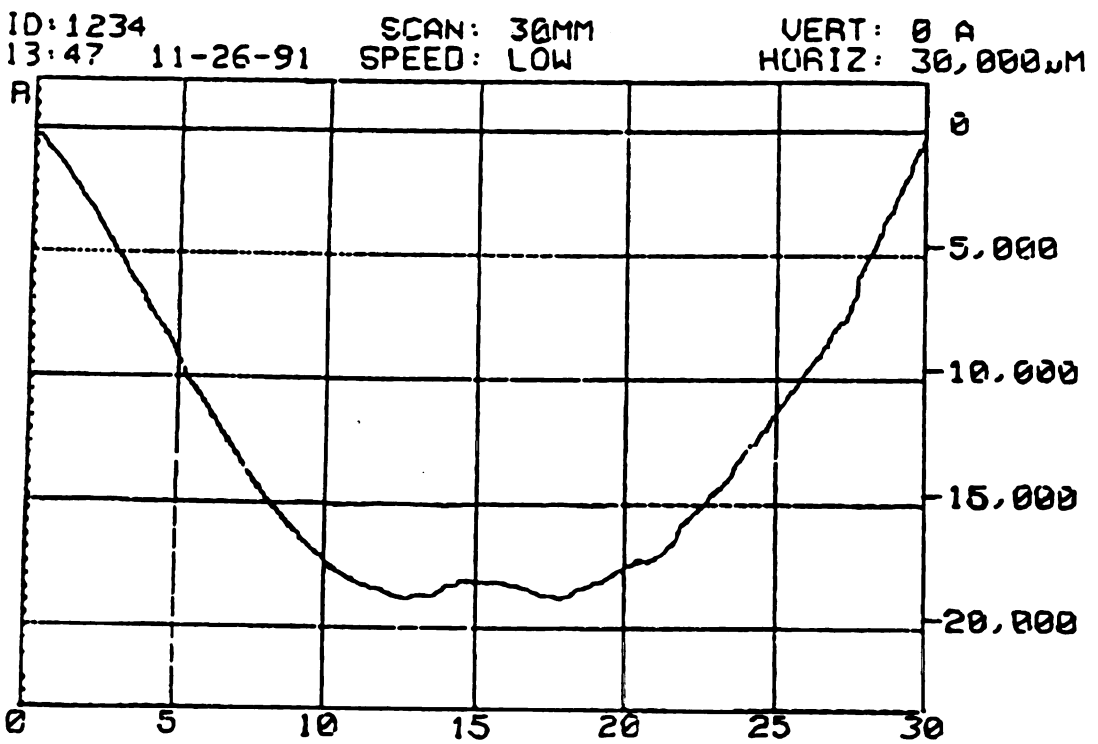

Figure 22. Surface profile of uncoated silicon 3 wafer taken with a dektak II on the polished side

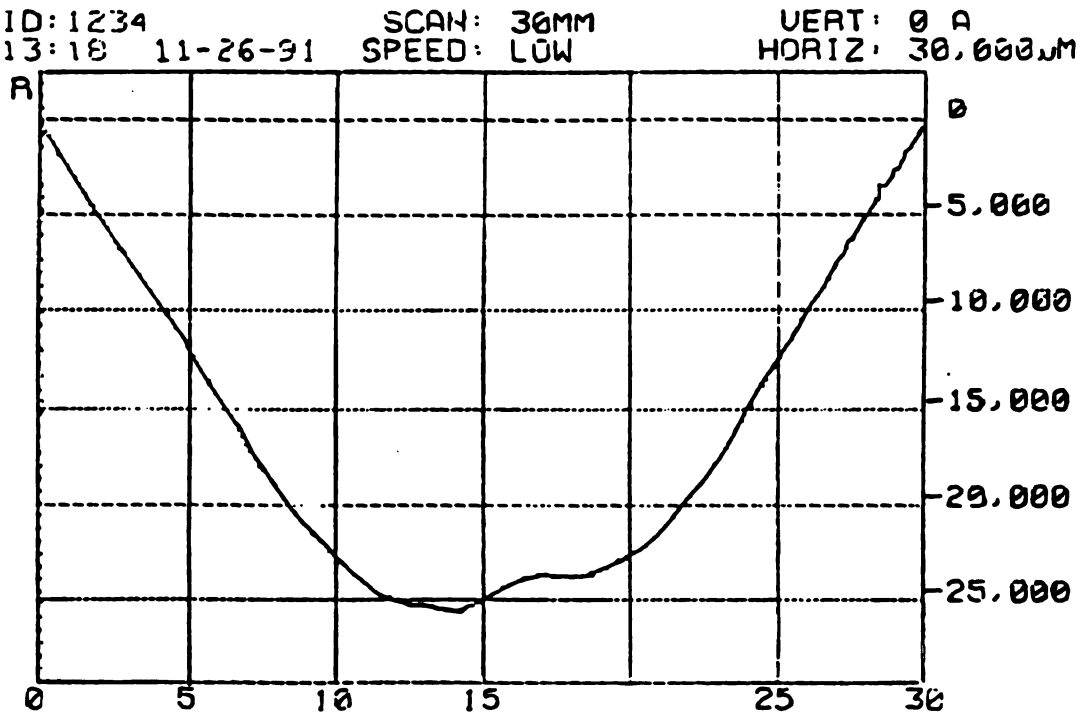

Figure 23. Surface profile of annealed and uncoated silicon 2 wafer taken with a dektak II on the polished side

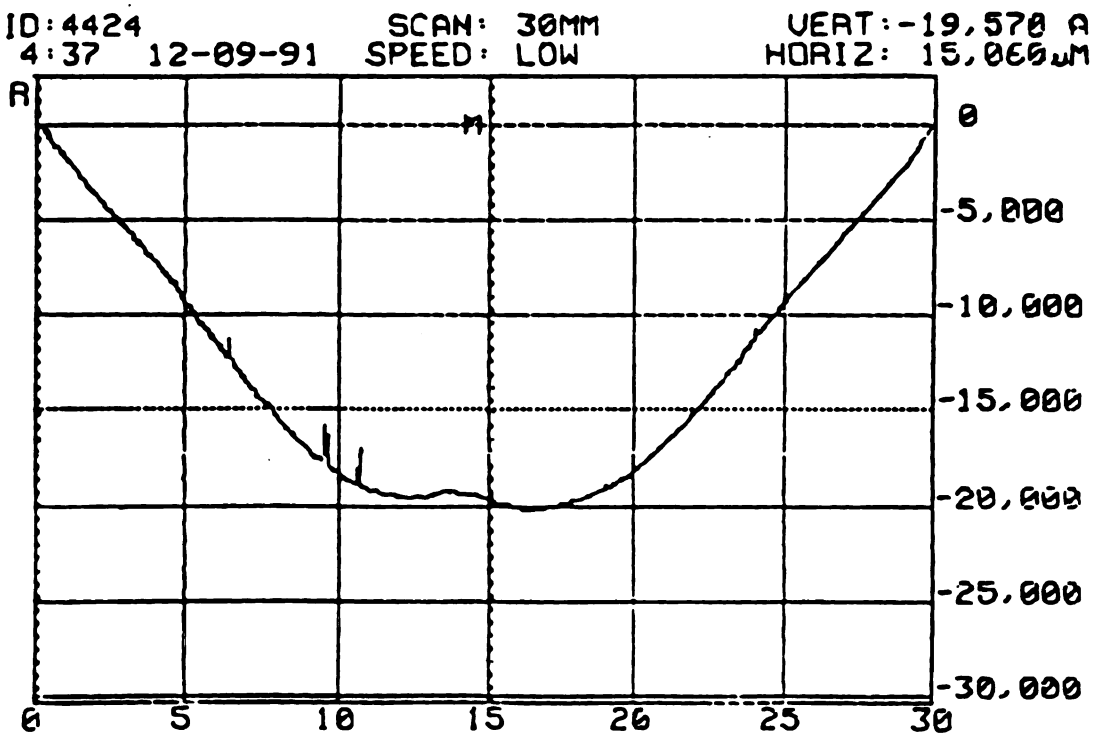

Figure 24. Surface profile of annealed and uncoated silicon 3 wafer taken with a dektak II on the polished side

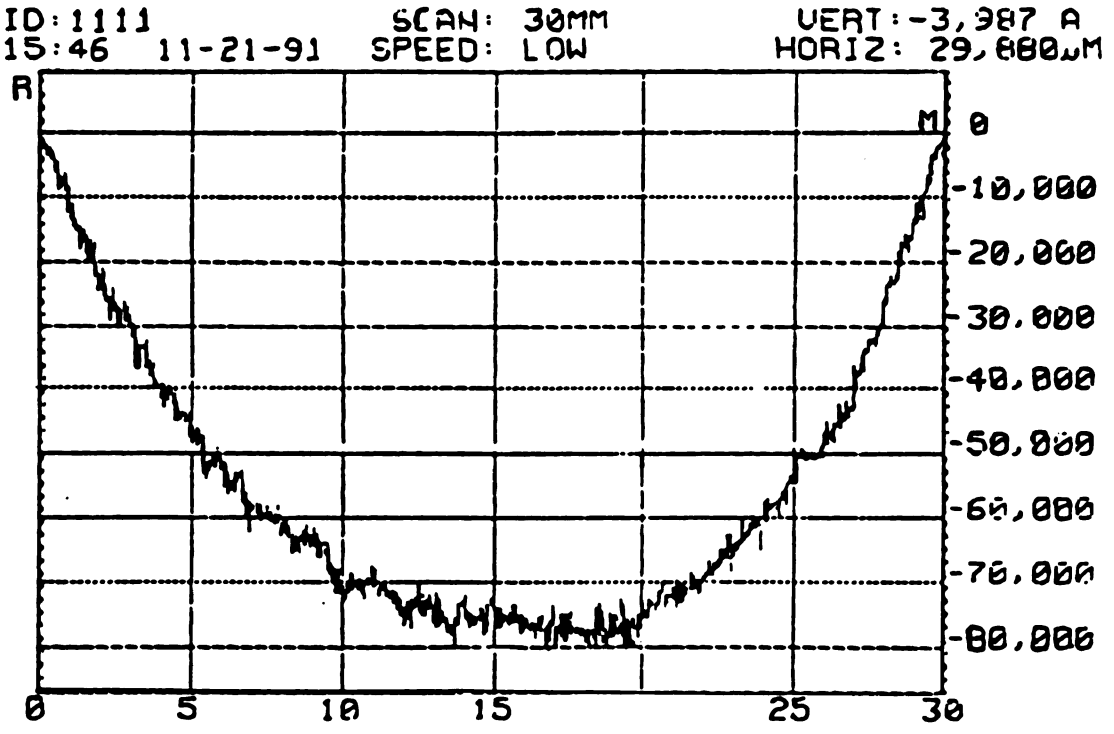

Figure 25. Surface profile of the diamond on silicon wafer in theas deposited state taken with a dektak II on thesilicon (unpolished) side.

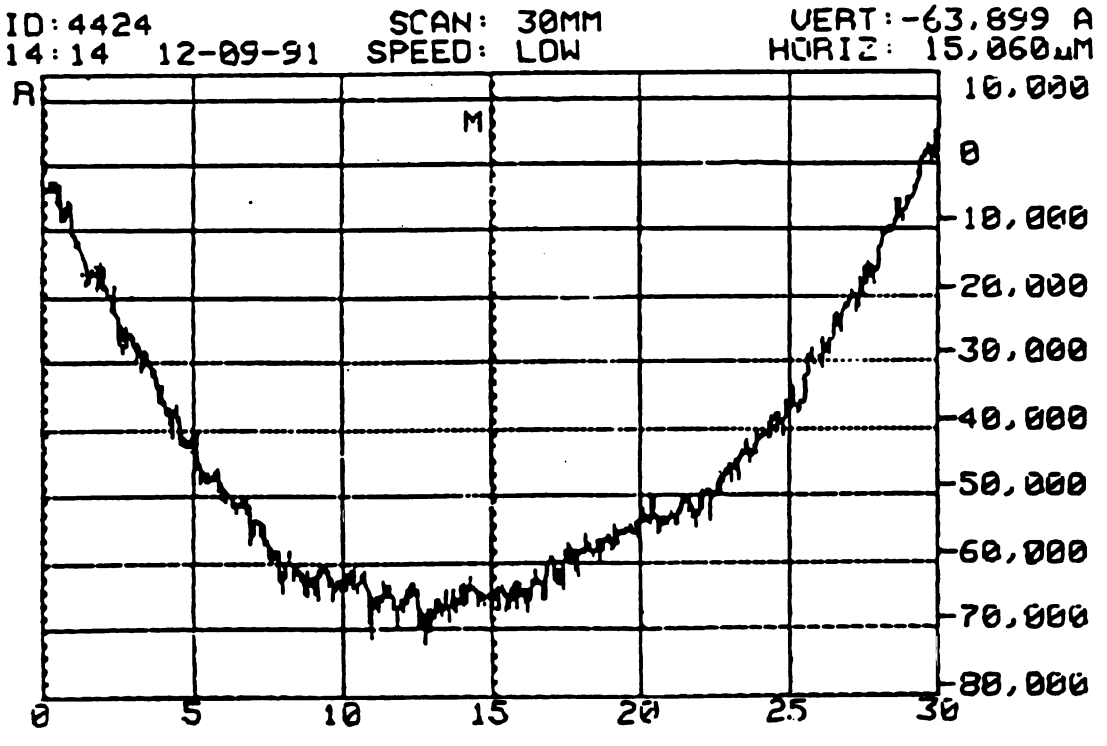

Figure 26. Surface profile of the diamond on silicon wafer in theannealed state taken with a dektak II on the silicon (unpolished)side.

7.2 Raman spectra and peak positions

The calibration spectrum obtained with toluene is given in figures 27 and 28. The calibration in figure 27 was done such that the error in peak position around the silicon peak is minimized. The calibration in figure 28 used for Raman spectra of diamond was centered around 1332 1/cm to minimize the error in the diamond peak position. Table 6 provides the toluene positions [86] and the measured toluene peaks after the calibration was done. The error in the peak position is also given. The measured values of the toluene peaks are read on the computer screen with the help of a cursor that can be moved to any point of the Raman spectrum. Since the position of the cursor is dependent the screen resolution, the variation in wavenumber corresponding to one screen pixel was measured to be 0.1 cm^{-1}. The calibration error due to the dependence of the cursor position on the screen pixel resolution is 0.05 cm^{-1}. The average error in the measured peak position (table 6) was 0.04 cm^{-1}. The error due to the calibration is thus taken as 0.05 cm^{-1} which is the larger of the two, since the two errors mentioned above are dependent.

The Raman spectra of the silicon 2 wafer on both surfaces in the as provided state are given in figures 29 and 30, and in figures 31 and 32 for the annealed silicon 2 wafer. Figures 33 and 34 give the Raman spectra of the silicon substrate surface before and after annealing, while the Raman spectra of the silicon substrate at the silicon diamond

interface are given in figures 35 and 36. Finally, the Raman spectra of the diamond film before and after the annealing heat treatment are given in figures 37 and 38 respectively. In all Raman spectra, the silicon and diamond peaks were isolated and expanded graphically without loss in resolution. A computer graphics software was used to expand the individual peaks given in figures 29a to 38a. Table 7 summarizes the results obtained for the peak position measurements

The method used here to determine the peak position is the same method described by Whalley [75] with 0.1 cm^{-1} error taken as the standard deviation for many repeated measurement [75]. The method was described in section 4.4.

7.3 Film thickness

Several film thickness measurements were taken on the SEM micrographs given in figures 39 to 43. All the measurements on figures 39 to 43 are from the same film-substrate sample. The silicon substrate thickness is uniform, since no variation greater than the measurement error were observed across the sample cut. The thickness of the diamond film however is not uniform. The film is thicker at the center of the wafer and becomes much thinner at the edges of the wafer. The diamond film thickness decreased from 1.25 microns at the center of the wafer to 0.5 microns at a radial distance of 20 mm from the center of the wafer. Several film thickness measurements were taken from figures 39

to 42 and resulted in an average diamond film thickness of 0.97 microns with a 0.11 microns standard deviation taken as the error in film thickness measurement. Along the 2 cm strip cut from the silicon-diamond wafer, most of the film is at a roughly uniform thickness of 1.2 microns. There was however a region of the film where the thickness is about 10 microns. The10 micron thickness region spreads only in an area of about 15 microns diameter and is not representative of the film thickness distribution. The average silicon wafer thickness was 0.456 mm with a 0.07 mm standard deviation (figure 43).

7.4 Grain size

The grain size of the diamond film was determined by the intercept method. The diamond film grain size was calculated to be 1.97 microns. The grain size seems to be uniformly distributed across the wafer as can be seen in figures 44 and 45 taken at two different locations on the diamond film. The diamond grains do not appear as sharp and as developed as MPCVD diamond grains in published works elsewhere [9]. The faces of the grains parallel to the silicon-diamond interface are clearly{111} family planes so that the normal to the film surface (necessary for the stress calculation from Raman shift) is of the<111> family directions.

Table 6. Toluene calibration peak positions and errors.

Toluene peak position (cm^{-1})	Toluene measured peak position (cm^{-1})	Error (cm^{-1})
521	521.0	0.0
622	622.1	0.1
786	785.9	0.1
1004	1003.9	0.1
1031	1031.0	0.0
1211	1211.0	0.0
1380	1380.0	0.0
1605	1605.1	0.1

Table 7. Raman peak positions of samples used.

Sample	State	Peak position (cm^{-1})	Measurement surface
Silicon 2*	as provided	520.62	polished
Silicon 2*	as provided	520.59	rough
Silicon 2*	annealed	520.49	polished
Silicon 2*	annealed	520.51	rough
Silicon substrate**	as provided	520.12	rough
Silicon substrate**	annealed	520.13	rough
Silicon substrate**	as provided	521.95	interface
Silicon substrate**	annealed	522.22	interface
Diamond	as deposited	1333.91	diamond
Diamond	annealed	1333.09	diamond

* uncoated wafer ** coated wafer

Silicon 2 refers to one of the hree uncoated silicon wafers numbered 1, 2 and 3 used in the experimental procedure.

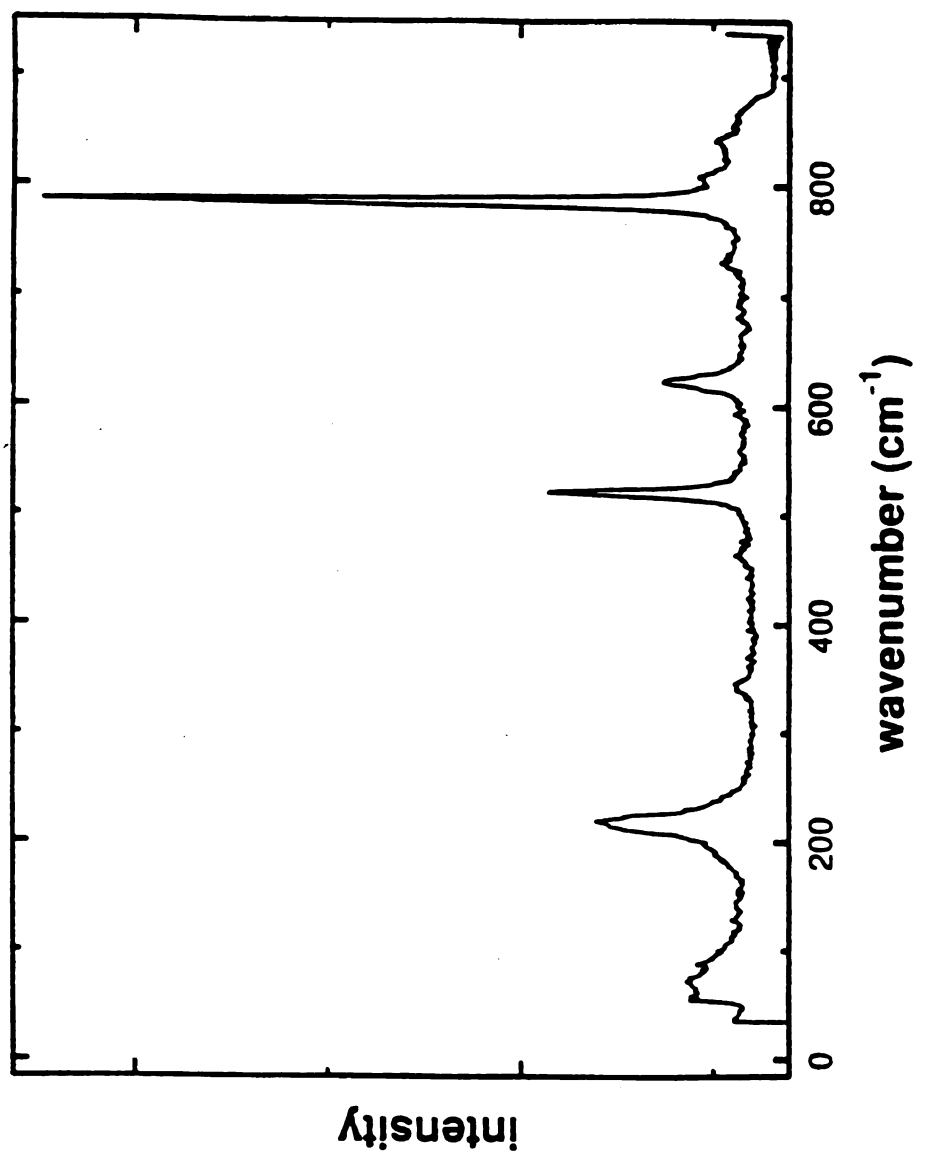

Figure 27. Raman spectrum of toluene used as calibration for silicon Raman spectra and taken with a 488 nm argon laser at 1800 g/mm and 100 microns slit width.

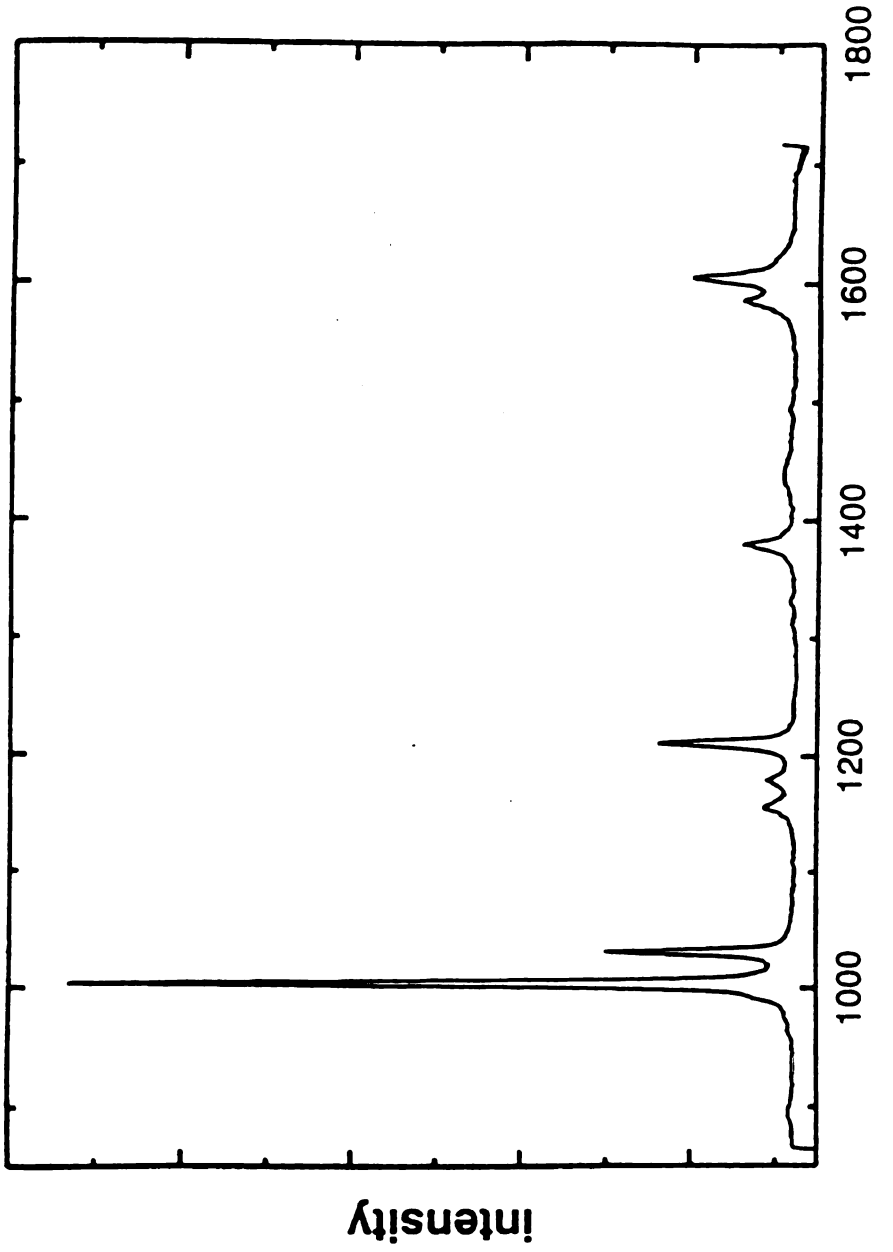

Figure 28. Raman spectrum of toluene used as calibration for diamond Raman spectra and taken with a 488 nm argon laser at 1800 g/mm and 100 microns slit width.

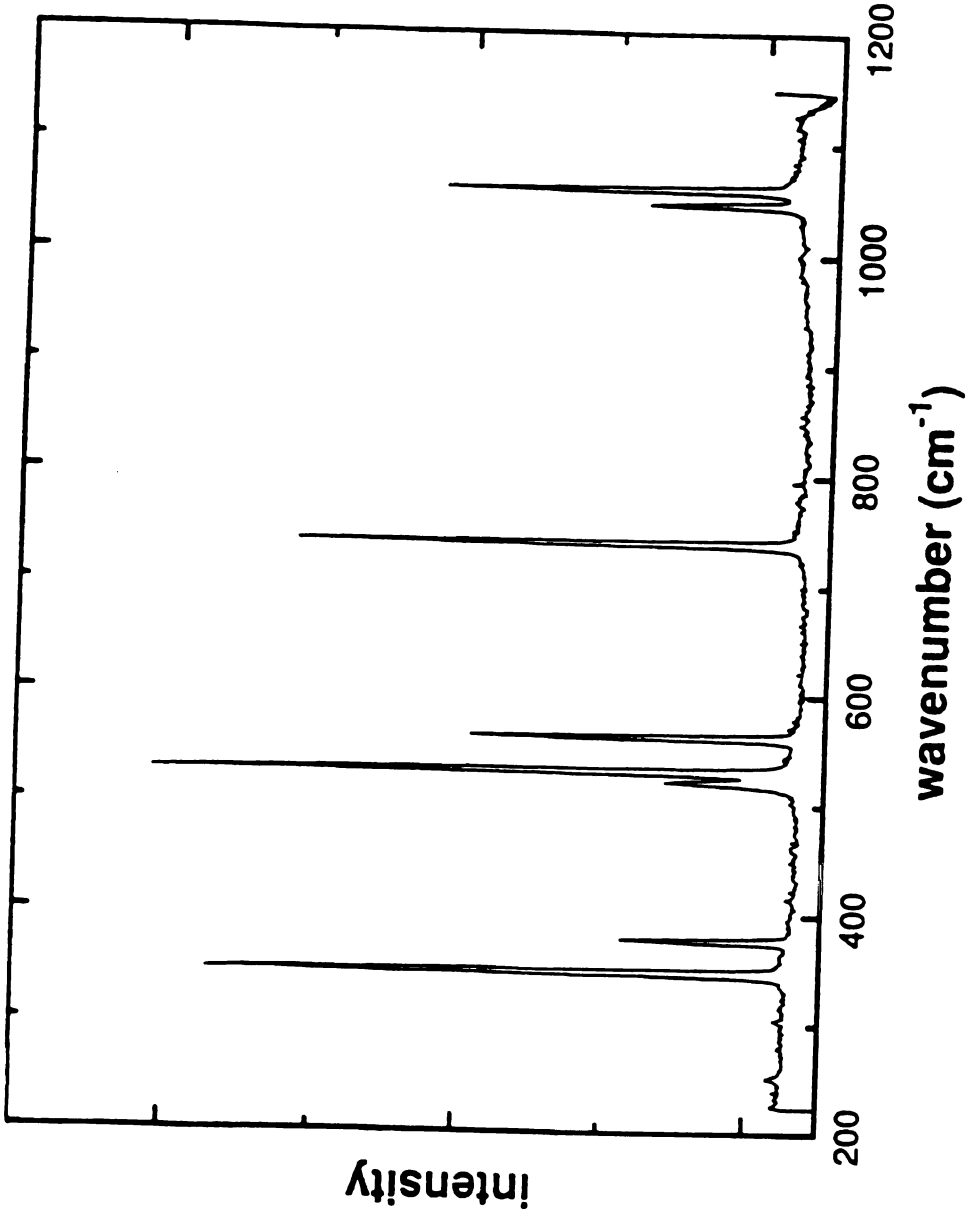

Figure 29. Raman spectrum of uncoated silicon 2 wafer on the rough side taken with a 488 nm argon laser at 1800 g/mm and 100 nms slit width.

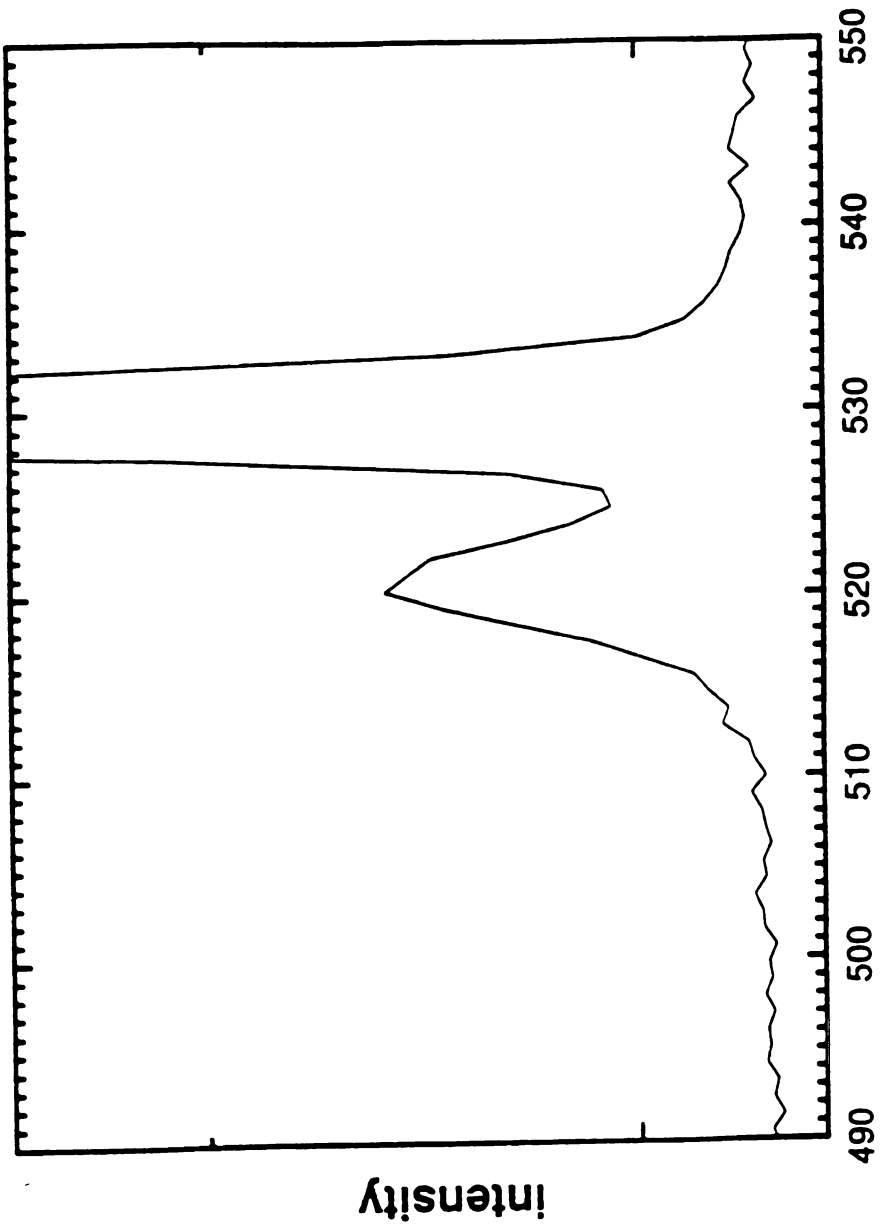

Figure 29a. Expanded silicon peak from the Raman spectrum of uncoated silicon 2 wafer on the rough side. Figure 29.

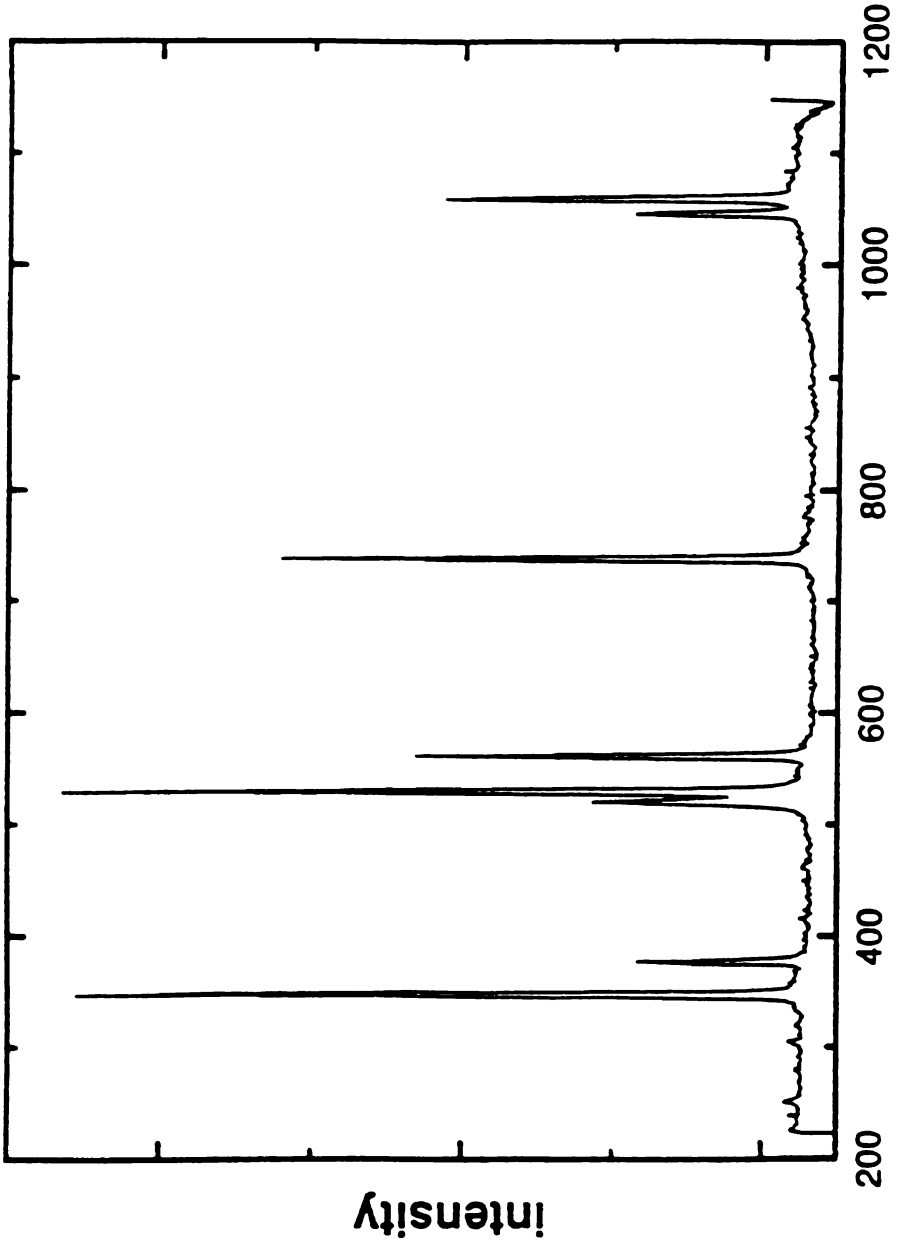

Figure 30. Raman spectrum of uncoated silicon 2 wafer on the polished side taken with a 488 nm argon laser at 1800 g/mm and 100 nms slit width

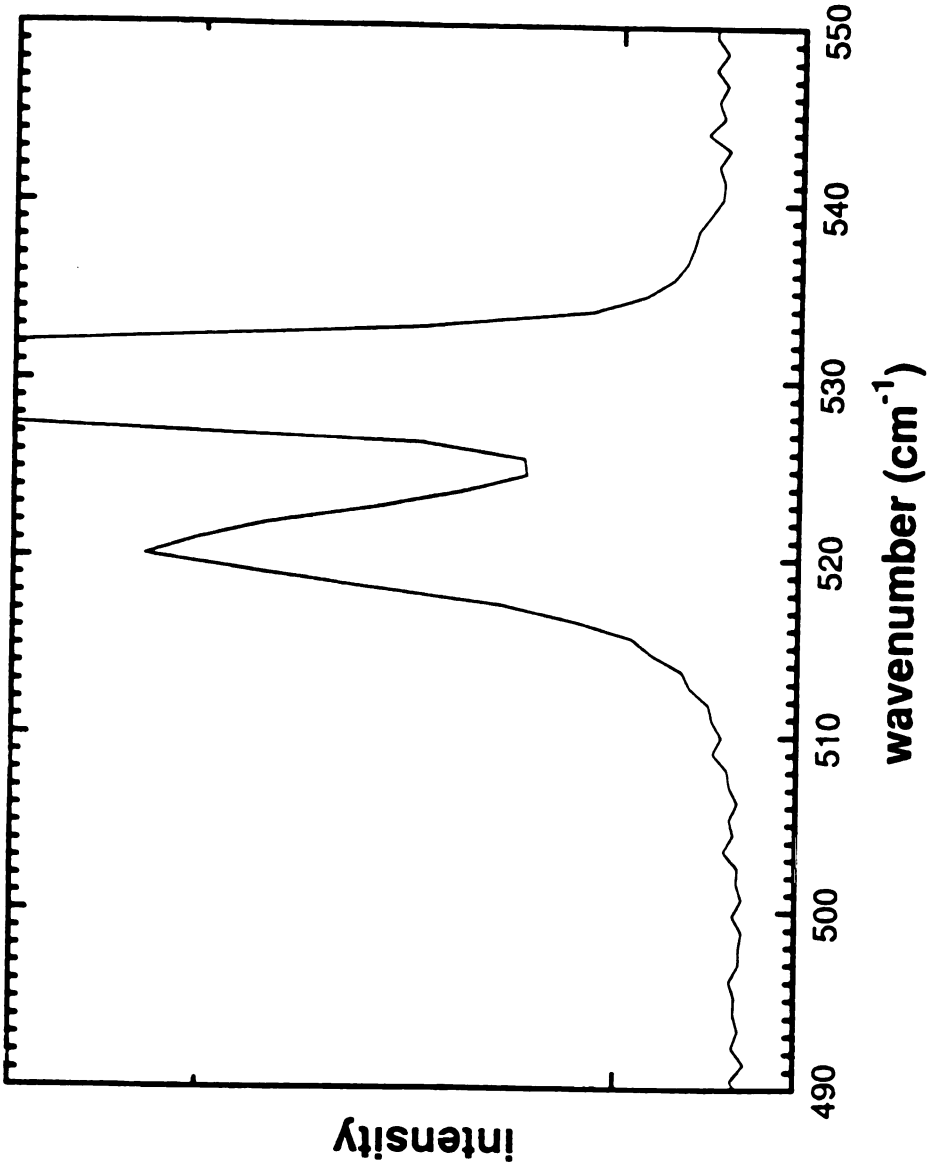

Figure 30 a. Expanded silicon peak from the Raman spectrum of uncoated silicon 2 wafer on the polished side. Figure 30.

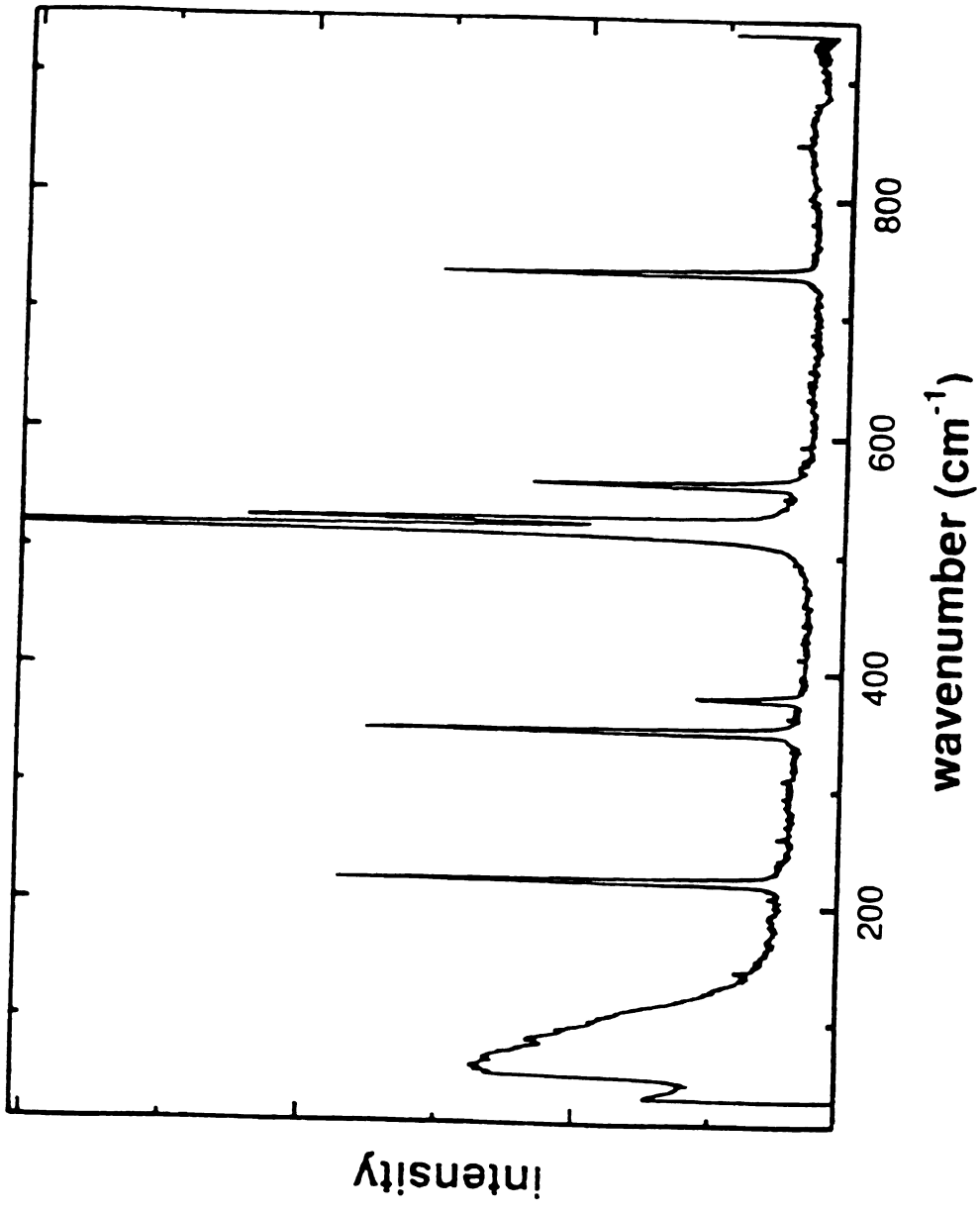

Figure 31. Raman spectrum of annealed & uncoated silicon 2 wafer on the rough side and taken with a 488 nm argon laser at 1800 g/mm an 100 nms slit width.

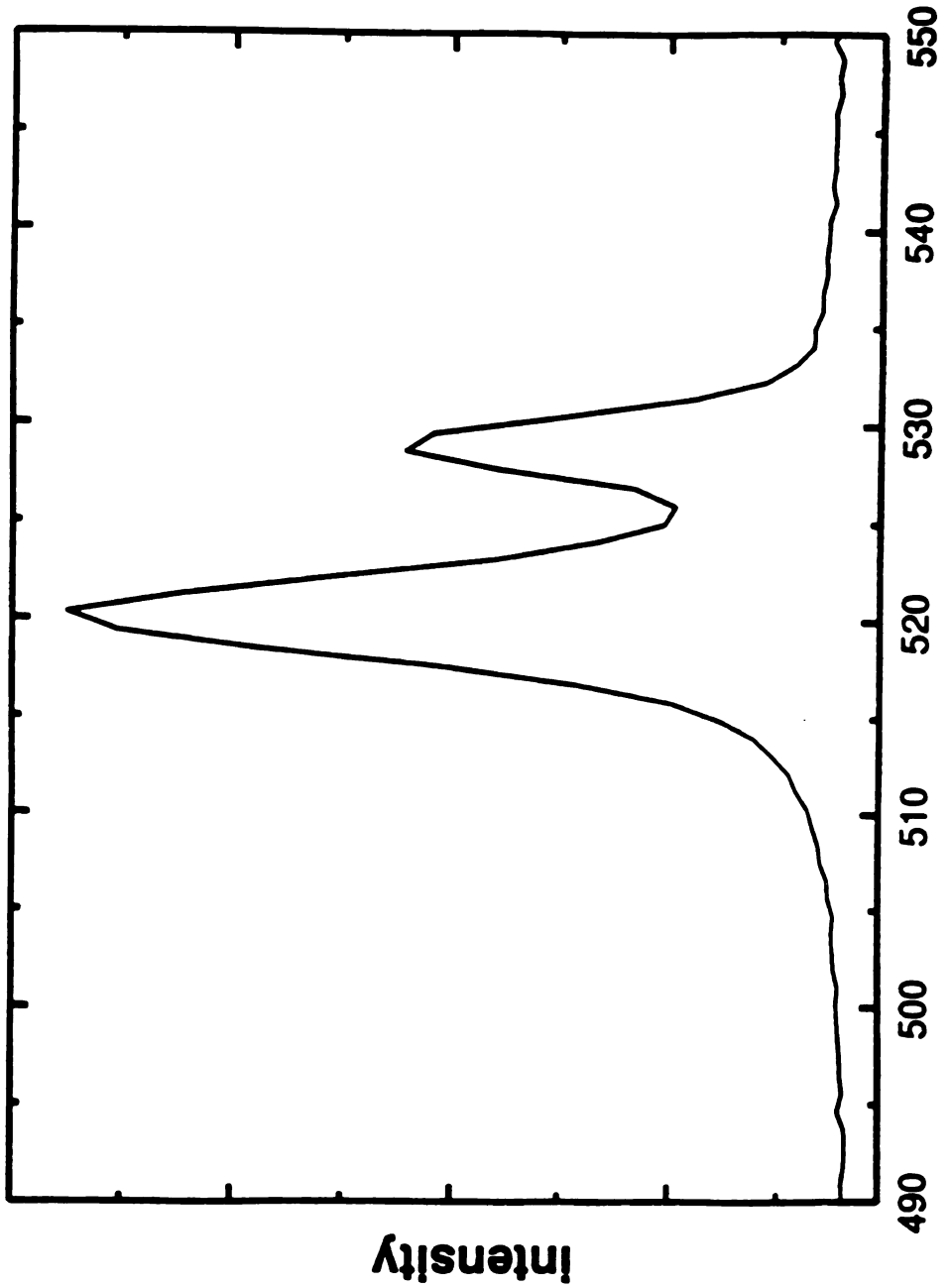

Figure 31a. Expanded silicon peak from the Raman spectrum of annealed & uncoated silicon 2 wafer taken on the rough side. Figure 31.

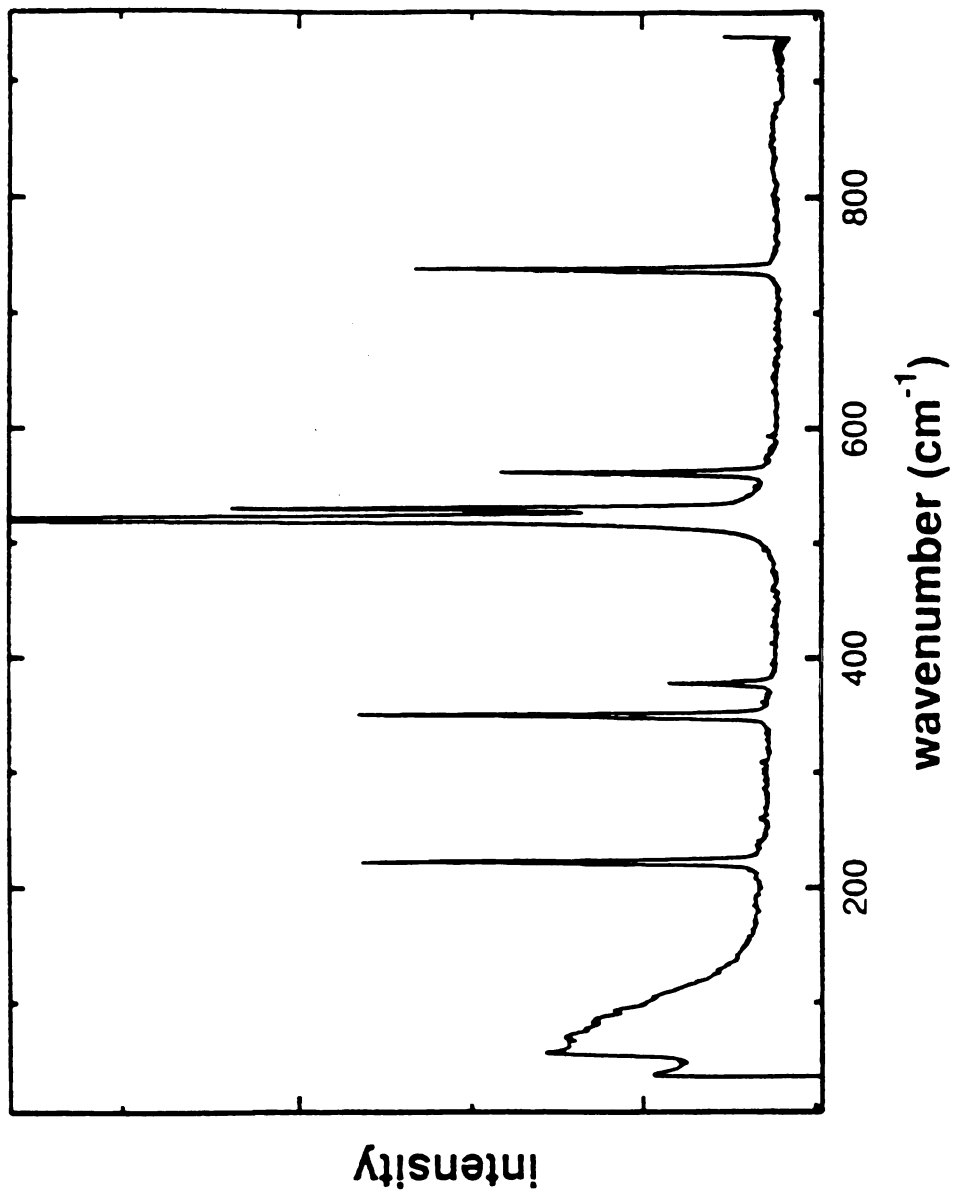

Figure 32. Raman spectrum of annealed & uncoated silicon 2 wafer on the polished and taken side with a 488 nm argonlaser at 1800 g/mm and 100 microns slit width.

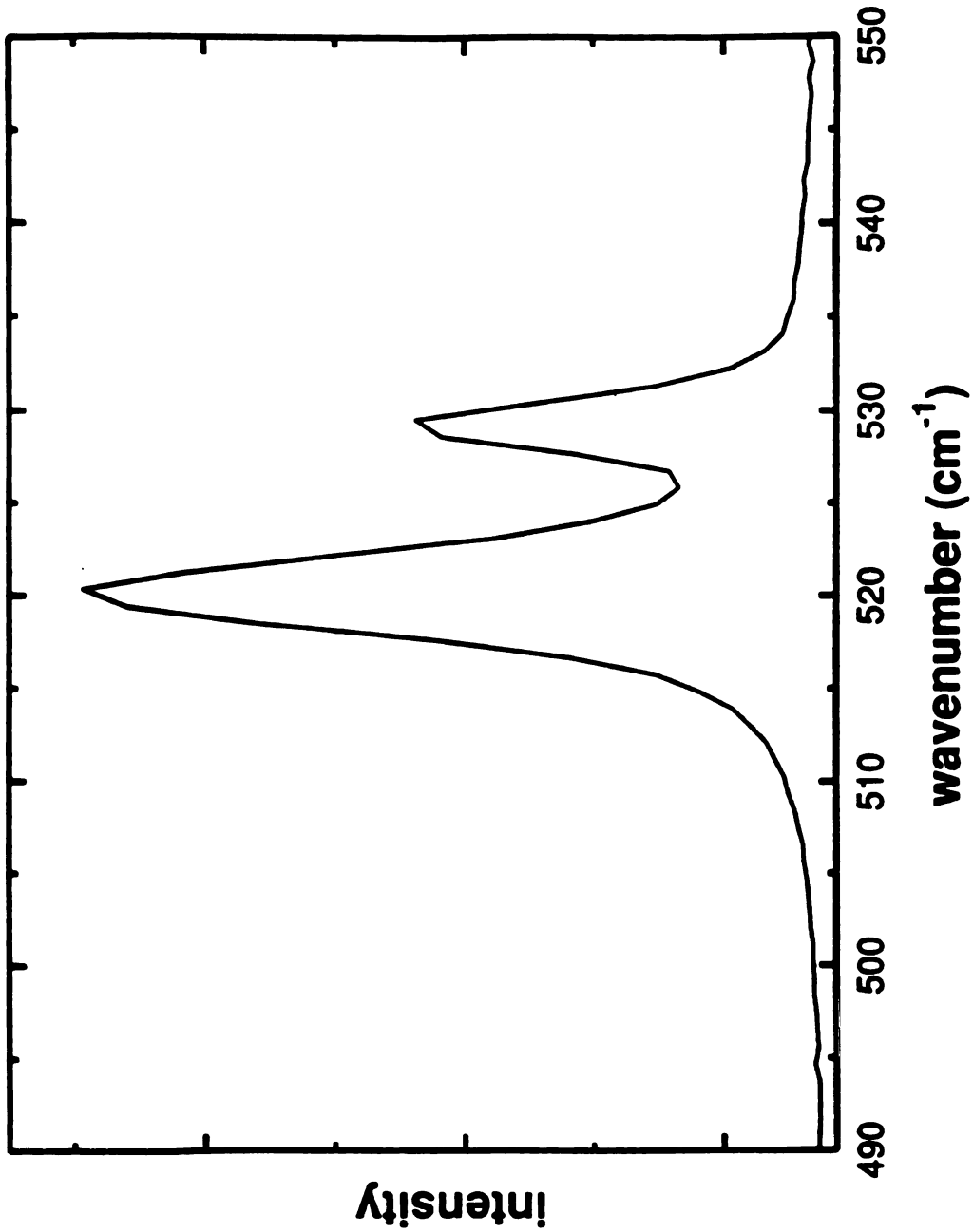

Figure 32a. Expanded silicon peak from the Raman spectrum of annealed & uncoated silicon 2 wafer taken on the polished side. Figure 32.

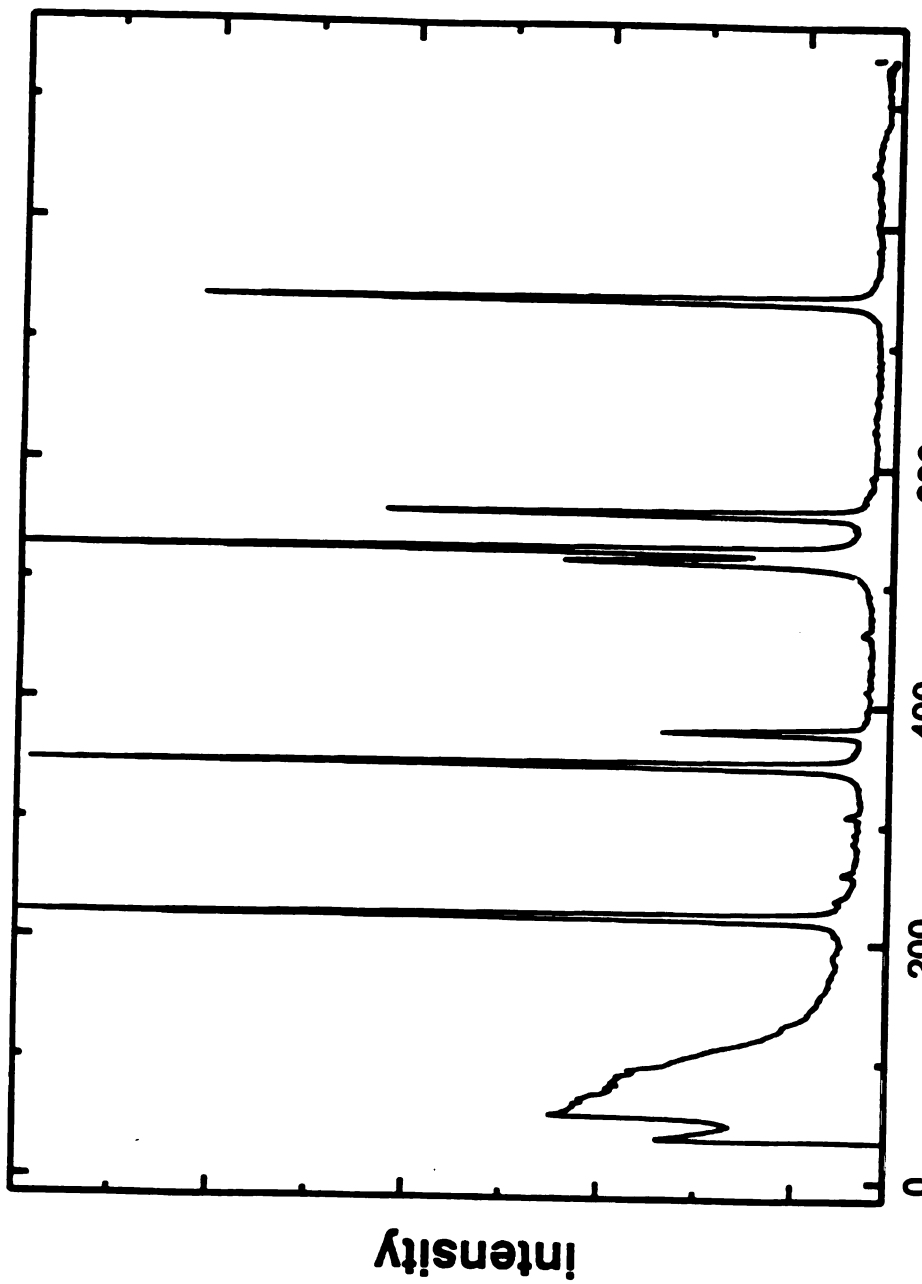

Figure 33. Raman spectrum of the coated silicon substrate on the back side (rough) of the silicon diamond sample and taken with a 488 nm argon laser at 1800 g/mm and 100 microns slit width.

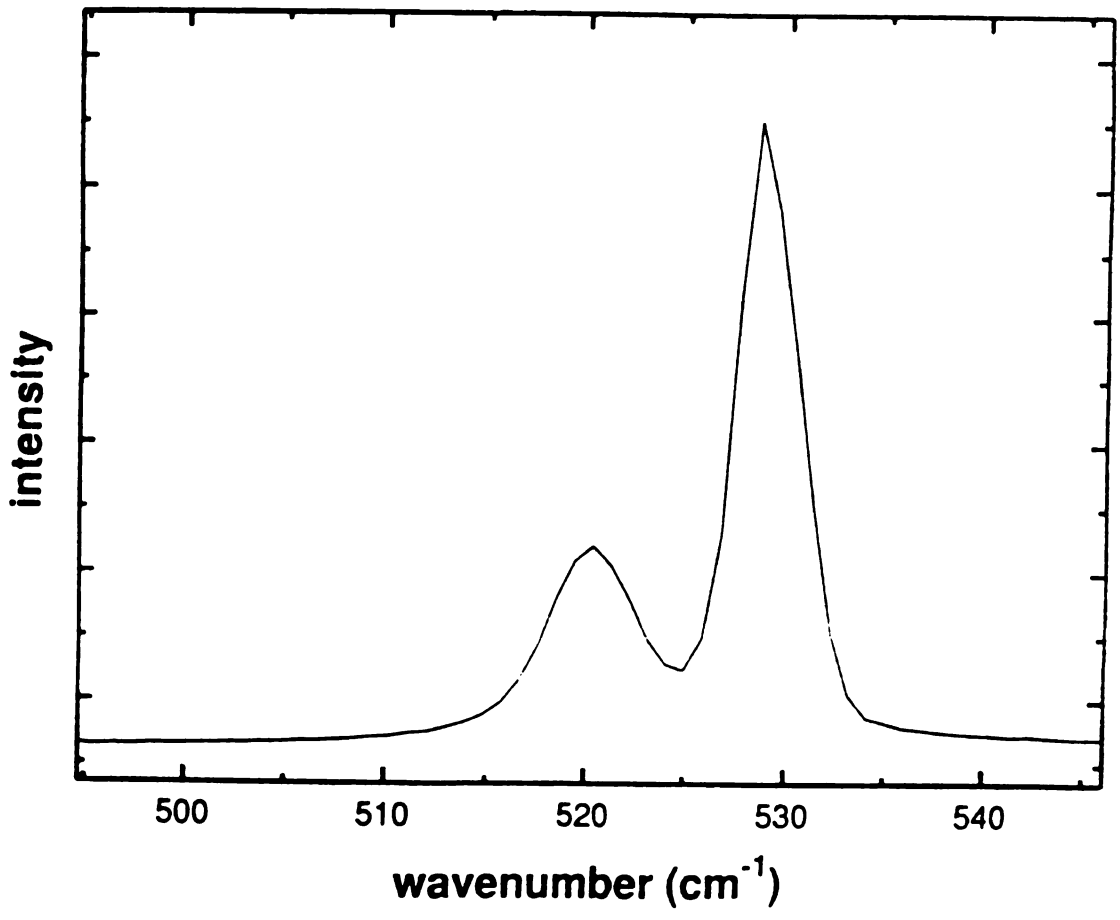

Figure 33a. Expanded silicon peak from the Raman spectrum of the coated silicon substrate on the back side (rough) of the silicon diamond sample. Figure 33.

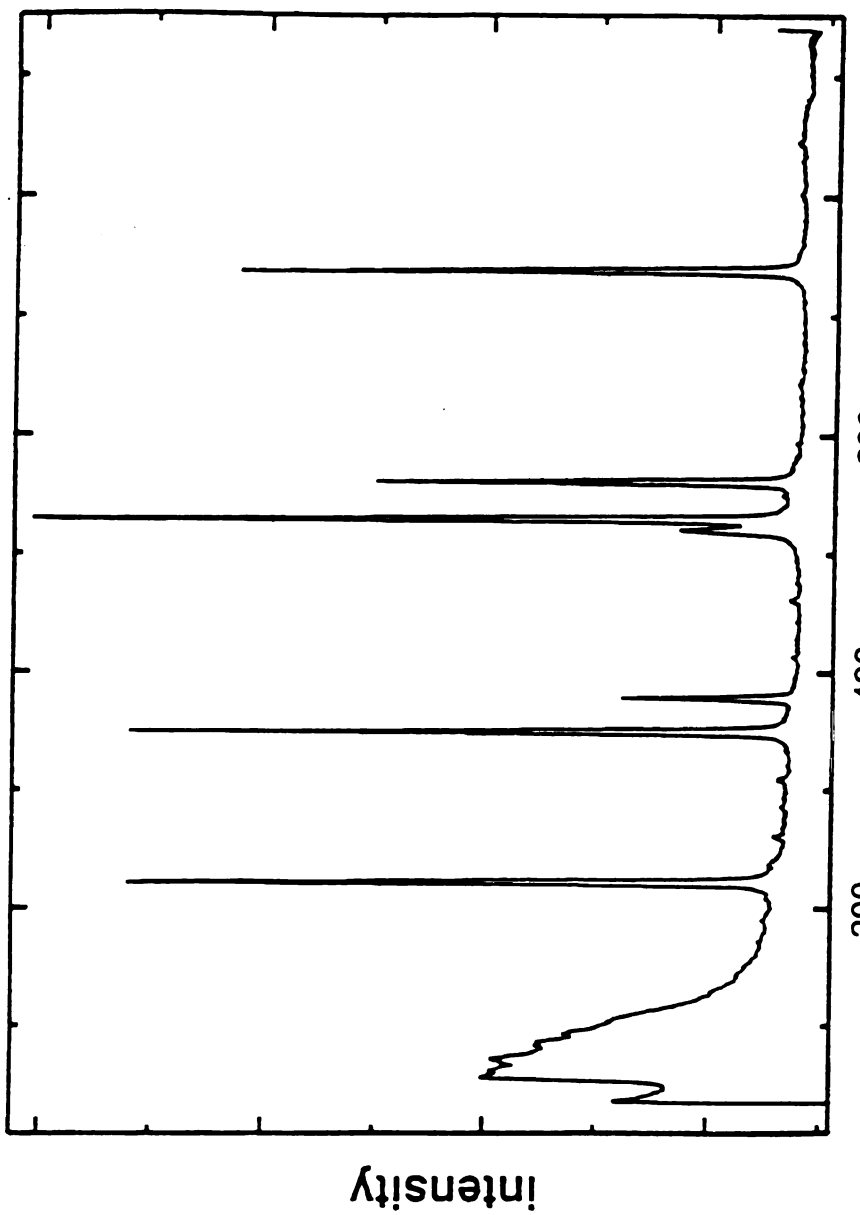

Figure 34. Raman spectrum of the silicon substrate on the back side (rough) of the annealed & coated silicon diamond sample and taken with a 488 nm argon laser at 1800 g/mm and 100 microns slit width.

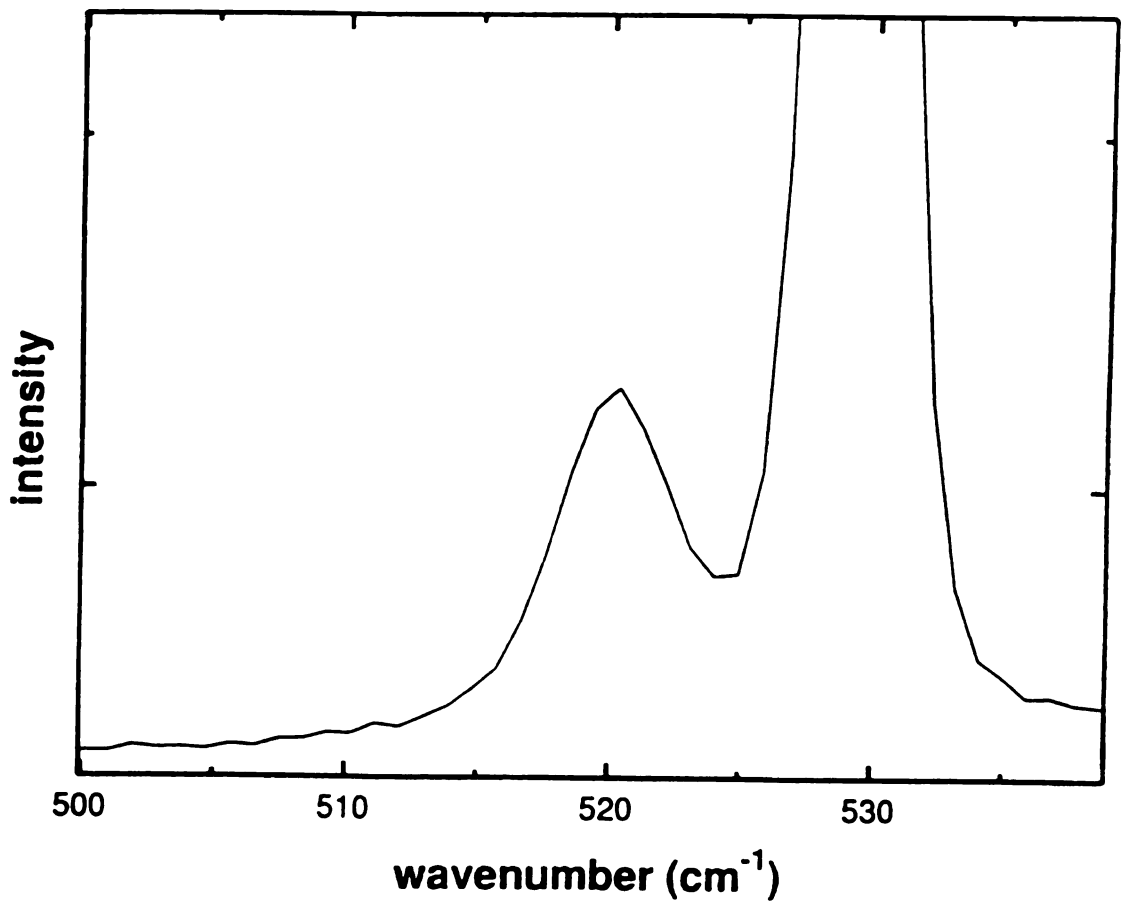

Figure 34a. Expanded silicon peak from the Raman spectrum of the coated silicon substrate on the back side (rough) of the annealed silicon diamond sample. Figure 34.

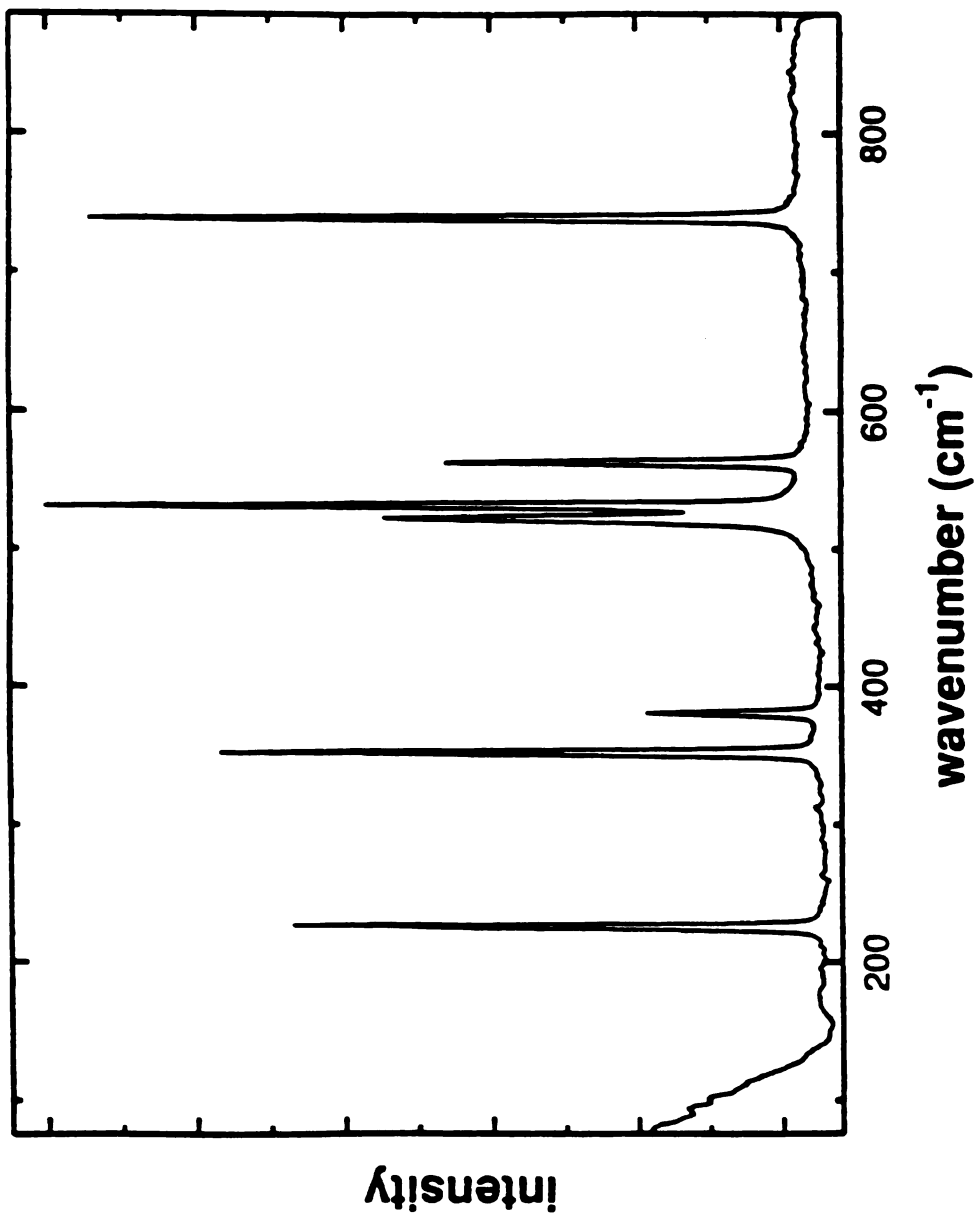

Figure 35. Raman spectrum of the silicon substrate at the interface side of the coated silicon diamond sample and taken with a 488 nm argon laser at 1800 g/mm and 100 microns slit width.

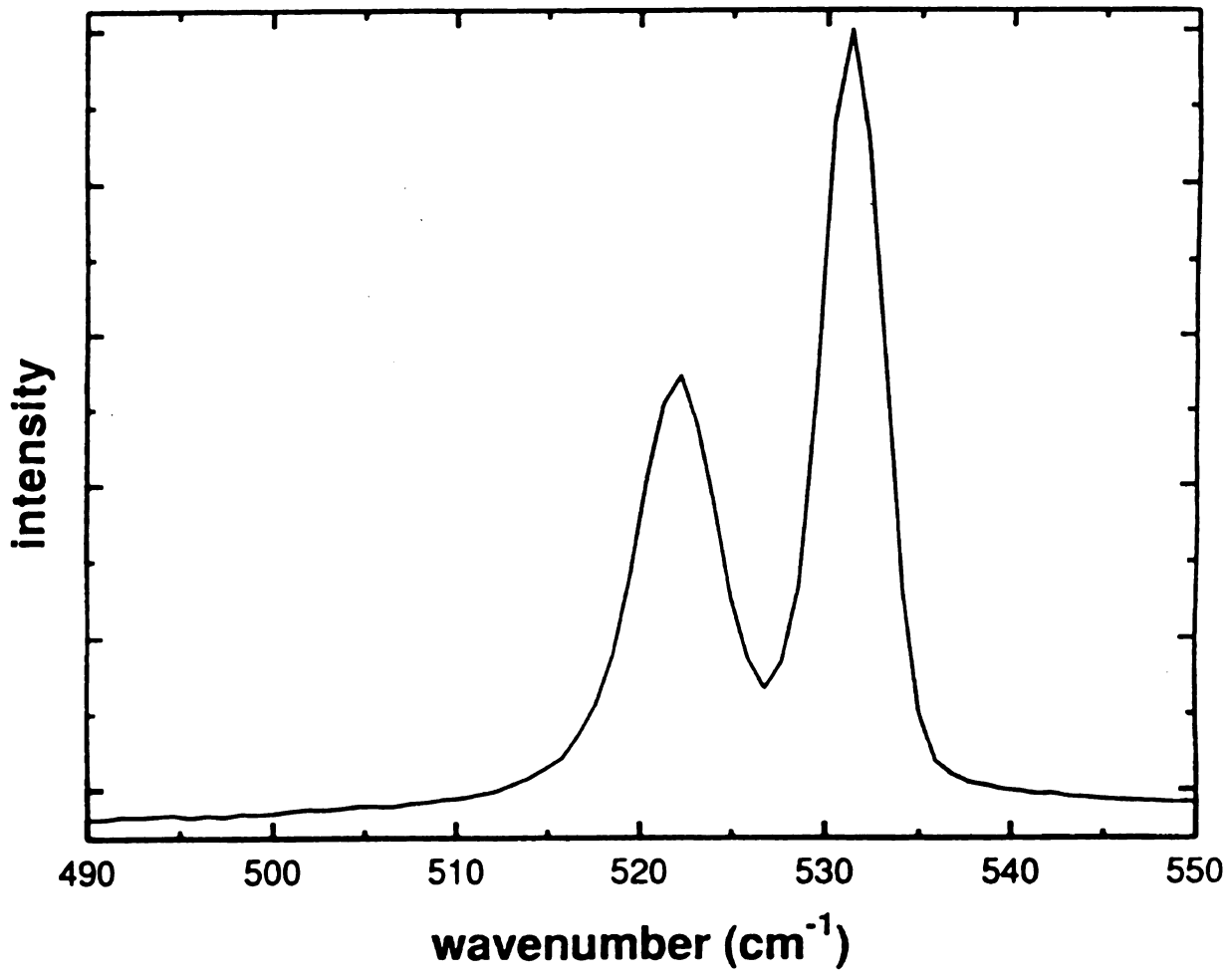

Figure 35a. Expanded silicon peak from the Raman spectrum of the coated silicon substrate at the interface of the silicon-diamond sample.

Figure 35.

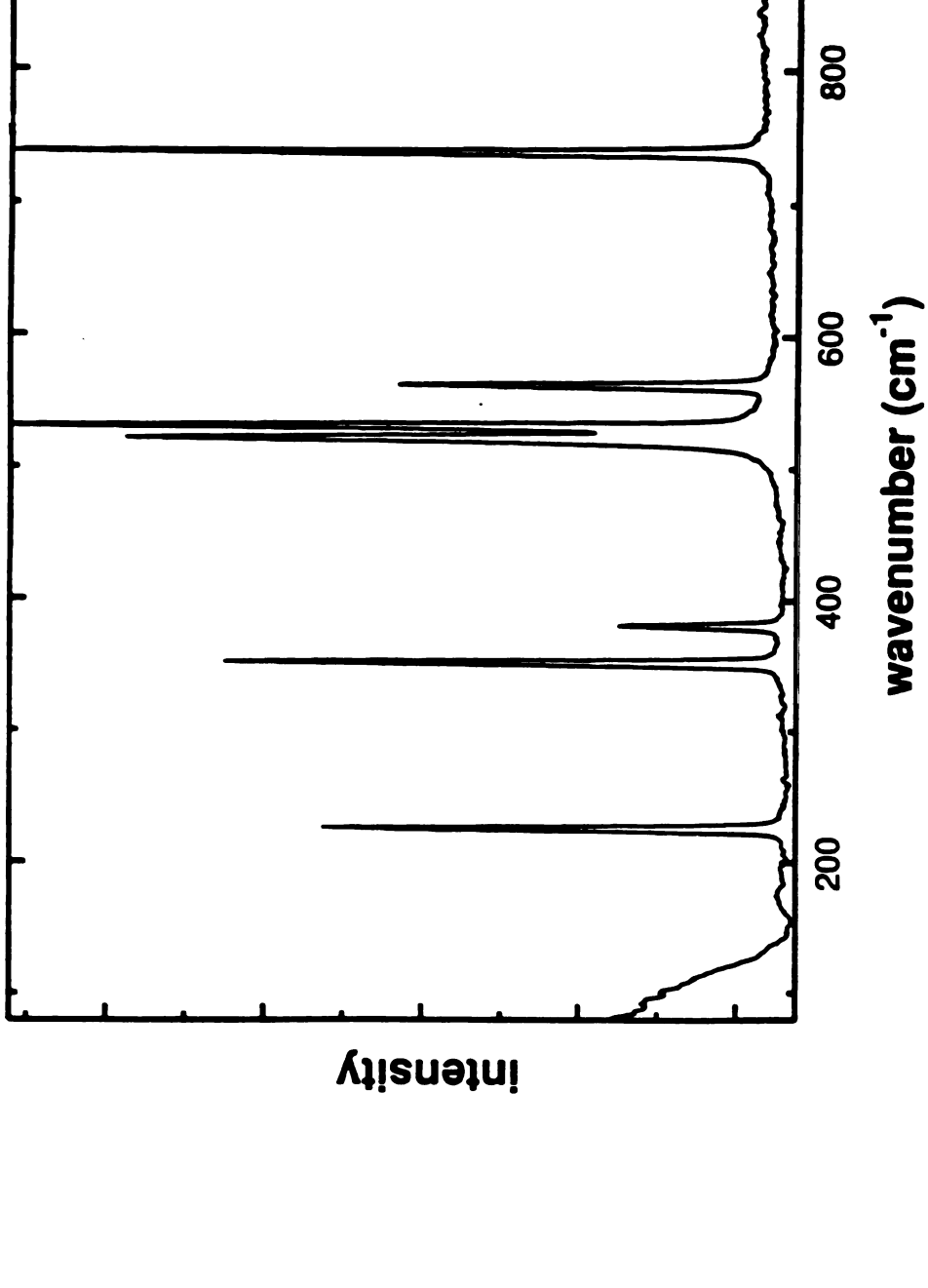

Figure 36. Raman spectrum of the annealed & coated silicon substrate at the interface side of the silicon diamond sample and taken with a 488 nm argon laser at 1800 g/mm and 100 microns slit width.

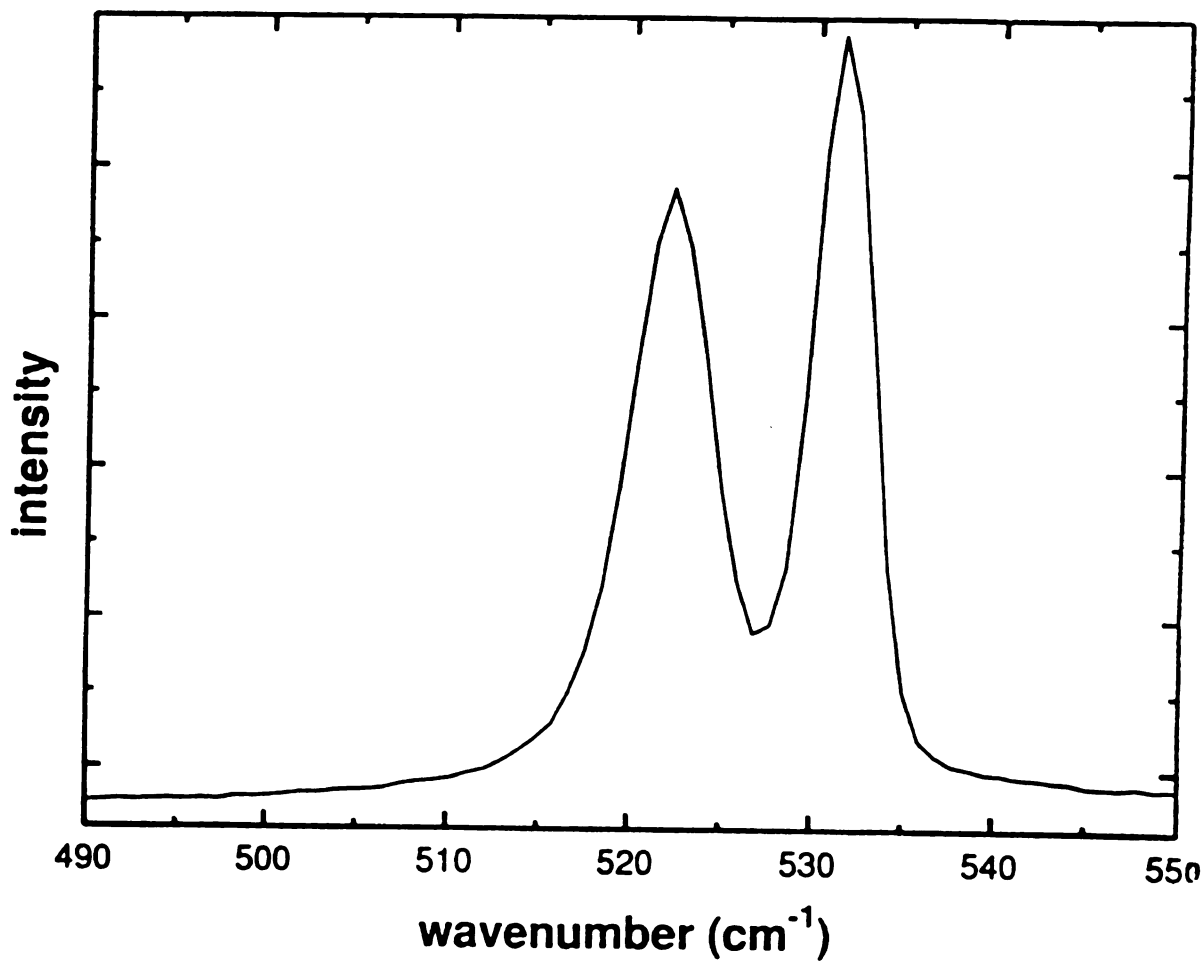

Figure 36a. Expanded silicon peak from the Raman spectrum of the annealed & coated silicon substrate at the interface of the silicon-diamond sample. Figure 36.

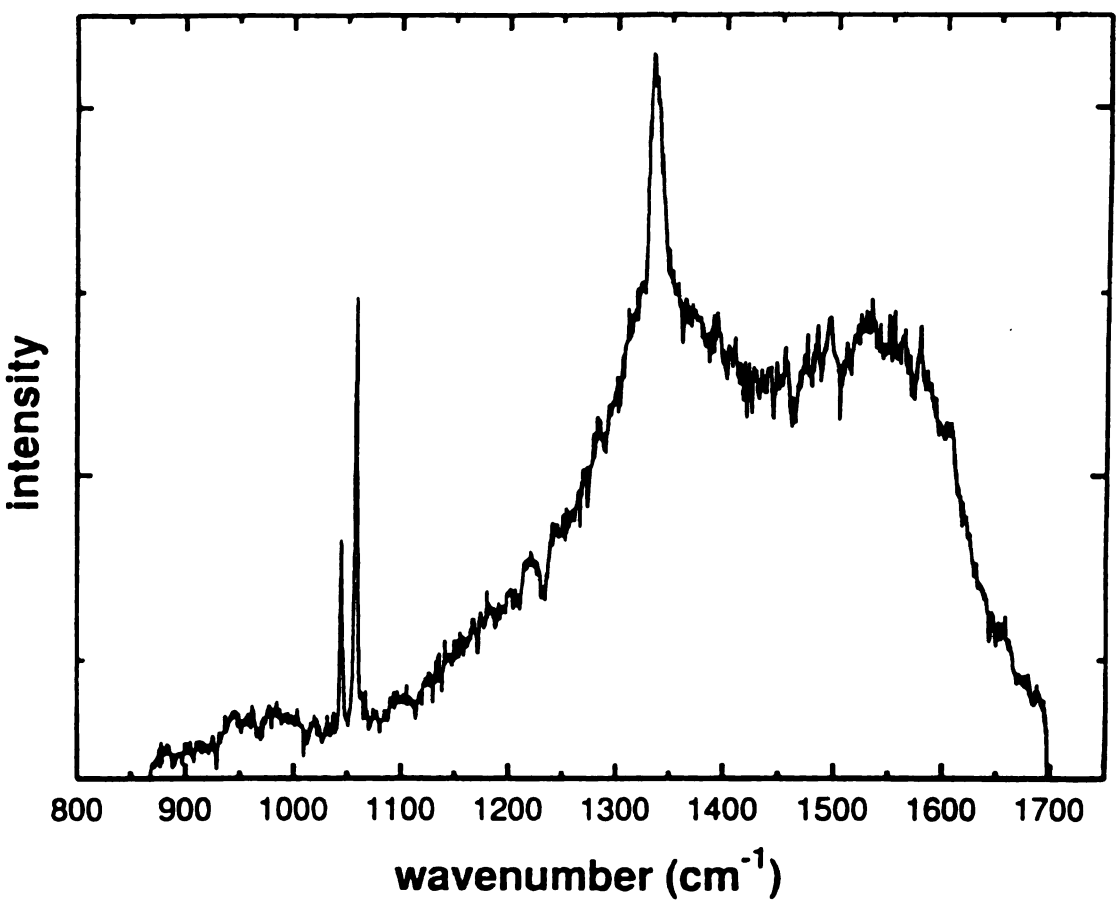

Figure 37. Raman spectrum of the diamond film in the as deposited state in the silicon-diamond sample and taken with a 488 nm argon laser at 1800 g/mm and 100 microns slit width.

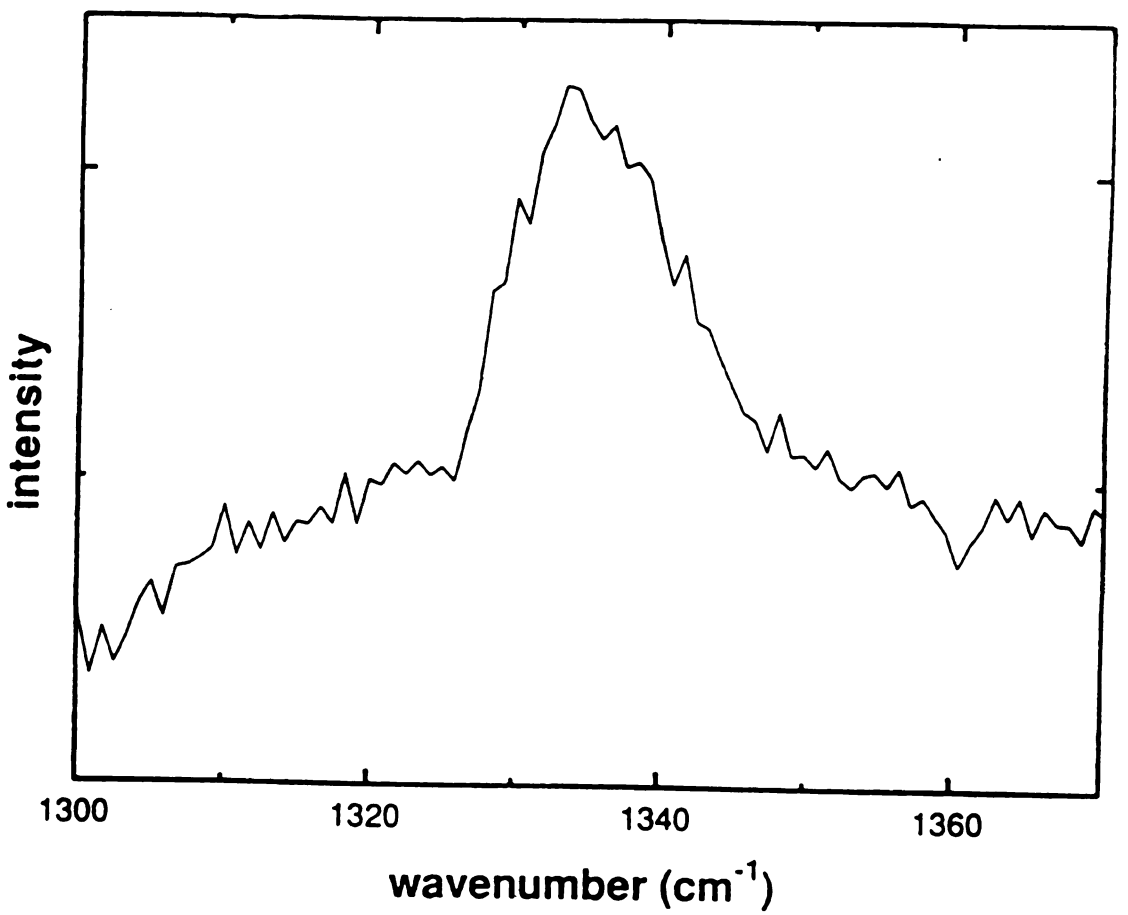

Figure 37a. Expanded diamond peak from the Raman spectrum of the diamond film in the as deposited state in the silicon-diamond sample.

Figure 37.

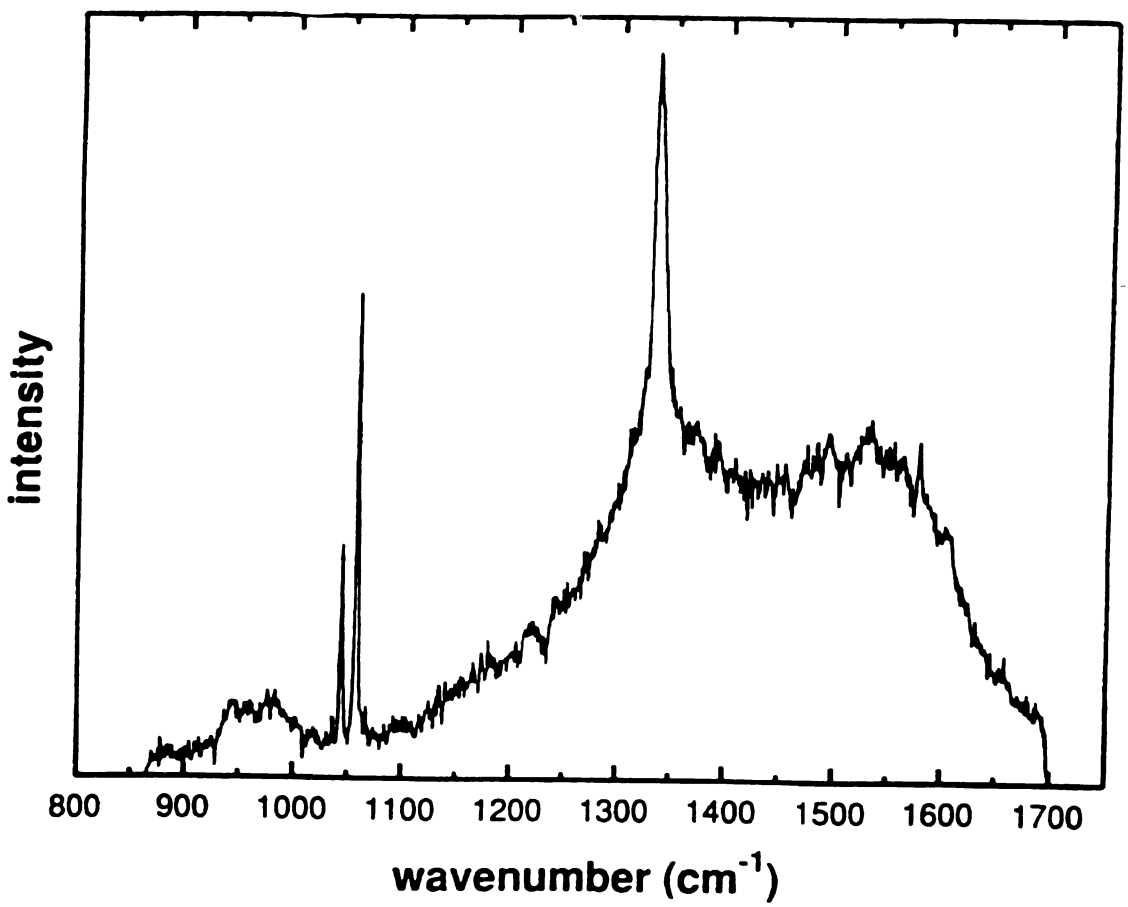

Figure 38. Raman spectrum of the diamond film in the annealed state in the silicon-diamond sample and taken with a 488 nm argon laser at 1800 g/mm and 100 micronsslit width.

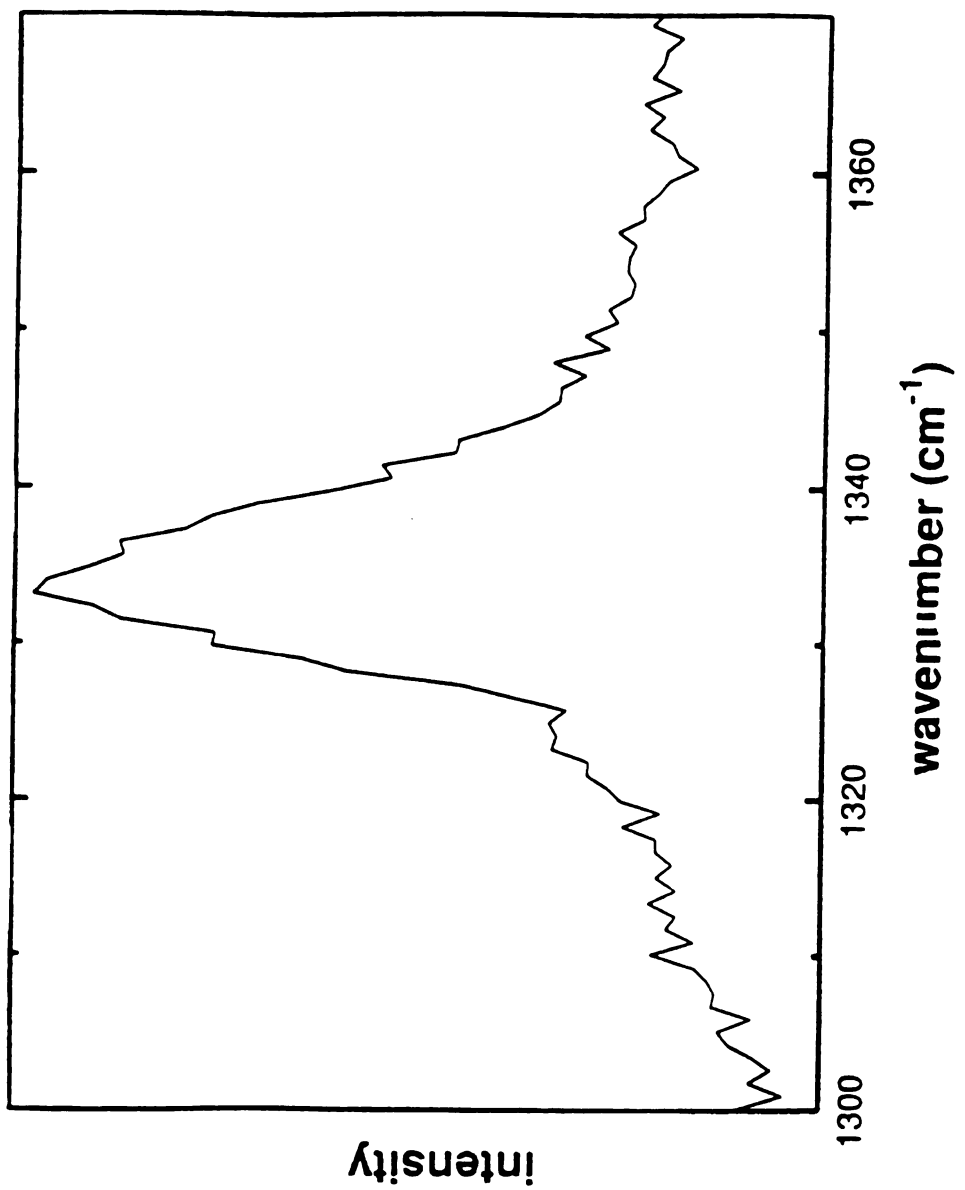

Figure 38a. Expanded diamond peak from the Raman spectrum of the diamond filmin the annealed state in the silicon-diamond sample. Figure 38.

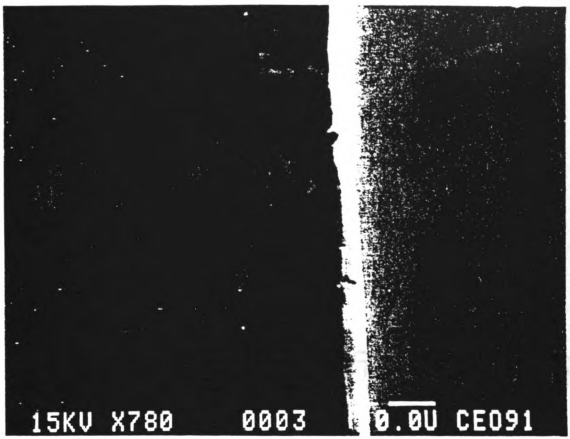

Figure 39. SEM micrograph of a cross section of the silicon-diamond sample at the interface showing the diamondfilm at 780 times magnification

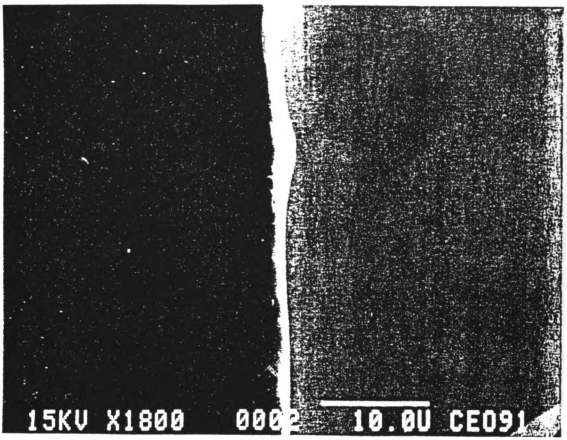

Figure 40. SEM micrograph of a cross section of the silicon-diamond sample at the interface showing the diamond film at 1800 times magnification. The location on the interface if different from that in figure 39.

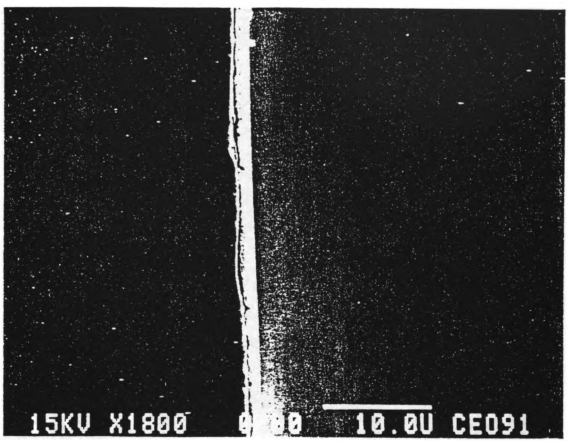

Figure 41. SEM micrograph of a cross section of the silicon-diamond sample at the interface showing the diamond film at 1800 times magnification. The location on the interface is different from that in figure 40.

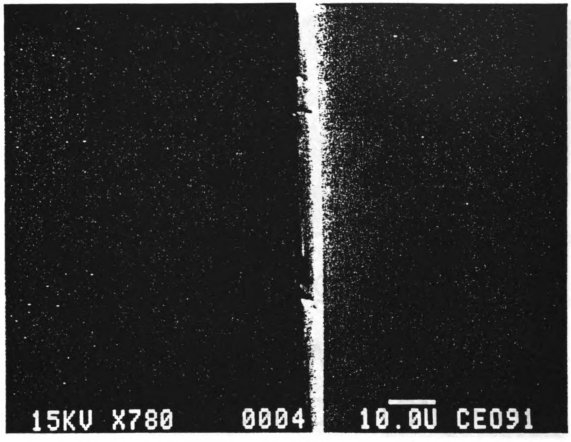

Figure 42. SEM micrograph of a cross section of the silicon-diamond sample at the interface showing the diamond film at 780 times magnification. The location on the interface if different from that in figure 41.

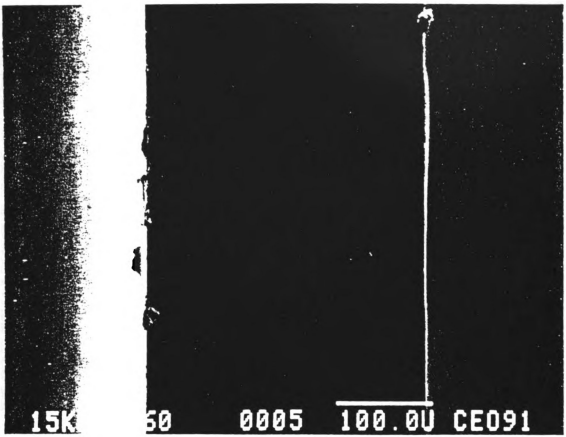

Figure 43. SEM micrograph of a cross section of the coated silicon wafer at the interface showing the full width silicon substrate at 160 times magnification.

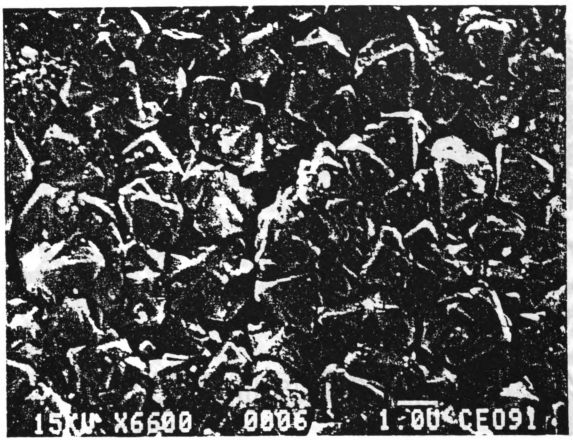

Figure 44. SEM micrograph of the diamond film showing the microstructure consisting of (111) oriented grains at 6,600 times magnification.

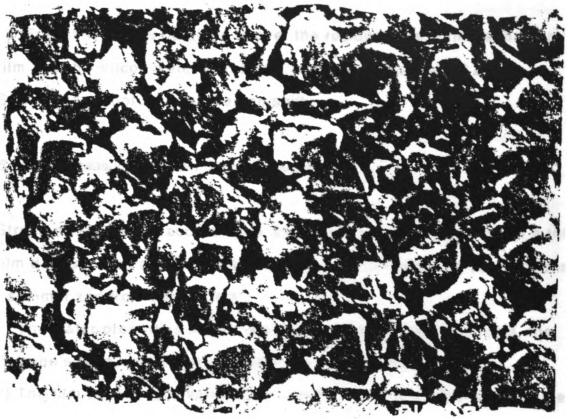

Figure 45. SEM micrograph of the diamond film showing the microstructure consisting of (111) oriented grains at 6,600 times magnification. The micrograph was taken at a different location from than in figure 44.

8- CALCULATION AND DISCUSSION

From the results obtained above, the residual stress in the diamond film and the silicon wafer at the interface will be calculated using Stoney's equation and the Raman shift.

8.1 Stress measurement from Stoney's equation

Stress measurement according to Stoney's equation in the case of a thin film deposited on a thicker substrate requires the following assumptions (summarized from section 4.3)

1) The wafer properties are known, the in-plane Young's modulus, the Poisson's ratio, and substrate thickness which must be uniform.

2) The film thickness is known and should be uniform. The value of the film thickness in Stoney's equation must be an average value.

3) The curvature of the substrate due to the stress in the film is known, and is independent of the orientation of the stylus scan measurement direction.

4) The film and substrate materials are isotropic.

5) The substrate is rigid (it is much thicker than the film) and thus, no stresses are developed in the substrate.

6) the interface bonding is strong enough not to allow slippage or spalling.

7) measured stresses are in the elastic range.

The applicability of Stoney's equation to measure the growth stress in thin diamond films deposited on (100) silicon wafers is argued here by checking the assumptions listed above against the obtained experimental results.

The mechanical properties of (100) silicon wafers are well known. The biaxial Young's modulus (includes the Poisson's ratio value) for (100) silicon is 180 GPa [10,59]. The substrate thickness was measured from an SEM micrograph and was 0.456 mm (figure 43). The substrate thickness was uniform. Thus assumption number one above checks well.

As stated above, the diamond film thickness is not uniform; the film becomes thinner towards the edge of the circular wafer. For MPCVD deposition of diamond films the non uniformity of the film thickness is not random and arises from the higher plasma density at the center of the deposition chamber as compared to the outer limits of the chamber [10,21]. Thus unless the deposition mechanism is improved, the variation in film thickness is a likely event in all MPCVD depositions. The film thickness of the sample used in this study dropped to 40 percent of the value at the center of the wafer at a radial distance of 20 mm. The thickness gradient is this study is similar to the thickness gradient reported by Windischmann [10,21]. Windischmann used MPCVD diamond films where the film thickness dropped to 50 percent of the center value at a radial distance of 25 mm [10,21]. The area of measurement had to be reduced to decrease the effect of thickness

gradient [10,21]. In this study, the DEKTAK II scan length was only 30 mm. Thus, the radius of curvature measurement involves a thickness gradient over a distance of only 15 mm on either side of the wafer center. Therefore, the thickness gradient over the 30 mm measurement distance is less severe than in the case where the whole 54 mm wafer is scanned.

The assumption of film uniformity is thus not well satisfied and therefore errors in the measured stress values are expected. One should note however that since Stoney's equation provides an average value of the stress in the film, the error in stress measurement due to thickness variation would be small if the calculated average thickness is close to the real average film thickness. It is also important to note that the film thickness variations is not random, but decreased steadily towards the wafer edges in a symmetric way. The average film thickness can therefore be determined more accurately than in the case where the film thickness variation is completely random.

The third assumption that the curvature should be spherical and independent of the measurement direction on the silicon wafer also is not well satisfied. The single crystal substrate wafer is highly anisotropic. The maximum in-plane difference in the elastic modulus of (100) silicon however is 16 percent [3], even though no important variations in curvature were observed for any orientation of the stylus with respect to the wafer when the film is uniform [3]. The Young's modulus in Stoney's equation representing the substrate should be the

average in plane modulus [3]. Using a single crystal for the substrate thus introduced an error in the stress value as calculated from Stoney's equation, since the elastic constant are not isotropic; they depend on the crystallographic orientation.

The assumption of isotropy of the film and substrate materials for Stoney's equation to be applicable should hold for the diamond film. The condition for isotropy is that $2\ C_{44}/(\ C_{11}-C_{12}) = 1$ (equation 27)[60], the ratio is equal to 1.21 for diamond and 1.56 for silicon. One should note however that the elastic constants ratio as a condition for isotropy is dependent on the reported value of elastic constants and thus can get closer or farther from 1 depending on the scatter in the values of the elastic constants. As expressed above, the silicon wafer is a single crystal and thus highly anisotropic. Cubic crystals are anisotropic with respect to the elastic modulus. However, the diamond film is polycrystalline with uniformly distributed grain size. Polycrystalline diamond can be macroscopically isotropic, unless the film has a texture (preferred orientation). Errors due to the anisotropy of the silicon wafer as well as any possible texture in the diamond film are inevitably introduced in the stress measured from the curvature. Evidence of possible anisotropy effect can be seen on figures 25 and 26; the wafer deflection profile is slightly off symmetric and obviously non spherical; it is rather elliptical. One can thus conclude that the assumption of material isotropy is not fully satisfied.

The assumption that the silicon wafer is rigid; all the deflection in the

wafer in due to the stress in the film, cannot be directly verified from Stoney's equation. Any stress in the silicon wafer can however be detected from the Raman peak position of the silicon wafer. Raman stress measurement (next section) revealed stresses in the silicon wafer that have opposite signs on the two sides of the wafer. The stress thus goes through a neutral plane. The magnitude of the interfacial strain on the silicon side of the interface was greater than the magnitude of the strain on the diamond side of the interface. When the two surfaces of a beam are under opposite stress signs (compression versus tension), the neutral plane where the stress is zero shifts if the beam is loaded.

The ratio of the substrate to film thickness for the sample used in this study is about 450 to 1. Thus the assumption that the film thickness is much smaller than the substrate thickness holds well. The error induced by neglecting the term ($1 - t_f / t_s$) is about 0.002 GPa, an insignificant error since the stress is determined only to within two significant digits.

From figures 39 to 42, one notices that while there is no spalling or cracking in the silicon-diamond interface, there is some limited interfacial cracking as can be seen in figure 41. It is however not possible to determine whether the interfacial cracking is due to a weak interfacial bond strength or to the cutting of the SEM sample from the original silicon-diamond sample. But since most of interface is not cracked, it is realistic to assume that the interfacial bonds are strong enough to avoid spalling or cracking at the interfacial plane.

All of the parameters and constants for stress determination by Stoney's equation are known and given below. The stress before and after annealing of the sample is thus calculated next.

t_f = 0.97 microns (diamond film thickness)

t_s = 0.456 mm (silicon substrate thickness)

$E_s/1-\mu$ = 180 GPa (biaxial Young's modulus of silicon)

L = 30 mm (stylus scanning distance)

δ_o = -95,150 angstroms

δ_a = -84,150 angstroms

δ_o and δ_a are the net center wafer deflection respectively before and after annealing. The stress in the diamond film is given by

$$\sigma_R = 4 E_s t_s^2 \Delta\delta \; / \; 3(1 - \nu_s) t_f L^2 \qquad (52)$$

where $\Delta\delta = \delta_a - \delta_o$. By substituting the above parameter values into Stoney's equation, the average residual stress in the diamond film on the(100) silicon substrate is given by

$$\sigma_R \text{ (GPa)} = -5.893 \quad \Delta\delta \text{ (meters)} \qquad (53)$$

Substituting the values of the center deflections of the wafer as provided and the annealed sample, the residual growth stress in the diamond film is -0.57 GPa. After annealing the silicon-diamond sample, the compressive residual growth stress was reduced to - 0.49 GPa. All of the deflection is assumed to be stress induced; the stress is calculated from shifts where the deflection of the uncoated wafer was subtracted. The annealing treatment thus resulted in a stress decrease of 13 percent.

The magnitude of the residual stress in the diamond film (-0.57 GPa) is only 0.05 percent of the Young's modulus of diamond. Thus, the stress magnitude measured from the radius of curvature is well within the elastic deformation range of diamond; assumption number 7 holds well.

The magnitude of the measured residual stress (-0.57 GPa) represents the macroscopic average stress in the entire diamond film. Since the film thickness is not constant, the value -0.57 GPa represents only an approximation to the value of the integrated force per unit with over the total thickness range. The accuracy of the obtained value - 0.57 GPa) depends on how closely the average diamond film thickness (0.97 microns) approximates the real average film thickness.

8.2 Stress measurement from the Raman peak position shift

The stress measurement from the Raman peak shift is not as straight forward as the measurement from the change in the curvature of the substrate. In section 4.4, the parameters controlling the calculation of the stress from the peak shift were discussed in detail as well as the application to the silicon-diamond composite system.

According to the discussion in section 4.4 the 3 X 3 secular equation results in two independent eigenvalues corresponding to the singlet and doublet frequencies of the strained cubic crystal lattices of both silicon and diamond. Only a singlet results under a hydrostatic stress while three independent singles result from a stress parallel to a <110> direction. From SEM micrographs (figure 44 and 45), the orientation of the diamond grains in the sample used in this work is assumed to be (111) such that (111) planes are parallel to the interface and perpendicular to the laser beam direction. The silicon single crystal is oriented such that the [100] direction is perpendicular to the interface and parallel to the laser beam. Both a singlet and a doublet frequencies result from the sample-stress configuration used, for both silicon and diamond. In section 4.4, it was also argued that under the current back scattering geometry, only the singlet is observed for both silicon and diamond. The equations of stress as a function of Raman peak shift were derived for a biaxial stress parallel to <100> planes as in the case of the silicon substrates. However, the equations derived

have to be readjusted for the <111> orientation of diamond.

For the (100) silicon single crystal, the equation for residual stress as a function of the singlet peak frequency shift was derived in section 4.4 and is given by

$$\sigma_R = \nu_0 \Delta\nu_s / [\, p\, S_{12} + q\, (\, S_{11} + S_{12}\,] \qquad (54)$$

where $\Delta\nu_s = \nu_s - \nu_0$ and ν_0 is the frequency of unstressed silicon. Table 3 gives the elastic constants and deformation potentials for both silicon and diamond. Using the values in table 3 for silicon, the stress-frequency shift relationship is given by

$$\sigma_s\,(\text{GPa}) = -0.25\ \ \Delta w_s\ (\text{cm-1}). \qquad (55)$$

For <111> diamond, the stress-frequency shift relationship is given by

$$\sigma_s\,(\text{GPa}) = -0.45\ \ \Delta w_s\ (\text{cm-1}). \qquad (56)$$

Equations 55 and 56 correspond to the sample geometry, orientation, laser polarization and back scattering geometry used in this study. The laser light used for the Raman scanning of the samples is polarized such that the electric field is parallel to the sample interface. As explained in section 4.4, the electric field parallel to the interface is also parallel to

the biaxial stress orientation and thus would result in detecting the maximum frequency shift of the singlet in both diamond and silicon (as given by equation 55 and 56).

As was the case for stress measurement from Stoney's equation, the major assumption made will be checked for the stress measurement from the Raman peak frequency shift.

To correctly measure the stress from the Raman peak frequency shift, the following assumption and conditions have to be satisfied:

1) p, q and r, the independent deformation potentials (derived with the assumption of harmonic motion as described is section 4.4) are accurate for the stress state of the samples used.

2) the stress measured is in the elastic range.

3) a singlet and a doublet result if the stress is truly a biaxial stress.

4) The crystallographic orientation of the sample is known.

5) The sample is a single crystal.

6) The laser light polarization and back scattering geometry is known.

7) The theoretically derived shift coefficient with stress (equations 55 and 56) do represent the sample-stress-laser beam orientation.

8) The relationship between stress and frequency shift is linear as predicted by the theoretical model.

The discussion of the above conditions (one to eight) was completed in section 4.4. A summary of the discussion is presented here. Conditions 2, 6, and 8 are well satisfied. From the stress values

measured with the change in the radius of curvature, the stress was indeed in the elastic range. The laser Raman set up uses a 180 degree back scattering geometry and the polarization of the laser light is accurately known. The relationship between stress and frequency shift is linear to stress magnitudes greater than 40 GPa. The stresses measured in thin diamond films hardly exceed the single digit range (in GPa) and thus the linearity assumption holds well.

The deformation potentials are critical to accurate stress determination. A scatter exists in the reported values in the literature, though the number of independently reported values is low. Furthermore, the reported values are for hydrostatic and uniaxial stress states. No deformation potentials have been reported (to the author's knowledge) for a true biaxial stress state for either diamond or silicon.

It is not feasible in this study to determine whether the stress in the diamond film is truly biaxial. In the case where the stress deviates from a true biaxial state, the error introduced is unknown.

The orientation of the silicon wafer is precisely known. However, the orientation of the diamond film can only be assumed to be <111> from SEM micrographs (figures 44 and 45).

The main problem with using Raman shifts to measure the stress in diamond films is that the film is polycrystalline. The theoretical derivation of the shifts due to stress is based on a single crystal with known orientation with respect to the laser beam. However, the calculated average grain size in the diamond film is about 2 microns.

Given that the beam spot size at the sample surface was also about 2 microns and given that the film thickness less than a micron, it is likely that the laser beam is focused on a single crystal or on the boundary between two grains. The infrared scattering is possible from only one or two grains, the theory may be applied. Whether the stress state within a single crystal represent the homogenous stress distribution in the diamond film is not known.

A compressive biaxial stress state in the diamond film parallel to the XY plane results in a tensile uniaxial stress in the Z direction. Thus the shift coefficient with stress under biaxial stress derived from theory can tentatively be compared with coefficients determined experimentally under a uniaxial stress along a <111> direction of diamond. A frequency shift coefficient with stress of 0.45 GPa/cm^{-1} [70] was reported for a uniaxial stress along the [111] direction; the diamond sample was a (111) single crystal plate and the stress range used was less than 1 GPa which makes it a very suitable case for comparison with the similar conditions used in this study. Both the theoretical and measured value of the shift coefficient are equal to 0.45 GPa/ cm^{-1} under almost identical conditions; thus the result can be used with some degree of confidence.

Stresses were calculated from the experimentally measured shifts using equations 55 and 56. The results are presented in table 8. The stress measurement results from both the change of radius of curvature and the shift in the Raman signal are summarized in table 9.

Several important results can be deduced from table 9. The residual stress measured by both methods has almost the same magnitude. A relative difference of only 3.3 percent is observed between the stress value obtained by the two methods for the as deposited diamond film. A relative difference of 4 percent is recorded for the stress values measured by the two methods for the annealed diamond film. The relative stress change in the diamond film after it was annealed was 20 percent from the Raman shift measurement and 14 percent from the change in curvature measurement (table 9).

The stresses measured by both method are very close for the as provided and annealed sample. Furthermore, the relative change in stress as a result of the anneal is also close for both methods. The immediate conclusion is one of two possibilities, either the stress is very uniform so that both methods are observing the same stress magnitude or that the two methods are measuring the same average stress in the diamond film. For a thick sample (thickness much higher than laser extinction distance) the stress measurement from the Raman shift would be the surface stress. In this work, the diamond film, which is less than one micron thick, all of the film is in focus and thus the stress measured from the peak shift is necessarily averaging both the interfacial and bulk stresses in the film. A supporting argument to the latter point made is that the strain measured at the interface from the peak shift of the silicon is greater than the strain measured in the diamond film. The interfacial strain is expected to be higher than the

Table 8. Stresses calculated from Raman peak shifts for silicon and diamond.

Sample	State	Measurement surface	Shift (cm^{-1})	Stress (GPa)
Silicon 2*	as provided	polished	-0.08	+0.02
Silicon 2*	as provided	rough	-0.11	+0.03
Silicon 2*	annealed	polished	-0.21	+0.05
Silicon 2*	annealed	rough	-0.19	+0.05
Silicon substrate**	as provided	rough	-0.58	+0.15
Silicon substrate**	annealed	rough	-0.57	+0.15
Silicon substrate**	as provided	interface	+1.25	-0.31
Silicon substrate**	annealed	interface	+1.52	-0.38
Diamond	as deposited	diamond	+1.31	-0.59
Diamond	annealed	diamond	+1.04	-0.47

* uncoated wafer ** coated wafer

Silicon 2 refers to one out of three uncoated silicon wafers numbered 1, 2 and 3 in the experimental procedure.

Table 9. Summary of stress measurment results.

Material	State	Stress (Raman) GPa	Strain (Raman) X 10^{-4}	Stress (Stoney) GPa	Strain (Stoney) X 10^{-4}
Diamond film	as deposit	-0.59	-5.03	-0.57	-4.86
Diamond film	annealed	-0.47	-4.01	-0.49	-4.18
Silicon * substrate interface	as deposit.	-0.31	-17.3	N/A	N/A
Silicon * substrate interface	annealed	-0.38	-21.52	N/A	N/A
Silicon * substrate backside	as deposit.	+0.15	+8.31	N/A	N/A
Silicon * substrate backside	annealed	+0.15	+8.31	N/A	N/A

* coated wafer

bulk strain since the compressive thermal expansion mismatch between the film and the substrate is greatest at the interface. Thus if the Raman shift provides the value of the interfacial strain rather than the average strain in the diamond film, the strain observed in the diamond film would have been about three times higher than the measured value to satisfy the condition that the strain is continuous at the interface. One can draw the conclusion that the stress measured in the 0.97 microns thick diamond film is the average stress over the film thickness in the volume probed by the laser beam. The origins and magnitude of the stress measured in the diamond film will be discussed later.

The immediate question that must be answered is whether the shift measured is actually a stress related shift or some other shift effect. It was argued in section 4.4 that for the silicon-diamond system and the laser Raman spectroscope used, there is no reason to expect any shifts other than stress induced shifts. The measured strain on the interface on the silicon side is greater than the strain in the diamond film. As expressed above, if the stress measured by the Raman shift is the average stress in the film, the average stress would be lower than the interfacial stress measured on the silicon side. The point to be made here is that even though the strains on both sides of the interface are not equal, the measured shifts are possibly stress induced, the stress measured in the diamond is averaged over the film thickness while the shift in the silicon wafer at the interface is sampled only 2 microns deep out of the 456 micron thickness (at the 488 nm wavelength [59]). Thus

the measured stress in diamond is an average value while the stress measured on the silicon side in an interfacial stress. It is therefore not unusual for the strain on the silicon side of the interface is greater than the strain on the diamond side.

A second indication that the measured shift is stress induced is the fact that the shift measured on either side of the silicon wafer are of opposite signs; the interface side of the silicon wafer is in compression (-0.31 GPa) and the back side is in tension (+ 0.15 GPa). Since the stress changes sign from one side to the other of the substrate, the stress (strain) must go through a neutral plane where the stress is zero. The stress profile across the thickness of the substrate is not expected to be symmetric about the half-thickness plane of the silicon substrate because the film and the substrate have different stiffness and thickness values. According to Oel and Frechette [57], the neutral axis position measured from the interface is given by

$$\eta_s = [S_f t_f^2 + 3 S_s t_s^2 + 3 S_s t_s t_f] / [-6 S_s (t_f + t_s)] \qquad (57)$$

where, S_f and S_s are respectively the stiffness of the film and the substrate. The term $3 S_s t_s^2$ was substituted in for the term $4 S_s t_s^2$ since η_s must approach ($t_s/2$) when t_f approaches zero.

Given that

t_f = +0.97 microns,

t_s = -0.456 mm,

s_f = 1.3 10-3 GPa/m,

and s_s = 82.3 10-3 GPa/m,

where the X=0 plane is taken at the interface, the distance η_s of the neutral axis of the silicon substrate away from the interface is 0.38 mm. Thus the neutral axis of the silicon substrate has moved away from the stiffer diamond. Since the neutral axis of the substrate is moved away from the interface, the stress on the interface side of the substrate in expected to be higher than the stress on the back side of the silicon substrate. Indeed, the stress on the interface side is twice as much as the stress on the back side stress in the silicon substrate respectively (-0.31 GPa versus 0.15 GPa (table 9)). The stresses in the silicon substrate after the anneal shows the same type of stress distribution as for the as-deposited state.

The annealing of the diamond film was carried to check if both methods are sensitive to the change in stress magnitude due to the anneal. As stated earlier, The relative stress relief due to annealing measured from the Raman shift was 20 percent while the same relative stress relief measured from the curvature change was 14 percent. An interesting feature occurred at the silicon interface. Upon annealing, the Raman shift of the silicon at the interface increased, indicating that

the stress state has become more compressive (from - 0.31 to 0.38 GPa), while the decrease in the shift of the diamond peak resulted from a decrease in the stress in the diamond film. A possible explanation of the stress change is the diffusion of hydrogen across the interface from the diamond side to the silicon side. Indeed, at the annealing temperature of 650 C for 1 hour, some limited diffusion of the hydrogen in the diamond film to the silicon substrate is expected. As a result, the stress in the silicon at the interface increased due to the hydrogen impurity that diffused in. It is a well established fact in the literature that hydrogen induces compressive stresses in both diamond [47] and silicon [55]. Incidentally, the relative increase in the stress magnitude due to annealing at the silicon (at interface) is 21 percent, just about the same magnitude of the stress decrease in diamond (20 percent). The annealing treatment reduced the stress only slightly. Annealing for more than one hour and/or at higher temperatures might be necessary to completely relief the stress in the diamond film.

Another point of concern is whether the silicon wafers have any stress before the deposition of diamond and whether the annealing of the silicon diamond system affects the silicon wafer separately. To answer the question, both the silicon wafer bow and Raman shift have been measured on separate silicon wafers before and after annealing under the same conditions as the silicon-diamond sample. The silicon wafers as provided by the supplier have a curvature due to the processing method, several treatment are carried to make sure that the

silicon wafers do not have any residual stress [85]. The original curvature of the wafers used is consistently the same for all the wafers annealed or not with the exception of one sample where the bow is much smaller than the other silicon wafers (table 5). The shift in the silicon peaks of the silicon wafers resulted in calculated stresses of 0.02 to 0.05 GPa, greater than the error in the stress measurement but roughly about 50 times smaller than the stresses in the diamond film. If the observed shifts in the separate silicon wafers are stress induced, their magnitude is small compared to the film stress and thus can be neglected. Annealing of a silicon wafer resulted in no change in the shift, furthermore the shifts on either side of the wafer were consistently the same for all wafer. Consequently, there is no reason to believe that neither the bow nor the Raman shifts are stress induced. Had the bow or shifts been stress induced, the annealing would have affected the magnitude of the shift and the sign of the shift on either side of the wafer would have been of opposite signs. The only possibility left is that the wafers are under a uniformly compressive stress, as indicated by the sign of the shift, rather than a bending stress.

Table 10 provides some reported stress measurements on diamond and carbon films. The magnitude of the compressive stress in the diamond film is lower than the calculated compressive stress that results from the thermal expansion mismatch after cooling to room temperature. The thermal stress that results from the thermal expansion mismatch between the film and the substrate upon cooling down from the

deposition temperature was calculated as a function of the deposition temperature. At the deposition temperature of 980°C, the compressive thermal stress is -0.83 GPa (figure 19). On top of the thermal mismatch stress, hydrogen and graphite component in diamond contribute to the compressive stress. Since the measured compressive stress (-0.57 GPa) is lower than the thermal compressive stress (-0.83 GPa) a tensile stress must have offset the compressive thermal mismatch stress and resulted in a lower measured compressive stress. One contribution of the tensile component of stress in the lattice mismatch stress. The lattice constant of silicon is larger than the lattice constant of diamond. As a result a compressive stress contribution develops at the silicon side of the interface and a tensile stress contribution on the diamond side. Windischmann [10,21] found diamond film under a tensile stress state. The magnitude of the stress was about +0.3 GPa. Windischmann explained the origin tensile stress with the grain boundary relaxation model (GBRM). The GBRM claims that films deposited under low adatom mobility and/or in the absence of energetic particle bombardment develops a porous microstructure. Tensile stresses develop in this type of microstructure (called Zone1) because of attractive atomic forces acting across the micropores and the grain boundaries [10].

Table 10. Reported residual stress values in diamond and carbon films

Ref.	Film material	Substrate material	Film thickness (μm)	Grain size (μm)	Internal Stress (GPa)	Stress Measuring Method (*)	Proposed stress mechanism (**)	Film deposition method (***)
10	Diamond	(100) Silicon	0.7	.02 to .12	+.565 to +.625	1	1	MPCVD
11	DLC	Silicon	N/A	N/A	2.0	2	2	IBSD
27	DLC	(100) Silicon	0.7	amorphous	-0.5 to -0.1	1	2,3	rf. Plasma
20	Diamond Membrane	Silicon	2.0	0.3 to 0.7	+.094 to +.139	3	3	MPCVD
12	DLC	Silicon	.03 to .12	amorphous	-.5 to -3.0	1	2	IBSD
21	Diamond Membrane	Silicon	1 to 3	.03 to .04	+.03 to +.15	1	2	MPCVD
87	Graphite	N/A	N/A	3mm	-0.3	4	4	N/A
26	Diamond	Alumina	N/A	10 to 20	-1.7 to -5.5	4	N/A	PACVD
		Tungsten carbide		10 to 20	-1.7 to -2.1			
		SiO_2 Glass		10 to 20	+2.1			
		SIALON		10 to 20	+1.7			
14	Carbon	Silicon	0.2	N/A	-3.5	N/A	N/A	IBSD
46	Carbon	Glass	0.2	N/A	-3.0	N/A	N/A	IBSD

(*)

1: stress calculated from change in substratecurvature, equation 9.
2: stress calculated from change in substrate defection, equation 25.
3: vibrating membrane method [20]
4: C-C bond length and crystallite size effect [87]

(**)

1: Grain boundary relaxation model
2: atom displacement, ion beam energy, and/or hydrogen effect
3: Differential expansion coefficient model
4: Stress calculated from shift in first order Raman spectrum.

(***)

MPCVD: Microwave plasma chemical vapor deposition
IBSD : Ion beam sputter deposition
PACVD: Plasma assisted chemical vapor deposition.

9- CONCLUSIONS AND RECOMMENDATIONS

A review of the literature revealed that the properties of diamond films deposited by MPCVD are dependent on the deposition parameters. Growth stresses are also dependent on the deposition parameters.

The thermal stress arising from the thermal expansion mismatch between the diamond film and the silicon substrate was calculated taking into account the temperature dependence of both the Young's modulus of diamond and the thermal expansion mismatch between the film and the substrate. The proposed model is believed to be an improvement over an existing model [10]. However, the assumptions made on the Young's modulus of diamond probably caused large errors in the magnitude of the calculated thermal stress. The estimated stress would become more accurate should data on the temperature dependence of the Young's modulus of diamond become available.

The magnitude of the residual stress measured in the diamond film was almost equal by the Raman shift and curvature change methods. Annealing of the silicon-diamond sample resulted in stress relief of 14 percent as measured from the curvature change and 20 percent as measured from the Raman peak shift. The two methods are measuring the average stress in the diamond film since the film thickness is not uniform and the stress is inversely proportional to the film thickness,

thus not uniform.

Diamond is transparent to the argon laser light used at 488 nm wavelength, thus the Raman shift are sampled over the entire film thickness of 0.97 micron.

The experimental results show that the observed Raman shift in this work are stress induced. Indeed, annealing of the silicon-diamond sample resulted in a measured stress relief equivalent to the magnitude of the stress relief measured from the curvature change. Raman shifts measured on opposite sides of the diamond coated silicon substrate are of opposite signs; one surface is in compression while the other surface is in tension. Furthermore, annealing of uncoated silicon wafers separately did not result in measurable Raman shifts or curvature changes, thus the measured shifts are due solely to the stress in the diamond film. Raman shift can consequently be treated as stress-induced and thus be used for stress measurement.

The stress relief in the diamond film as result of the annealing at 650 degree Celsius for one hour in nitrogen is interpreted from the diffusion of hydrogen from the diamond to the silicon across the interface; the magnitude of the Raman silicon shift (thus the stress) at the interface increased upon annealing.

The measured strain at the interface was not continuous as predicted by the theory; the Raman shift (and thus the strain) was considerably higher on the silicon side of the interface. Two explanations were offered. First, the strain (thus stress) measured on

the diamond film was an average value since all of the film in the laser focus, while the shift on the silicon side of the interface results from the interfacial strain; the laser beam is sampling within 2 microns deep out of the 456 microns wafer thickness. The interfacial strain in the silicon is higher than the average strain in the diamond film. Second, the assumptions made to derive the stress-shift relationship are well satisfied for the single crystal silicon with known orientation, while it is not the case for the polycrystalline diamond film whose orientation was assumed as (111); to be able to apply the equation to stress measurement. Since the stress-shift relation was derived for a single crystal with known orientation with respect to the stress and the laser beam, the magnitude of the Raman shift from the polycrystalline diamond film cannot be directly converted into stress. For silicon, the shifts can be converted to stress more confidently. Continuity of the strain at the interface would thus provide us with the value of the interfacial strain and thus stress from the measured strain on the silicon side of the interface. The average or macroscopic stress in the film cannot however be measured reliably from the Raman shift.

For the stress measurement from the curvature change, the isotropy assumption is not satisfied for either the silicon or the diamond. However, since the diamond is polycrystalline, it might be macroscopically isotropic with respect to the elastic modulus. Stress measurement in the diamond film from the change in curvature is more reliable than from the Raman shift.

The magnitude of the stress measured in the diamond film (-0.57 GPa) is lower than the calculated thermal expansion mismatch stress. Tensile stresses must have offset the compressive stress. Lattice mismatch stress and attractive forces across grain boundaries and pores (GBRM [10]) could have contributed to the tensile stress. However, the calculated thermal stress (-0.83 GPa) could have been exaggerated due to the several critical assumptions made to derive the stress equation.

Finally, contribution of the processing method to the curvature in the diamond coated wafer is not known; a more meaningful study would involve measuring a silicon wafer curvature and Raman shift, deposit the film on the same wafer, then measure the shifts and curvatures before and after annealing. Furthermore, experimental studies on the stress dependence of the Raman peak position for polycrystalline samples under a true biaxial stress are needed for comparison with theoretical models and accurate stress determination in thin deposited diamond films. A theoretical model for stress-Raman shifts calculation taking into account the polycrystalline nature of a material would also be very helpful for accurate stress measurement in polycrystalline films.

LIST OF REFRENCES

REFERENCES

1. Stoney, G. G., *Proc. Roy. Soc.* (London), **A82**, 172, 1909.
2. Marshall, D. B., *J. Appl. Phys.*, **56** [10], 2632, 1984.
3. Argon, A. S., Gupta, V., Landis, H. S., Cornie, J. A., *J. Mater. Sci.*, **24**, 1207, 1989.
4. Sugo, M., Uchida, N., Yakamoto, A., Nishioka, T., *J. Appl. Phys.*, **65** [2], 591,1989.
5. Blumberg, R. H. and Seraphin, D. P., *J. Appl. Phys.*, 33, 163, 1962.
6. Freedman, J. F., *IBM J. Res. Develop.*, **6**, 449, 1962.
7. D' Heurle, F. M., *Thin Solid Films*, **171**, 81, 1989.
8. Hoffman R. W., Physics of Thin Films, edited by, Hass, G. and Thun, R. E., Academic press, New York and London, vol **3**, 211 -271,1966.
9. Yoshikawa, M., Katagiri, H., Ishitani A., *Appl. Phys. Lett.*, **55** [25], 2608, 1989.
10. Windishmann, H., Epps, F. G., *J. Appl. Phys.*, **69**, 2231, 1991.
11. Nir, D., *J. vac. Sci. Technol.*, **A4** [6], 2954, 1986.
12. Nir, D., *Thin Solid Films*, **146**, 27, 1987
13. Green, D. J., *J. Mater. Sci.*, **19**, 2165, 1984.
14. Gille, G., *Thin Solid Films*, **120**, 109, 1984.
15. Hoffman, D. W., Kukla, C. M., *J. vac. Sci. Technol.*, **A3** [6], 2600,1985.

16. Davidson, J. L., Ramesham, R., Ellis, C., *J. Electrochem. Soc.*,**137** [10], 3206,1990.

17. Cullity, B. D., Elements of x-ray diffraction, Addison-wesley Publishing company, Inc. p. 447-526, 1987.

18. Berman, R., Physical properties of diamond, Oxford University Press, London, 1965.

19. Tsai, H-C., Bogy, D. B., *J. vac. Sci. Technol.*, **A5** [6], 3287, 1987.

20. Berry, B. S., Pritchet, J. J., Guarnieri, C. R., *Appl. Phys. Lett.*, **57** [3], 302, 1990.

21. Windishmann, H., Epps, F. G., *J. Appl. Phys.*, **68**, 5665, 1990.

22. Buckley, R. G., Moustakas, T. D., Ye, L., Varon J., *J. Appl. Phys.*, **66** [8], 3595, 1989.

23. Enke, K., Dimigen, H., Hubsch, H., *Appl. Phys. Lett.*, **36**, 291, 1980.

24. Chrenko, R. M., L. *Appl. Phys. Lett.* **63** [12], 5873, 1988.

25. CRC Handbook of chemistry and physics, 59th edition,CRC press, Florida, 1986.

26. Knight, D. S., White, W. B., *J. Mater. Res.*, **4**, [2], 385, 1989.

27. Amaratunga, G. A. J., Welland. M. E., *J. Appl. Phys.*, **68**, 5240, 1990.

28. Albin, S., Watkins, L., *IEEE Elect. Dev. Lett.*, **2**, [4], 159,1990.

29. Takata, Y., Edamatsu, K., Yokoyama, T., Seki, K., Tohnan, M.,Okada, T., Ohta, T., *Jpn. J. Appl. Phys.*, **28** [7], L1282, 1989.

30. Clausing, R. E., Heatherly L., Spetch, E. D., More K. L. and Begun G. M., *Carbon*, **28** [6] ,762,1990.

31. Wang, X. H., Pilione L., Zhu, W., Yarbrough W., Drawl, W., Messier, R., *J. Mater. Res.*, **5** [11], 2345, 1990.

32. Endo, M., *J. Appl. Phys.*, **63** [8], 2769, 1988.

33. Liou Y., Inspektor, A., Weimer, R., Knight, D. S., Messier, R., *J. mater. Res.*, **5** [11], 2305, 1990.

34. Grill, A., Patel V., Meyerson, B. S., *J. Mater. Res.*, **5** [11], 2351, 1990.

35. Harshavardhan, K. S., *J. Appl. Phys.*, **68** [7], 3303, 1990.

36. Yarborough, W., Messier R., *Science*, **247**, 688, 1990.

37. Yoshikawa, M., Katagiri, G., Ishitani, A. and Akamatsu, T., *J. Appl. Phys.*, **64** [11], 6464, 1988.

38. Ohsawa, Y., Tamou Y., Kikuchi, N., *J. Mater. Sci.*, **26**, 3748, 1991.

39. Sundgren, J. E., Hentzell, T. G., *J. vac. Sci. Technol.*, **A4** [5], 2275, 1986.

40. Kato, H., Nagasima, K., Hasunuma, H., *Oyo Butsuri*, **30**, 533, 1959.

41. Kimbara, A., Haraki, H., *J. Appl. Phys.* Japan, **4**, 243, 1965.

42. Horikoshi, H., Ozawa, Y., Hasunuma, H., *J. Appl. Phys.* Japan, **1**, 304, 1962.

43. Horikoshi, H., Tamura, N., *J. Appl. Phys.* Japan, **2**, 328, 1963.

44. Kimbara, A., *Oyo Butsuri*, **30**, 496, 1961.

45. Blackburn, H., Campbell, D. S., in "Eigth National Symposium Vacuum Technology Transactions," p.943. Perganon Press, New York,1961.

46. Matuda, N., Baba, S., Kimbara, A., *Thin Solid Films*, **8**, 301, 1981.

47. Zelez J., *J. Vac. Sci. Technol.*, **A1** [2], 305, 1983.

48.. Hoffman D. W., *Thin Solid Films*, **40**, 355,1977.

49.. Davidenkov, N. N., *Soviet phys.-Solid state English Tansl.*, **2**, 2595, 1961.

50. Priest, J., Caswell, H. L., Budo, Y., *J. Appl. Phys.*, **34**, 347, 1963.

51. Finegan, J. D., Hoffman R. W., in "Eigth National Symposium Vacuum Technology Transactions," p.935. Perganon Press, New York,1961.

52. Blackburn, H., Campbell, D. S., *Phil. Mag.*, **8**, 823, 1963.

53 Halliday, J. S., Rymer, T. B., Wright, H. R., *Proc. Roy. Soc.* (London), **A 225**, 548, 1954.

54. Fleet, S. G., *Mullard Res. Lab. rep.*, 466,1963.

55. Windischmann, H., Collins, R. W. and Cavese J. M., *J. Non cryst. sol.*, **85**, 261, 1986.

56. Rossignton, C., Evans, A. G., *J. Appl. Phys.*, **56**, 2639, 1984.

57. Oel, H. J., Frechaette, V. D., *J. Amer. Ceram. Soc.*, **50** [10], 542, 1967.

58. Rubin, M., Hopper, C. B., Cho, N-H., *J. Mater. Res.* **5**, [11], 2538, 1990.

59. Trimble, L. E., Celler, G. K., Schimmel, C., Y. Lu, Nakahara, S. and Fauchet, P. M., *J. Mater. Res.*, **3** [3], 514, 1988.

60. Cardinale, G. F. and Tustison, R. W., *J. Vac. Sci. Technol.*, **A9**, 2204, 1991.

61. Cerdeira, F., Buchenauer, C. J., Pollak, F. H., Cardona, *Phys. Rev B.*, 5 [2], 580, 1972.

62. Gezan, S., Maradudin, A. A. and Oitmaa, *J., Annals of Physics*, **56**, 556, 1970.

63. Sharma, S. K., *Journal of Raman Spectroscopy.*, **16** [5], 350,1985.

64. Nishioka, T., Shinoda, Y., Ohmachi, Y., *J. Appl. Phys.*, **57** [2], 276, 1985.

65. Hanfland, M. and Syassen K., *J. Appl. Phys.* **57** [8], 2752, 1985.

66. Diebold, A. C. and Steinhauser, S. W., *J. Vac. Sci. Technol.*, **B7** [2], 365, 1989.

67. Mukaida, H., Okumura, H., Lee, J. H., Daimon, H., Sakuma, E., Misawa, S., Endo, K. and Yoshida, S., *J. Appl. Phys.*, **62** [1],

68. Engler, TH. and Abstreiter, G., *Solid State Electronics*, **23**, 31, 1980.

69. Tardieu, A., Cansell, F., and petitet, J. P., *J. Appl. Phys.*, **68** [7], 3243, 1990.

70. Grimsditch, M. H., Anastasskis, E., Cardona, M., *Phys. Rev. B.*, **18**, 901,1978

71. Gupta, Y. M, Horn, P. D., Yoo, C. S., *Appl. Phys. Lett.*, 55

72. Hanfland, M., Syassen, K., Fahy, S., Louie, S. G., *Physica* **139& 140B**, 516,1986.

73. Boppart, H., *Phys. Rev. B.*, **32** [2], 1423, 1985.

74. Hanfland, M. and Syassen, K., *Phys. Rev. B*, **31** [10], 6896, 1985.

75. Whalley, E., Lavergne, A. and Wong, T. T., *Rev. Sci. Instrum.*, **47** [7], 845, 1976.

76. Grimsditch, M. H. and Ramdas, A. K., *Phys. Rev. B*, **11** [8], 3139, 1978.

77. Fitzer, E., *Carbon*, **26** [4],594,1988.

78. Knight, D. S., Weimer, R., Pilione L. and White, W. B, *Appl. Phys. Lett.*, **56** [14], 1320, 1990.

79. Watchman, J. B., Tefft, W. E., Lam D. G. and Apstein, C. S., *Phys. Rev. B.*, **122** [6], 1574, 1961.

80. Anderson L. O., *Phys. Rev. B.*, **144** [2], 553.1966.

81. Glen, A. and Bartram, S. F., *J. Appl. Phys.*, **46** [1], 89, 1975.

82. Lammer, A., *Mater. Sci. Technol.*, **4**, 949, 1988.

83. Simmons G. and Wang, H, "Single Crystal Elastic Constants and Calculated Aggregate Properties: A HANDBOOK", second edition, The M.I.T. press, 185-186, London, 1971.

84. Sze, S., "VLSI Technology", second edition, Mc Graw Hill book company, New York,1988.

85. Gamlen, C. A., Adhesion of Diamond Thin Films to Silicon Wafer and FTIR Spectroscopy of Damaged Materials, Thesis for the degree of M. S.,1990.

86. Kiefer, B., *Applied Spectroscopy*, **25**, 500, 1971.

87. Kitajima, M., and Nakamura, K., *Journal of Nuclear Materials*, **175**, 251, 1990.